Earth-Science Reviews 202 (2020) 103089

Contents lists available at ScienceDirect

Earth-Science Reviews

journal homepage: www.elsevier.com/locate/earscirev

The Rio Apa Terrane reviewed: U—Pb zircon geochronology and provenance studies provide paleotectonic links with a growing Proterozoic Amazonia

W. Teixeira[a,*], U.G. Cordani[a], F.M. Faleiros[a], K. Sato[a], V.C. Maurer[b], A.S. Ruiz[c], E.J.P. Azevedo[d]

[a] Institute of Geosciences, University of São Paulo, Brazil
[b] Department of Geology, School of Mines, Federal University of Ouro Preto, Brazil
[c] Faculty of Geosciences, Federal University of Mato Grosso, Brazil
[d] Brazilian Geologic Survey, CPRM, Brazil

ARTICLE INFO

Keywords:
Rio Apa Terrane
U-Pb zircon ages and sedimentary provenance
Paleo- to Mesoproterozoic evolution
Amazonian Craton
LIP

ABSTRACT

New and compiled data of zircon U-Pb ages and geochemical-isotopic constraints provide new insights into the orogenic evolution of the Rio Apa Terrane (RAT) and its close affinity with the Amazonia throughout the Proterozoic. Two terranes with distinct evolutionary histories built the RAT. The Porto Murtinho (2070–1940 Ma) and Amoguijá (1870–1820 Ma) magmatic arcs generated the Western Terrane which is mainly composed of short-lived crustal components. Granitoid rocks (1870 Ma) in the distal Corumbá Window indicate that the RAT is much larger in extent. The Caracol accretionary arc (1800–1740 Ma) and the associated Alto Tererê back-arc basin formed away from the Amoguijá belt, being roughly coeval with the adjoining Baía das Garças suite (1776 Ma) and Paso Bravo granitoid rocks (1774–1752 Ma). These tectonic units constitute the Eastern Terrane, whilst the Nd—Hf isotopic constraints indicate derivation from a predominantly juvenile magma source with the minor input of crustal-derived contaminants. The youngest detrital zircon grains from the Alto Tererê samples gave 1740–1790 Ma ages and unimodal age spectra were mainly present. The basin infill was, therefore, most likely concomitant with the exhumation of the Caracol belt. Alto Tererê provenance study also included detritus from passive to active margin settings. The RAT underwent regional cooling between 1.35 and 1.27 Ga, documented mainly by $^{40}Ar—^{39}Ar$ and K—Ar ages. This age pattern matches a collisional episode that formed the accretionary margin of Amazonia, suggesting that the RAT was a close neighbor at Ectasian times. The geodynamic interplay between them lasted until 1.1 Ga ago, highlighted by some shared-components of a LIP event.

1. Introduction

The Rio Apa Craton (Almeida, 1967; Cordani et al., 2010), also named Rio Apa Province (Ruiz, 2005), Rio Apa Block (Lacerda Filho et al., 2016), or Rio Apa Terrane – RAT (Faleiros et al., 2016) crops out as a structural high, 220 km long and 60 km wide, largely overlain by Neoproterozoic-Ediacaran and Quaternary sedimentary rocks (Fig. 1). Basement rocks, occurring in another window in the Corumbá region, located ca. 100–150 km away from the southwestern portion of the Amazonian Craton (present coordinates), are probably coeval with the RAT due to the similarity of their ages. Considering the Neoproterozoic framework, the RAT is a very large basement dome encompassed within the Paraguay belt, a tectonic unit formed during the process of assembly of Western Gondwana (e.g., Boggiani and Alvarenga, 2004). The Paraguay belt has a vergence towards the SE edge of the Amazonian Craton, highlighted by NW-trending nappes with metamorphosed pelitic-carbonatic rocks. Fig. 1 also shows the associated Neoproterozoic Tucavaca belt, which started as an aulacogen developed within the cratonic crust (Cordani et al., 2010; Lacerda Filho et al., 2016).

The geological knowledge of the RAT has increased significantly over the last two decades, due to systematic mapping of the Brazilian Geologic Survey (CPRM), in addition to geochemical and geophysical data. Moreover, Cordani et al. (2010) conducted a systematic U—Pb, Rb—Sr, Sm—Nd and K—Ar study in order to focus on the geodynamic evolution of the unit, previously inferred by regional mapping and age dating (Araújo et al., 1982; Lacerda-Filho et al., 2006). According to these authors, the RAT consists of distinct tectonic domains, formed by accretionary events roughly between 2.0 and 1.7 Ga. Eventually, the resulting arc complexes underwent crustal shortening and metamorphism, as part of a major collision along the active margin of the continental segment called Amazonia, occurred in Mesoproterozoic times (e.g., Cordani and Teixeira, 2007; Bettencourt et al., 2010;

* Corresponding author.
E-mail address: wteixeir@usp.br (W. Teixeira).

https://doi.org/10.1016/j.earscirev.2020.103089
Received 26 February 2019; Received in revised form 14 January 2020; Accepted 14 January 2020
Available online 23 January 2020

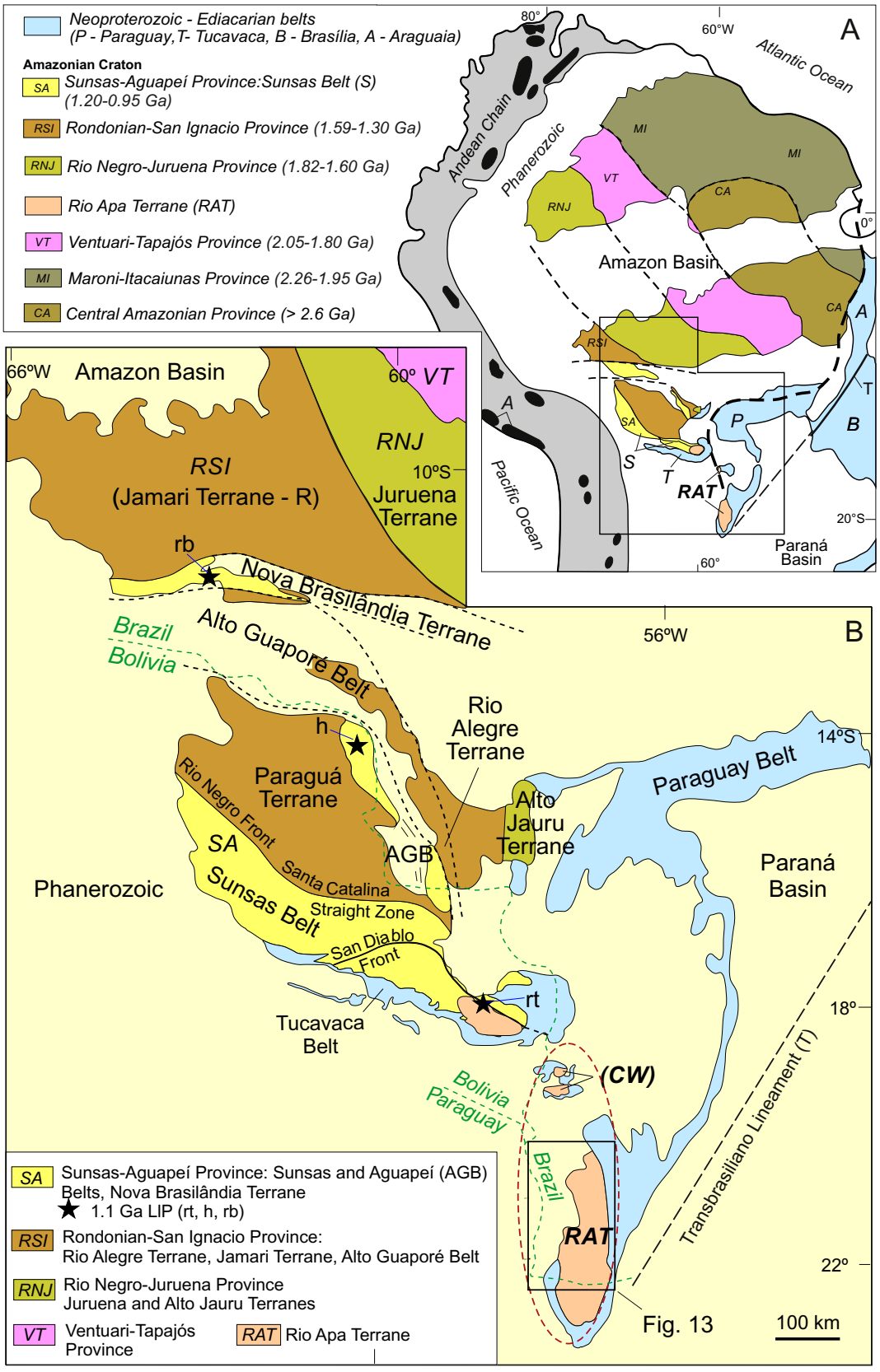

Fig. 1. A) tectonic sketch of the Amazonian Craton. Basement inliers (reworked in the late Mesoproterozoic) in the Andean chain are also shown in black (A = ca. 2.0 Ga-old Arequipa Terrane); B) Geologic outline of the SW Amazonian Craton, showing the distal Rio Apa Terrane (present coordinates) and the northern structural high with correlative rocks (CW = Corumbá Window). Keys: AGB (Aguapeí fold and thrust belt; R (Mesoproterozoic reworking of the Jamari Terrane). Stars in the SW Amazonian Craton represent 1.11 Ga LIP components: h (Huanchaca sills and dikes; rt. (Rincón del Tigre complex); rb (Rio Branco suite). Geologic framework adapted from Cordani et al. (2010), Casquet et al. (2012) and Teixeira et al. (2019b). See text for details.

Table 1
Geologic-tectonic aspects of the Ventuari-Tapajós (VT), Rio Negro-Juruena (RNJ), Rondonian-San Ignacio (RSI) and Sunsas-Aguapeí (SA) provinces, highlighted by the age and geochemical-isotopic constraints and major magmatic and tectonic episodes. See text and Fig. 1 for an explanation.

Province	Relevant events and major geologic-tectonic characteristics
Sunsas- Aguapeí (*SA*) (1.20–0.98 Ga)	1.11 Ga Rincón del Tigre-Huanchaca LIP. 1.10–1.00 Ga Sunsas collisional orogeny. Aguapeí fold-and-thrust belt (c. 0.96 Ga) Nova Brasilândia Terrane (1.18–1.12 Ga). Regional shear zones (e.g., San Diablo, Santa Catalina). Syn- to late-tectonic plutons (1.08–1.05 Ga). Nova Brasilândia Terrane (1.11 Ga) within the RSI (coeval with the Sunsas collision). 1.11 Ga Rincón del Tigre-Huanchaca LIP. Anorogenic plutonism (1.00–0.95 Ga). Crystalline basement (1.92 Ga).
Rondonian-San Ignacio (RSI) (1.59–1.30 Ga)	Cachoeirinha (1.59–1.52 Ga), Rio Alegre (1.51–1.48 Ga), Alto Central Brazil (1.44–1.43 and 1.35–1.33 Ga), Santa Helena (1.44–1.42 Ga) belts. San Ignacio orogeny (1.37–1.34 Ga): Pensamiento suite (Paraguá Terrane: 1.82–1.76 Ga). Crustal shortening and collisional metamorphism (~1.35 Ga) inboard the RNJ and RAT. Cratonization: 1.30–1.25 Ga. Tectonic reactivation and crustal reworking triggered by the Sunsas orogeny. Anorogenic plutonism (1.08–1.05 Ga), including the Rondônia Tin Granites (0.99–0.95 Ga).
Rio Negro-Juruena (RNJ) (1.82–1.60 Ga)	Basement window: gneisses (2.05–2.03 Ga) and granitoid suites (1.99–1.93 Ga and 1.89–1.87 Ga). Juruena orogen (1.82–1.74 Ga). Teles Pires suite and coeval mafic suite (1.78–1.76 Ga). Colider and Roosevelt Groups (1.78–1.74 Ga). Alto Jauru granite-greenstone terrane (1.80–1.70 Ga). Collisional high grade metamorphism and deformation (1.69–1.63 Ga). Serra da Providência suite (1.60–1.51 Ga). Anorogenic plutons (1.45–1.35 Ga). Metamorphic overprints: 1.57–1.50 Ga and ~1.35 Ga. Cratonic area for the RSI and SA orogenies.
Ventuari-Tapajós (VT) (2.05–1.80 Ga)	Multiple accretionary belts: calc-alkaline gneiss complexes (2.04–1.90 Ga) and granitoid suites (1.89–1.88 Ga). Uatumã SLIP (1.89–1.87 Ga) and coeval granitoid rocks (1.88 Ga). Cachimbo Graben: basal metavolcanosedimentary sequence (ca. 1.74 Ga). Cratonic area for the RNJ and RSI orogenies.

Rizzotto et al., 2013).

The detailed evolution of particular domains within the RAT, including the provenance sources of the supracrustal sequences, is still poorly known. In this study, new U−Pb LA-ICP-MS ages from detrital zircon grains of key samples were obtained to better understand their tectonic role. Some additional U−Pb zircon SHRIMP dating was also carried out on the granitoid rocks that may have been their sources. The novel approach integrated the geochronological and isotopic-geochemical interpretation to address the geodynamic evolution of the RAT and the possible correlations with the Paleo- to Mesoproterozoic accretionary-collisional history of Amazonia. The potential implications in the context of supercontinent Columbia are also discussed. Finally, we reassess a peculiar intraplate mafic magmatism (1.11 Ga) occurring in the RAT, which shows a similar age with a Large Igneous Province (LIP) episode documented in the SW Amazonian Craton, which allows a global barcode match in supercontinent Rodinia.

2. The Amazonian Craton

The Amazonian Craton (Fig. 1) essentially comprises two major crustal segments, the Archean-Paleoproterozoic tectonic provinces in the NE and the late Paleo- to Mesoproterozoic ones in the SW (e.g., Teixeira et al., 1989; Tassinari and Macambira, 2004; Cordani and Teixeira, 2007). In the eastern and south-eastern parts, the craton is bounded by the Araguaia and Paraguay belts whose rocks underwent deformation and metamorphism during the development of the Transbrasiliano lineament (Fig. 1). This lineament is a major suture along which a large Pharusian-Goias ocean disappeared during the process of agglutination of West Gondwana (Cordani et al., 2016a). From a paleotectonic point of view, the closure of this ocean that separated the Amazonian - West African cratons from the São Francisco and Rio de la Plata cratons eventually produced Brasiliano-Pan African belts at Neoproterozoic - Eocambrian times (e.g., Cordani et al., 2009; Ganade et al., 2016; D'Agrella-Filho and Cordani, 2017). We summarize below relevant tectonic-geological aspects of the Proterozoic history of the Amazonian Craton that can be used to establish correlations with the RAT, the focus of the study.

The oldest segment consists of one ancient core - the Central Amazonian tectonic province (> 2.6 Ga) - and the adjacent Maroni-Itacaiunas tectonic province (2.45–1.93 Ga) to the north. The first province, largely exposed within the Carajás and Rio Maria domains, is essentially composed of Meso- to Neoarchean granite-greenstone associations, medium- to high-grade terrains, and granitoid rocks (e.g., Bettencourt et al., 2016). The second province, mostly exposed in the Guiana shield, consolidated during the Transamazonian orogeny by means of accretionary and collisional arcs, hosts some Archean blocks and/or inliers (e.g., Kroonenberg et al., 2016 and references therein; Borghetti et al., 2018). Both provinces document LIP scale events, namely the Avanavero and Uatumã, dated at 1.89–1.87 and 1.79–1.78 Ga, respectively. These two igneous events have barcode matches in the context of the Columbia supercontinent (Teixeira et al., 2019b and references therein).

The southern Ventuari-Tapajós (2.05–1.80 Ga), Rio Negro-Juruena (1.82–1.60 Ga), Rondonian-San Ignacio (1.59–1.30 Ga) and Sunsas-Aguapeí (1.20–0.95 Ga) tectonic provinces (Fig. 1) are the result of long-lived accretionary orogens coupled with plate convergence and B-type subduction outboard of the Central Amazonian province (e.g., Cordani and Teixeira, 2007; Bettencourt et al., 2010; Teixeira et al., 2010). We roughly followed the original model of Cordani and Teixeira (2007) for the Proterozoic accretionary growth of the Amazonia, in which the continued plate convergence in association with soft collision and accretion dynamics would favor spontaneous and induced nucleation of oceanic slabs (Stern, 2004), producing lateral accretion and stacking of successively younger arc complexes and intervening terranes through time and space. Such a “mobilistic” concept is used as a case for the tectonic evolution of the RAT. In addition, we have considered recent geophysical and geologic information on the SW Amazonian Craton, including U−Pb zircon dating and geochemical-isotopic constraints, which also defined particular orogenic events and tectonic settings of the lithostratigraphic units (e.g., Fernandes et al., 2011; Rizzotto et al., 2013, 2014; Scandolara et al., 2013a, 2017).

Table 1 summarizes the geologic-geochronologic characteristics of the Ventuari-Tapajós, Rio Negro-Juruena, Rondonian-San Ignacio and Sunsas-Aguapeí tectonic provinces with focus on the Central Brazil shield (also termed Central Brazil shield). Special emphasis is given to the Paleo- and Mesoproterozoic tectonic-magmatic events that allowed potential implications for the RAT evolution.

The Ventuari-Tapajós province was formed in the Orosirian period (e.g., Cordani and Teixeira, 2007) by means of accretionary-collisional arcs. In the Central Brazil shield (Tapajós-São Felix do Xingu region; not shown), the multiple magmatic arcs developed between 2.04 and 1.90 Ga, resulting in a complex geologic framework with calc-alkaline tonalitic, monzogranitic and monzonitic gneisses, amphibolites and associated metavolcanic-sedimentary sequences (back-arc). Voluminous plutonic-volcanism (1.89–1.87 Ga) was also apparent in this portion of the shield (e.g., Santos et al., 2000, 2001, 2004; Lamarão et al., 2002; Fernandes et al., 2011), collectively ascribed to the Uatumã silicic large igneous province - SLIP (e.g., Teixeira et al., 2019b and references therein).

From a geodynamic point of view, the gneissic rocks may have

generated, as a response of the northward subduction, successive slabs beneath the Archean/Paleoproterozoic continental margin. The Uatumã SLIP should be the rift-related activity over the adjoining stable area, induced by a possible flattening in the angle of the subducting plate (Fernandes et al., 2011). Nevertheless, the complexities of such a dynamic setting, including timing and duration of crustal addition and reworking are still under debate because of insufficient geochronologic-isotopic information and scarce geophysical investigation (e.g., Rosa et al., 2016). The available Sm−Nd one-stage depleted mantle model T_{DM} ages (hereafter termed as T_{DM} ages) for the Tapajós rocks are between 2.5 and 2.2 Ga (e.g., Lamarão et al., 2005; Tassinari and Macambira, 2004; Cordani and Teixeira, 2007) with positive to slightly negative $\varepsilon_{Nd(t)}$ values (Sato and Tassinari, 1997; Santos et al., 2000). This suggests a predominant juvenile nature for the accretionary arcs, though including ancient crustal components in the magma genesis.

The Rio Negro-Juruena tectonic province formed in the late Orosirian-Statherian, as a continuation of the soft collision and accretion dynamics that originated the previous Ventuari-Tapajós province, as described by Cordani et al. (2016b) for the northwesternmost part of the Guiana shield. The southwestern part of the Rio Negro-Juruena province, in the Central Brazil shield, is made up of distinct arc complexes as old as 1.82 Ga, overlain in places by siliciclastic strata that fill tectonic basins of Meso- to early Neoproterozoic ages (e.g., Leite and Saes, 2003; Reis et al., 2013).

Scandolara et al. (2017), based on systematic structural, geophysical and isotopic studies, proposed a tectonic model for the southwestern part of the province, with the Juruena orogeny originating the Juruena (1.82–1.74 Ga) and the adjoining Jamari (1.79–1.74 Ga) terranes, respectively (see Fig. 1), where most T_{DM} ages varied from 2.1 to 1.9 Ga (e.g., Sato and Tassinari, 1997; Santos et al., 2008). Recently, Rizzotto et al. (2019b) postulated that some portions of both terranes could be intracontinental, composed dominantly of rocks (1.82–1.76 Ga) with A-type geochemical characteristics. We note that the Jamari Terrane underwent widespread reworking and magmatism during the Mesoproterozoic, as reported by Bettencourt et al. (2010), indicating that the tectonic unit is part of the younger Rondonian-San Ignacio province to be dealt with later (see Fig. 1B and Table 1).

According to Scandolara et al. (2017), much of the eastern portion of the Juruena Terrane (Alta Floresta region; not shown) comprise calc-alkaline and alkaline felsic plutonic rocks (e.g., 1.78–1.76 Ga Teles Pires suite), and includes a mafic suite of tholeiitic affinity (Scandolara et al., 2014). Such a widespread plutonic-volcanic episode was tectonically related to their Juruena orogeny. The Teles Pires suite is roughly coeval with nearby volcano-sedimentary units (1.78–1.74 Ga), known as the Colider and Roosevelt groups (e.g., Santos et al., 2000).

A cratonic block has been recognized in the eastern portion of the Juruena Terrane (e.g., Rizzotto et al., 2019a), where arc-type migmatitic orthogneisses (2.05–2.03 Ga) predominate, intruded by two granitoid suites (1.99–1.93 Ga and 1.89–1.87 Ga). Crustal remnants as old as 2.80 Ga are locally present. The gneissic rocks and the oldest granitoid suite show calc-alkaline affinities of medium-K and juvenile isotopic signatures (Siderian-type T_{DM} ages), while the youngest (1.89–1.87 Ga) intrusive suite has chemical characteristics compatible with intraplate settings (e.g., Scandolara et al., 2013a; Rizzotto et al., 2019a). This framework is considered relevant to the scope of our study.

The eastern portion of the Rio Negro-Juruena province is north bounded by the Cachimbo Graben (Scandolara et al., 2017). This graben is filled by two distinct lithostratigraphic units: a lower, rift-type volcano-sedimentary sequence (< 1.74 Ga), and an upper, significantly younger sedimentary one (< 1.03 Ga). Detrital provenance study for a quartz-sandstone from the rift sequence indicated major age peaks at 1.98, 1.84 and 1.81 Ga and a relatively significant younger zircon population at ca. 1.74 Ga (Reis et al., 2013). Given the age match, this basin is roughly penecontemporaneus with the Colider and Roosevelt groups occurring to the south.

The southwestern part of the Rio Negro-Juruena province underwent a collisional process with high-grade metamorphism dated at 1.67–1.63 Ga (Tassinari et al., 1996; Santos et al., 2008) and/or 1.69–1.63 Ga (Scandolara et al., 2017), when most of the paragneisses within the Juruena Terrane formed. According to these authors, the crustal shortening involved movement from south to north and produced E-W overprint on the older rocks as well as in the Roosevelt Group. The country rocks are crosscut by plutonic rocks with ages between 1.60–1.51 Ga (Serra da Providência suite) and 1.45–1.35 Ga (Dall' Agnol et al., 1999; Payolla et al., 2002; Bettencourt et al., 2010; Scandolara et al., 2013b, 2014). In the entire province, T_{DM} ages vary from 1.5 Ga (e.g., intrusive granites) to up to 2.2 Ga (see Table 1). Therefore, some proportion of crustal and juvenile components contributed to the different magmatic arcs.

At the southern end of the Rio Negro-Juruena province, the Alto Jauru granite-greenstone terrane (see Fig. 1B) presents U−Pb zircon ages between 1.82 and 1.79 Ga and T_{DM} ages between 1.9 and 1.8 Ga with juvenile-like $\varepsilon_{Nd(t)}$ values. This terrane hosts granitoid plutons with ages between 1.59 and 1.42 Ga, produced by the accretionary-collisional magmatic arcs akin to the adjoining Rondonian-San Ignacio province. This province is a product of a Mesoproterozoic orogeny that lasted ca. 260 Myr, involving magmatic-arc convergence, ocean closure, and a continental collision of an intervening Paraguá Terrane (see Fig. 1B) against the active margin of the Rio Negro-Juruena province (e.g., Bettencourt et al., 2010; Rizzotto et al., 2014). According to Bettencourt et al. (2010), four orogenic pulses, corresponding to successive stacking of magmatic arcs, can be distinguished, namely: Cachoeirinha (1.59–1.52 Ga), Rio Alegre (1.51–1.48 Ga), Santa Helena (1.44–1.42 Ga), and Alto Central Brazil (1.35–1.33 Ga). The Rio Alegre belt, also termed Rio Alegre Terrane (Ruiz, 2005), is bounded to the west by the Paraguá Terrane and the deformed sedimentary rocks of the Aguapeí Group (1.17–1.15 Ga) that belong to the Sunsas-Aguapeí tectonic province which is the youngest of the Amazonian Craton. The arc complexes of the Rondonian-San Ignacio province yielded T_{DM} ages between 2.10 and 1.50 Ga (see Table 1), indicating that different crustal components contributed to the magma genesis over time (e.g., Geraldes et al., 2001; Rizzotto et al., 2014).

The Paraguá Terrane (Fig. 3) - or Paraguá Craton (Litherland et al., 1986) - comprises a polycyclic crust, including basement rocks as old as 1.82 Ga (Santos et al., 2008), encompassed by the Lomas Maneches granitoid suite and the Chiquitania paraderived complex. Reconnaissance scale U−Pb geochronology (zircon cores) indicated that the latter unit originated from predominantly 1.76–1.73 Ga protoliths, and was deposited after ca. 1.69–1.63 Ga, as suggested by the youngest age peak in a detrital zircon population. The emplacement of the Lomas Maneches suite occurred between 1.69 and 1.66 Ga according to the U−Pb zircon ages. Both units and the basement rocks underwent a metamorphic overprint at ca. 1.35–1.32 Ga, given by U−Pb ages in zircon rims (Boger et al., 2005; Santos et al., 2008). Available T_{DM} ages varied between 2.1 and 1.6 Ga (e.g., Santos et al., 2008 and references therein). Rb−Sr and K−Ar ages ranged between 1.40–1.25 and 1.16–0.90 Ga (Litherland et al., 1989; Teixeira et al., 1989).

Crustal-derived plutonic rocks are also present in the Paraguá Terrane, collectively known as the Pensamiento Granitoid Complex (Litherland et al., 1986; Matos et al., 2009) or Pensamiento suite (Nedel et al., 2017), yielding U−Pb zircon ages between 1.37 and 1.34 Ga and variable T_{DM} ages between 1.9 and 1.5 Ga. These rocks have been traditionally related to the San Ignacio orogeny in the Precambrian shield of Bolivia (Bettencourt et al., 2010 and references therein). Moreover, they are also included in the Alto Central Brazil orogeny of Rizzotto et al. (2014), active from 1.44 to 1.33 Ga.

The Alto Central Brazil orogeny played a major role in the consolidation of the Rondonian-San Ignacio province and is considered here as relevant for the Mesoproterozoic history of the RAT. It includes well-preserved passive-margin strata, intra-oceanic remnants, and *syn*- to late-kinematic plutonism, such as the Pensamiento intrusive suite

and coeval plutons in the Brazilian counterpart (Santos et al., 2008; Rizzotto et al., 2014; Nedel et al., 2017 and references therein). Ophiolitic remnants and associated chemically-derived assemblages with juvenile-like Nd isotopic signatures mark its early accretionary phase (1.44–1.43 Ga) (Rizzotto et al., 2013, 2014). Its collisional stage (1.35–1.33 Ga) eventually sutured the Paraguá Terrane to the Rio Negro-Juruena province, and was traditionally termed as the San Ignacio orogeny in Bolivia (e.g., Litherland et al., 1986. Medium- to high-grade metamorphism and deformation occurred in the tectonic province, as well as partial melting of pre-existing material. During the collisional stage gabbroic rocks and granites emplaced the Paraguá Terrane (Bettencourt et al., 2010 among others).

The Rondonian-San Ignacio province behaved as a tectonically stable continental mass shortly after ca. 1.30 Ga (Ruiz, 2005; Rizzotto et al., 2014 and references therein), exemplified by a platform-like cover Huanchaca sequence (see Fig. 1B) occurring in the northern portion of the Paraguá Terrane (Litherland et al., 1986). The sedimentary cover is intruded by the Huanchaca 1.11 Ga sills and the E-W trending dikes akin to the Rincón del Tigre-Huanchaca LIP of widespread occurrence in the SW portion of the Amazonian Craton (Teixeira et al., 2015, 2019a, 2019b). This province hosts a large number of significantly younger plutons in Bolivia (1.08–1.05 Ga), anorogenic-type, and the Rondônia Tin Granites in Brazil with U—Pb zircon ages between 0.99 and 0.95 Ga (Teixeira et al., 2010 and references therein). (Table 1).

The tectonic history of the Sunsas-Aguapeí province (Teixeira et al., 2010 and references therein) lasted ca. 250 Myr, and included the ~1.1 Ga Sunsas collisional-type orogeny (Litherland et al., 1989; Boger et al., 2005; Teixeira et al., 2010). From a global perspective, the Sunsas orogeny matches the Rigolet orogenic pulse of the Grenville orogeny (Laurentia), which eventually led to the formation of the Rodinia supercontinent (e.g., Tohver et al., 2006).

The passive-margin stage resumed at ~1.2 Ga ago, during which the Sunsas/Vibosi groups formed by the erosion of Paleo- to Mesoproterozoic sources, as documented by U—Pb provenance studies (Leite and Saes, 2003). For example, granitoid rocks as old as 1.92 Ga with T_{DM} ages of ca. 2.9 Ga occur in the SE edge of the Sunsas belt, bounded to the north by the San Diablo Front (Vargas-Matos et al., 2011, see Fig. 1B). The Sunsas contractional/transpressional stage produced syn- to late-orogenic granites (1105–1047 Ma), which predominate to the south of the Rio Negro Front–Santa Catalina straight zone (Litherland et al., 1986, 1989; Boger et al., 2005). The San Diablo Front, where the K—Ar ages on cataclastic rocks fall between 1000 and 870 Ma, is a major transcurrent/transpressive ductile shear zone related to the Sunsas belt rather than a suture zone between two distinct terranes (Nedel et al., 2017).

The Sunsas collision and the consequent crustal shortening generated bimodal magmatism inland under transpressive conditions in the Nova Brasilândia belt (Tohver et al., 2004), also termed Nova Brasilândia Terrane (e.g., Bettencourt et al., 2010; Teixeira et al., 2010; Tohver et al., 2006, see Fig. 1B). According to Teixeira et al. (2015), the age of this bimodal magmatism, namely the Rio Branco suite, is practically identical to the age of 1.11 Ga determined for the Rincón del Tigre-Huanchaca LIP (Fig. 1B). The Sunsas collision formed regional tectonic offshoots in the Rondonian-San Ignacio province, such as the Aguapeí fold and thrust belt and associated shear zones in the Alto Jauru Terrane (e.g., Ruiz, 2005; Bettencourt et al., 2010; Rizzotto et al., 2014 and references therein).

3. The Rio Apa Terrane

The RAT, focus of the study, locates in the state of Mato Grosso do Sul, Brazil, and northeastern Paraguay, as a structural high composed of Rhyacian/Statherian rocks (Fig. 1A, B). One small basement window with coeval rocks – the Corumbá Window -, occurs in the vicinity of the town of Corumbá, located at about 150–200 km towards north. Both domains are largely covered by recent sediments of platform-like cover sequences.

The RAT primarily comprises arc-type orthoderived rocks and metavolcanic-sedimentary sequences, overlain by Vendian/early Cambrian pelitic-carbonatic assemblages of the Paraguay belt (e.g., Boggiani and Alvarenga, 2004; Faleiros et al., 2016). These latter assemblages exhibit tectonic and metamorphic polarity that increases towards the RAT, which stands up therefore as the foreland domain for the Paraguay belt. Cordani et al. (2010) in the light of U—Pb zircon and $^{40}Ar—^{39}Ar$ dates and Sm—Nd T_{DM} ages demonstrated that the RAT formed between 1990 and 1700 Ma and comprises two terranes (Western and Eastern) with different age frames. Further studies (Redes et al., 2015; Faleiros et al., 2016; Santos et al., 2019) showed that the intrusive granitoid rocks of the Western Terrane are correlative with the Taquaral and Coimbra batholiths of the Corumbá Window, indicating that the RAT is much larger, although hidden by sediments.

Lacerda Filho (2015) carried out an important study on the RAT using systematic field mapping with geochemical and geochronological data, and later he proposed a tectonic model for the unit (Lacerda Filho et al., 2016). Faleiros et al. (2016) also conducted a relevant work on the evolution of the RAT based on systematic field mapping carried out by the Brazilian Geological Survey, CPRM, and U—Pb zircon geochronology. Recently Plens (2018) produced a detailed geochemical-isotopic study on the Eastern Terrane and documented the first zircon Lu—Hf measurements in the RAT.

Fig. 2 shows the geologic units of the RAT and its paleotectonic scenario, when the Western and Eastern terranes came together along a hypothetical suture at ca. 1.67 Ga, when a regional reset of the Rb—Sr systematics occurred on the country rocks (Cordani et al., 2010). This prominent tectonic limit is referred hereafter as the Aldeia Tomázia shear zone (Faleiros et al., 2016). It is defined as a major thrust system between the Western and Eastern Terranes, which shows a coherent low angle ductile deformation with top tectonic transport (vergence) moving to NWW. In it, the rocks display foliated arrangement with dominant mylonitic and protomylonitic textures oriented N10-20NE/10–30 SW. Lacerda Filho et al. (2016) reported U—Pb ages on monazite grains from a mylonite, with 1308 ± 39 Ma. This age is broadly equivalent to several K—Ar and $^{40}Ar—^{39}Ar$ datings (1370–1270 Ma) documented in the RAT, indicating regional metamorphic overprint and crustal exhumation. At first glance, the geochronological and field evidences correlate with the timing of the collisional phase of the Alto Central Brazil orogeny that consolidated the Rondonian-San Ignacio province (e.g., Cordani et al., 2010; Lacerda Filho et al., 2016) - see Table 1.

The Porto Murtinho banded gneiss (Cordani et al., 2010), also known as Rio Apa Complex (Lacerda-Filho et al., 2006), and hereafter termed as Porto Murtinho Complex (Faleiros et al., 2016), constitutes the basal lithostratigraphic unit of the Western Terrane. It is intruded by the Alumiador granitic batholith which is coeval with the felsic volcanic rocks of the Serra da Bocaina Formation (Fig. 2). From a tectonic point of view, such a plutonic-volcanic association is a product of the magmatic processes of the Amoguijá continental arc (e.g., Cordani et al., 2010 and references therein). The Serra da Alegria and Triunfo mafic complexes, as well as the Fazenda Matão mafic-ultramafic layered suite, are also intrusive into portions of the Porto Murtinho Complex. Scattered supracrustal sequences (mainly quartzites and schists) occupying small areas in the Western Terrane were termed as separate units (Alto Tererê, Amolar, and San Luiz) from place to place by different authors.

The Eastern Terrane comprises the widespread Caracol leucocratic gneisses (i.e., Caracol Gneiss) and the Baía das Garças granitic rocks that are tectonically ascribed to the evolution of the Caracol magmatic arc. The associated metavolcanic-sedimentary assemblage of the Alto Tererê Group overlies discontinuously most of these meta-igneous units as sinuous tectonic slices (Figs. 2 and 3). The Eastern Terrane also hosts the Morraria basement and the Paso Bravo province (Cordani et al.,

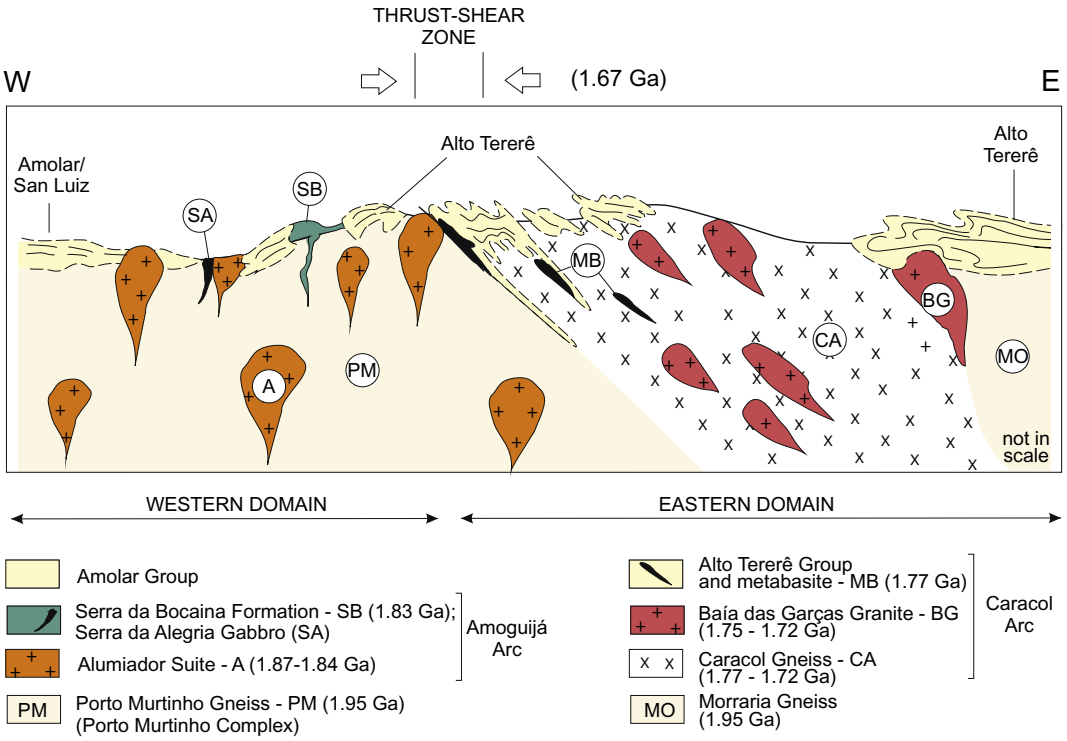

Fig. 2. Hypothetical crustal section of the Rio Apa Terrane highlighted by the major lithostratigraphic units of the Western and Eastern Terranes. The juxtaposition of both terranes along a thrust-shear zone is also shown (adapted from Cordani et al., 2010, Lacerda Filho et al., 2016; Faleiros et al., 2016).

2010 and references therein), and are made up of gneisses and migmatites.

Most RAT rocks show a complex structural framework, given by deformation with variable attitudes of the planar fabric and dip angles always to the SW (Faleiros et al., 2016). According to these authors, the supracrustal strata of the Western Terrane exhibit a dominant thin-skin structural pattern, in contrast with much of the country rocks. Brittes et al. (2013) demonstrated that the Serra da Bocaina volcanic rocks show two compressive ductile to ductile-brittle deformational phases. Whereas the younger phase was associated to local retrometamorphism developed at a shallow crustal level, the older one was related to the development of a penetrative foliation (S_1) in association with the most intense and dominant regional deformation (D_1) under greenschist facies conditions. The nearby siliciclastic sequences (e.g., Amolar, San Luiz Groups) underwent a similar deformation and metamorphism, though the primary sedimentary structures were preserved. The D_1 deformation was contemporary with the onset of a shear zone whose kinematic indicators pointed to a reverse movement with top transportation to the WNW dominated by frontal slopes of low-to-medium dipping. Plens et al. (2013) documented a similar feature along another sinuous shear zone that occurs to the east, around Serra da Esperança. Ruiz et al. (2014) showed that $^{40}Ar-^{39}Ar$ plateau ages on muscovite from the mylonites yielded 1302 ± 4 and 1295 ± 6 Ma which agree well with the previous published K–Ar and $^{40}Ar-^{39}Ar$ ages of ca. 1300 Ma interpreted to be related to a regional tectonothermal overprint.

In the Eastern Terrane, the country rocks exhibit an overall structural-metamorphic pattern that characterizes again a westward movement, though with a peculiar thick-skin low-angle thrusting (Remédio and Faleiros, 2014). Plens (2018) observed the important role of three deformational phases in the tectonic evolution of the Eastern Terrane. The earliest phase (D_1) produced the gneissic banding observed in the country rocks whereas the second (D_2) one overprinted both the basement rocks and the Caracol Gneiss. This is a well-developed penetrative foliation with subhorizontal dip angles. The youngest deformation (D_3) produced the regional low-dip penetrative foliation, which is associated with the ductile shear zones with top tectonic vergence to NWW (see Section 3).

Nearby the Aldeia Tomázia shear zone (Fig. 3) the lithologies with quite different rheological properties disclose isoclinal folding. This structure tectonically bounds lithologies formed at significantly distinct crustal levels, exemplified by the slightly deformed lower greenschist-facies metavolcanic-sedimentary rocks which are common in the Western Terrane, overlain by highly deformed amphibolite facies rocks akin to the Eastern Terrane (e.g., Cordani et al., 2010; Faleiros et al., 2016). The latter rocks have always been termed “Alto Tererê Group”, and its depositional age was estimated at 1769 ± 9 Ma using a U–Pb zircon age obtained in interlayered metabasic rocks (Lacerda Filho et al., 2016). In contrast, different names were given to those supracrustal sequences that occur across the Western Terrane (see above), which are therefore a matter of dispute.

E-W trending mafic dikes of the Rio Perdido suite crosscut all the above mentioned lithostratigraphic units of the RAT and crystallized at 1110.7 ± 1.4 Ma according to a U–Pb baddeleyite age (Teixeira et al., 2019a, 2019b). This age is identical, within error, to that of the Rincón del Tigre-Huanchaca LIP (Fig. 1B), which occurs in the SW Amazonian Craton (Teixeira et al., 2015), allowing a close tectonic relationship for the Rio Perdido suite. Table 2 shows the geochronological background of the RAT, which is considered relevant for our study.

We summarize below, in Sections 3.1–3.3, the tectonic-geologic framework of the RAT, roughly following the paleotectonic model shown in Fig. 2, but based on some new field information and U–Pb geochronological data reported by Faleiros et al. (2016), as depicted in Fig. 3.

3.1. The Western Terrane

Distinct Paleoproterozoic orogenic processes formed the Western Terrane as indicated by the geologic-geochronologic constraints. The oldest one is the Porto Murtinho Complex, which is dominantly

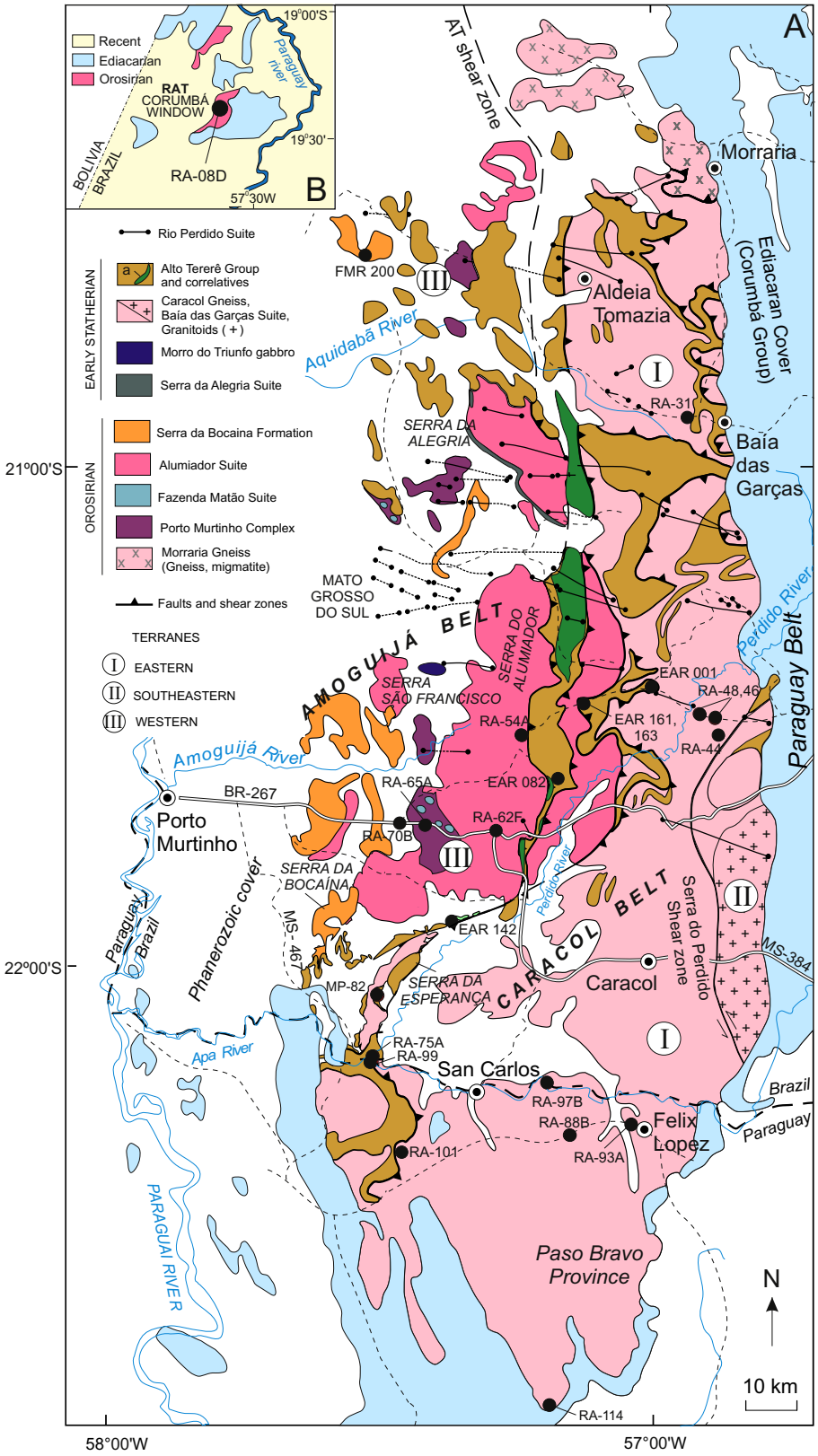

Fig. 3. A) Geologic outline of the Rio Apa Terrane – RAT (after Cordani et al., 2010; Faleiros et al., 2016 and Lacerda Filho et al., 2016). B) The Corumbá Window (granitoid rocks of the Amoguijá belt). The location of the studied samples is also shown. See text for explanation.

composed of gneisses and migmatites, aged between 2.07 and 1.96 Ga. The youngest (1.86 and 1.81 Ga) is the Amoguijá continental arc, which is mainly formed by a plutonic-volcanic association (see Table 2).

3.1.1. Porto Murtinho complex

This complex consists mainly of greenschist-facies (retro-metamorphic) migmatites and banded orthogneisses of monzogranitic, granodioritic and tonalitic composition, locally mylonitic. Amphibolites

Table 2
Geochronologic background of the Rio Apa Terrane.

Western Terrane	Significant ages zircon U-Pb; *[Sm–Nd T_{DM} ages]*	Eastern Terrane	Significant ages zircon U-P; *[Sm–Nd and Lu–Hf T_{DM} ages;]*	Southeastern Terrane	Zircon U–Pb ages
Rio Perdido suite (mafic dikes): Amolar, San Luiz and/or Alto Tererê Groups	1110.7 ± 1.4 Ma (ih-zr > 1.59 Ga) Maximum depositional age (siliciclastic rocks): 1.74–1.78 Ga *[2.0–2.3 Ga]* K–Ar age: 1280 Ma	Rio Perdido suite Alto Tererê Group	1768 ± 6 Ma (amphibolite) *[1.9, 2.2–2.3, 2.7–2.9 Ga]* Maximum deposition ages (siliciclastic rocks): 1.70–1.77 Ga. *[1.9–2.0 Ga]* Metamorphic overprint (mo; U–Pb): 1308 ± 39 Ma; K–Ar ages: 1370; 1300–1267 Ma Mylonites; ^{40}Ar–^{39}Ar ages: 1302–1295 Ma	Rio Perdido suite	
Extension-type intrusions	~1790 Ma Serra da Alegria suite *[2.5–2.6 Ga];* 1811 ± 7 Ma Aquidabã Granite *[2.3–2.6 Ga].*	Baía das Garças Granite; Cerro Porã Granite*	1719 ± 11 to 1754 ± 42 Ma; 1749 ± 49 Ma* *[2.0–2.1 Ga]* (U–Pb isotopic reset: 1440–1230 Ma) K–Ar ages: 1342–1315 Ma	Post-orogenic granite	1791 ± 19 Ma
Rio Naitaca Formation (?)	1813 ± 18 Ma (basal meta-andesite)	Caracol Gneiss# and coeval volcanics	1781 ± 7 to 1748 ± 19 Ma; 1721 ± 25 Ma *[1.8–2.2 Ga][1.9–2.3 Ga#]* ^{40}Ar–^{39}Ar ages: 1310–1270 Ma. Local isotopic reset (^{40}Ar–^{39}Ar): 1130 Ma		
Serra da Bocaina Formation (Amoguijá arc)	1831 ± 12; *[2.1–2.4 Ga]*	Basement (Orthogneiss)	1822 ± 6 Ma *[2.0 Ga]*	Augen gneiss	1822 ± 18 Ma
Alumiador suite, São Francisco** and Santa Otília Granites (Amoguijá arc)	1841 ± 15 to 1830 ± 12; 1878 ± 7 Ma** *[2.2; 2.5–2.6 Ga]*				
Extension-type activity	1902 ± 12 Ma (Chatelodo), 1878 ± 7 Ma (S.Francisco); 1878 ± 9, 1899 ± 9 Ma (Rhyolites) 1946 ± 6 Ma (Fazenda Matão)	Paso Bravo Province (Granitoid crust)	*[2.2–2.4 Ga]*		
Porto Murtinho Complex (Orthogneiss and Migmatite)	2074 ± 7 to 1989 ± 11 1947 ± 9 to 1941 ± 13; Ma (ih-zr: 2.05 to 3.44 Ga) *[2.4–2.6; 3.1 Ga]*	Morraria Gneiss	1950 ± 23 Ma ^{40}Ar–^{39}Ar ages: 1308–1292 Ma	Basement rocks	–

Note: U–Pb ages: zr (zircon), ih-zr (inherited zircon), mo (monazite). Data compilation from Ruiz (2005), Plens et al. (2013), Redes et al. (2015), Lacerda Filho (2015), Ruiz et al. (2014); Cabrera (2015), Brittes et al. (2016), Lacerda Filho et al. (2016), Faleiros et al. (2016), Cordani et al. (2010). See text for details.
U–Pb dates: zr (zircon); ih-zr (inherited zircons), mo (monazite). Regional cooling ages are mostly on biotite (K–Ar and ^{40}Ar–^{39}Ar dating). The U–Pb, K–Ar and Ar/Ar ages are in million years (Ma). Sm–Nd T_{DM} (one-stage) ages are in Giga years (Ga). The Caracol (Eastern Terrane) disclose zircon Hf T_{DM} ages between 2.3 and 1.9 Ga (Plens, 2018). The Western and Eastern Terranes document a regional isotopic reset of the Rb–Sr systematics at 1.67 Ga (Cordani et al., 2010). Data compiled from Cordani et al. (2010), Plens et al. (2013); Cabrera (2015) Faleiros et al. (2016), Lacerda Filho et al. (2016), Plens (2018). See text for explanation. The symbols *, ** and # were used for linking the name of a given rocks with its data.

are subordinate (e.g., Lacerda-Filho et al., 2006; Lacerda Filho et al., 2016; Cordani et al., 2010). These rocks are scattered across the Western Terrane and are largely hidden by an extensive Phanerozoic cover, as depicted in Fig. 3.

U–Pb zircon crystallization ages ranged from 2074 ± 7 to 1941 ± 13 Ma (Lacerda Filho, 2015; Cordani et al., 2010; Faleiros et al., 2016). The last authors carried out a systematic U–Pb geochronological survey of the RAT and documented isotopic evidence of partial melting in the Córrego Jibóia high-grade orthogneiss, highlighted by inherited zircon cores dated at 1989 ± 11 Ma while the magmatic crystallization occurred at 1947 ± 9 Ma (zircon rims). In a similar manner, the intrusive relationships between the Fazenda Matão suite (1946 ± 6 Ma; Costa, 2017) and a migmatitic gneiss provides additional indirect information of high-grade metamorphism and partial melting some time before the emplacement of this suite. In other words, crustal shortening and thickening of the Porto Murtinho Complex has occurred during the Orosirian. The available T_{DM} ages (2.1–3.1 Ga) suggest that the Porto Murtinho rocks may have evolved in an active continental margin, which is consistent with their subduction-related calc-alkaline signature (e.g., Faleiros et al., 2016 and references therein). Noteworthy, the same authors also reported a Concordia plot for a gray orthogneiss (retrometamorphic) with a nearly continuous spread of inherited zircon ages between 1.90 and 1.95 Ga and 3.20 Ga. The youngest grains indicated the maximum depositional age of this particular rock, whereas the morphology of most zircon grains suggested the role of sedimentary protoliths in an anatectic magma genesis. In a similar manner, Lacerda Filho (2015) documented inherited zircon grains with $^{207}Pb/^{206}$ Pb ages between 2.05 and 3.42 Ga in a banded gneiss, where most analytical points defined a lower intercept age of 1985 ± 20 Ma. This rock probably underwent a later overprint, as indicated by some zircon grains dated at 1880 ± 37 Ma.

Finally, the Porto Murtinho Complex also hosts a gabbroic intrusion (1969 ± 5 Ma) and the Serra da Alegria gabbro-anorthosite suite (1791 Ma), which yielded T_{DM} ages between 2.6 and 2.4 Ga (Nogueira et al., 2013; Lacerda Filho, 2015; Lacerda Filho et al., 2016), as well as the Morro do Triunfo Gabbro (e.g., Cordani et al., 2010 and references therein). Moreover, the crystalline basement is cut by various granitic intrusions, of which the Alumiador batholith is the largest. Other plutons include the Chatelodo granite (1902 ± 12 Ma; Faleiros et al., 2016) and the São Francisco Granite (1878 ± 7 Ma), with dikes locally intruding volcanic rocks, dated at 1899 ± 9 Ma (Souza et al., 2016). The significantly younger Aquidabã Granite (1811 ± 7 Ma) yielded T_{DM} ages between 2.6 and 2.3 Ga (Nogueira et al., 2013), indicating crustal derivation (see Table 3).

3.1.2. Amoguijá continental belt

The Amoguijá belt comprises the voluminous granitic rocks of the Alumiador suite and the associated felsic volcanic rocks of the Serra da Bocaina Formation. The Alumiador suite is predominantly composed of hornblende-biotite gneisses with monzogranitic composition. They usually show high-K calc-alkaline signature akin to orogenic settings (Lacerda-Filho et al., 2006; Manzano et al., 2012). However, some of the granitic rock types of the Alumiador suite have alkaline signatures typical of post-orogenic or anorogenic settings (Manzano et al., 2012; Godoy et al., 2014). As such, a complex magmatic history for the Alumiador suite is probable. The U–Pb zircon crystallization ages varied from 1841 ± 15 Ma to 1839 ± 33 Ma (see Table 2). The variable T_{DM} ages (2.6–2.2 Ga) and the negative $\varepsilon_{Nd(t)}$ values (−5.91 to −0.68) indicate that distinct crustal components participated in the precursor magmas. From a geodynamic point of view, the Amoguijá magmatic arcs evolved in a continental margin setting, where the Santa Otília Granite (1830 ± 12 Ma) and the Córrego do Cervo Granite (1841 ± 15 Ma) also developed, given the similarities in age (e.g., Faleiros et al., 2016 and references therein).

The associated Serra da Bocaina Formation crops out discontinuously in the central and southern portions of the Western Terrane. This lithostratigraphic unit includes pyroclastic and felsic volcanic assemblages with medium- to high-K calc-alkaline and peraluminous geochemical signature, typical of volcanic arc settings (Araújo et al., 1982; Godoy et al., 2010; Brittes et al., 2013; Faleiros et al., 2016). The rocks show low-grade metamorphism, but have a well-developed penetrative foliation and mylonitic textures near the regional Aldeia Tomázia shear zone (Figs. 2 and 3). This zone also formed reverse/thrust slices of the Alumiador plutonic rocks towards NNW (Brittes et al., 2013). A rhyolite sample from the Serra da Bocaina Formation yielded a U–Pb zircon SHRIMP age of 1831 ± 12 Ma, interpreted as genetically linked to the Amoguijá magmatic arc (Brittes et al., 2016). The volcanic rocks yielded T_{DM} ages mostly between 2.1 and 2.4 Ga, and variable negative $\varepsilon_{Nd(t)}$ values (Lacerda-Filho et al., 2006; Brittes et al., 2013). According to these authors, these data suggest that the parental magmas of the Serra da Bocaina Formation derived in a continental arc setting, in agreement with the documented geochemical affinity. Finally, volcanic rocks very similar to the Serra da Bocaina assemblage yielded two additional U–Pb zircon ages that are significantly older (1878 ± 9 and 1899 ± 9 Ma; see Table 2), suggesting that not all volcanic rocks in the Western Terrane belong to the Amoguijá tectonic framework.

3.1.3. Supracrustal sequences

The supracrustal associations across the Western Terrane have been

Table 3
GPS location of the study samples with the respective age methods applied in this study.

Sample	Coordinates	Interpreted geologic unit	Terrane/ Province	Age method
RA-65A	21°44′36″ 57°26′54″	Porto Murtinho	Western	SHRIMP
RA-54A	21°34′52″ 57°12′46″	Alumiador	Western	SHRIMP
RA - 62F	22°39′60″ 57°19′25″	Alumiador	Western	SHRIMP
RA-08D	19°19′21″ 58°38′56″	Granitoid	Corumbá Window	SHRIMP
FMR-200	20°43′40″ 57°18′33″	Serra da Bocaina	Western	SHRIMP
EAR- 082	21°38′13″ 57°09′54″	Alto Tererê	Western	LA-ICPMS
RA - 44	21°35′22″ 56°50′07″	Caracol	Eastern	SHRIMP
RA - 46	21°33′40″ 56°49′40″	Caracol	Eastern	SHRIMP
RA - 48	21°32′47″ 56°54′32″	Caracol	Eastern	SHRIMP
RA-101	22°24′04″ 57°27′52″	Caracol	Eastern	SHRIMP
RA - 31	21°02′40″ 57°03′15″	Baía das Garças	Eastern	SHRIMP
RA-88B	22°17′07″ 57°07′27″	Caracol	Paso Bravo	SHRIMP
RA-97A	22°13′46″ 57°12′35″	Caracol	Paso Bravo	SHRIMP
RA-93A	22°21′13″ 56°57′59″	Caracol	Paso Bravo	SHRIMP
RA-114	22°41′36″ 57°13′32″	Caracol	Paso Bravo	SHRIMP
EAR- 001	21°29′50″ 57°00′36″	Alto Tererê	Eastern	LA-ICPMS
EAR- 142	21°53′49″ 57°19′35″	Alto Tererê	Eastern	LA-ICPMS
MP-82	22°05′28″ 57°28′32″	Alto Tererê	Eastern	LA-ICPMS
EAR-161	21°29′49″ 57°07′08″	Alto Tererê	Eastern	LA-ICPMS
EAR-163	21°30′04″ 57°08′18″	Alto Tererê	Eastern	LA-ICPMS
RA-75A/RA-99	22°10′18″ 57°31′06″	Alto Tererê	Eastern	LA-ICPMS

the focus of several studies, including unpublished Doctoral theses showing that they have contrasting metamorphic, structural and stratigraphic characteristics. For instance, Cabrera (2015) conducted detailed stratigraphic studies on most of the occurrences, including provenance studies in two samples: a metasandstone collected in the Serra da Alegria region and a massive quartzite occurring nearby the Serra da Esperança (see Fig. 3). These samples though using a few tens of U—Pb zircon analyses, yielded similar maximum depositional ages of ca. 1800 Ma. However, analogous provenance studies, conducted in the nearby siliciclastic rocks attributed to the Amolar Group (Lacerda Filho, 2015), defined relatively younger maximum ages in the detrital population at ca. 1710–1750 Ma. The coupled Sm—Nd T_{DM} crustal residence ages on these rocks gave negative to slightly positive $\varepsilon_{Nd(t)}$ values (see Table 2), implying that the original material derived from eroded Rhyacian to early Orosirian crust. An additional $^{40}Ar—^{39}Ar$ age in a quartz-muscovite schist collected close to the Serra da Esperança gave a plateau age of 1287 ± 5 Ma, as depicted in Table 2 (Cabrera, 2015). This indicates that the region underwent a much younger regional thermal overprint, as previously proposed by Cordani et al. (2010) on the basis of K—Ar and $^{40}Ar—^{39}Ar$ ages in the country rocks of the RAT.

Faleiros et al. (2016) coined the name "Rio Naitaca Formation" for one particularly immature sedimentary assemblage with minor interlayered volcanic and pyroclastic rocks in the NW portion of the Western Terrane (see Fig. 3). Previously, this package had been interpreted as the low metamorphic equivalent of the Alto Tererê Formation (e.g., Cordani et al., 2010). The Rio Naitaca Formation consists of quartzite, metasandstone, meta-arkose, metagraywacke, metaconglomerate and phyllite that underwent metamorphism under chlorite-grade conditions. In particular, the basal metasandstone includes centimetric-to-metric layers of meta-andesite, meta-dacite and meta-rhyolite, as well as pyroclastic rocks (Faleiros et al., 2016). These authors reported a U—Pb zircon SHRIMP Concordia age of 1813 ± 18 Ma for the basal andesitic lapilli tuff, constraining the timing of sedimentation for their Rio Naitaca Formation. This age roughly matches the maximum depositional ages of two siliciclastic samples (Cabrera, 2015), as well as to the crystallization age of the Serra da Bocaina rhyolite (Brittes et al., 2016). Four remaining zircon dates from the pyroclastic rock yielded concordant U—Pb ages between 1918 ± 11 and 2003 ± 11 Ma, interpreted as detrital inputs (Faleiros et al., 2016).

3.2. The Eastern Terrane

This terrane comprises distinct gneissic, migmatitic and granitoid rocks, making up the Morraria and the widespread Caracol gneisses, as well as the Baía das Garças granitic suite (Cordani et al., 2010), which is intrusive into the Morraria gneisses, as well as the Paso Bravo Province in Paraguay (Wiens, 1986). The entire terrane is partially overlain by the highly deformed and metamorphosed metavolcanic-sedimentary rocks of the Alto Tererê Group, as outlined in Fig. 3.

3.2.1. Morraria and Paso Bravo gneisses and migmatites

The Morraria Gneiss crops out as a basement window in the northernmost part of the Eastern Terrane, overlain by the Quaternary sediments of the Pantanal Formation (see Fig. 3). It comprises medium- to high-grade banded gneisses with amphibolite intercalations and migmatitic rocks with calc-alkaline signature (Faleiros et al., 2016). One strongly foliated orthogneiss yielded a U—Pb zircon SHRIMP age of 1935 ± 15 Ma (Cordani et al., 2010). The $^{40}Ar—^{39}Ar$ muscovite and biotite plateau ages for the Morraria Gneiss range between 1283 and 1265 Ma, whereas a K—Ar hornblende age was 1374 Ma (see Table 2).

Similarly to the Morraria Gneiss, the Paso Bravo Province (see Fig. 3) comprises medium-grade metamorphic tonalitic gneisses and migmatites. Strongly foliated granite gneisses are exposed in the western portion of this province (Wiens, 1986). No meaningful U—Pb ages are available for these rocks due to the difficulties of the isotopic systematic, such as the high U contents producing metamict zircon grains (Cordani et al., 2010). Two T_{DM} ages of 2.4 and 2.2 Ga were obtained from the rocks (see Table 2), indicating that they derived from short-lived protoliths, as exemplified by the $\varepsilon_{Nd(t)}$ values of −0.50 and −1.13, respectively. The available $^{40}Ar—^{39}Ar$ plateau ages (amphibole and biotite) from some gneissic and granitoid rocks varied from 1308 to 1292 Ma (Cordani et al., 2010), suggesting that this portion of the RAT underwent a tectonothermal event in the Ectasian.

3.2.2. Caracol Gneiss and Baía das Garças suite

The Caracol Gneiss, also named Caracol suite, consists mainly of polydeformed, amphibolite-facies leucocratic orthogneisses of granitic composition, showing K-high calc-alkaline and/or A-type, alkaline signatures (Cordani et al., 2010; Faleiros et al., 2016; Plens, 2018). The last author documented some subordinate effusive rocks in the Eastern Domain. U—Pb zircon crystallization ages for the Caracol gneisses ranged from 1783 ± 18 to 1721 ± 25 Ma, with most results forming a cluster at 1770–1760 Ma (Table 2).

The available T_{DM} ages for the Caracol Gneiss gave values from 1.8 to 2.2 Ga with mostly positive $\varepsilon_{Nd(t)}$ values between 3.2 and 0.7 (Cordani et al., 2010; Lacerda Filho, 2015; Plens, 2018). This latter author also reported the first zircon Lu—Hf data carried out on distinct lithological facies of the Caracol Gneiss which gave Hf-T_{DM} model ages between 1.9 and 2.3 Ga and variable positive and negative $\varepsilon_{Hf(t)}$ values. The Eastern Terrane also contains slightly older orthogneisses (tonalitic to monzogranitic in composition), as indicated by a U—Pb zircon crystallization age of 1822 ± 6 Ma, with a coupled slightly positive $\varepsilon_{Nd(t)}$ value and T_{DM} age of 2.0 Ga (Plens, 2018). Several $^{40}Ar—^{39}Ar$ biotite ages were also reported for the Eastern Terrane, mostly ranging between 1342 and 1270 Ma, similar to those of the Paso Bravo rocks (Cordani et al., 2010).

The Baía das Garças suite, consisting mostly of high-K calc-alkaline granites, is intrusive into the metavolcanic-sedimentary rocks of the Alto Tererê Group and crops out in the northern portion of the Eastern Terrane (see Figs. 2 and 3). The published U—Pb zircon ages ranged from 1719 ± 11 Ma to 1754 ± 42 Ma (Cordani et al., 2010; Faleiros et al., 2016). The documented T_{DM} ages ranged from 2.0 to 2.1 Ga, and are similar to those of the Caracol Gneiss (see Table 2), but showing a larger range in the $\varepsilon_{Nd(t)}$ values (−5.2 to +2.0). Finally, the A-type Cerro Porã Granite, located in the SW portion of the Eastern Terrane, yielded a U—Pb zircon age of 1749 ± 45 Ma (Plens et al., 2013). Therefore, this pluton is roughly coeval with both the Caracol Gneiss and Baía das Garças suite. This granite yielded one $^{40}Ar—^{39}Ar$ muscovite age of 1280 ± 9 Ma (see Table 2).

3.2.3. The Alto Tererê Group

According to Lacerda Filho et al. (2016), the Alto Tererê Group is mainly composed of garnet-muscovite-quartz, muscovite-quartz, and biotite-quartz schists, and feldspathic quartzites. Kyanite-staurolite schists with interlayered amphibolite, epidote-chlorite-actinolite schists, and amphibole schists are subordinate. An amphibolitic layer crops out as discontinuous slices tectonically interspersed within the basal metasedimentary strata (see Figs. 2 and 3). The amphibolitic body crystallized at 1768 ± 6 Ma (U—Pb zircon age), constraining the age of the Alto Tererê Group (Table 2). Xenocrysts from that amphibolite yielded three age groups (1973 ± 36, 1983 ± 7 and 2032 ± 19 Ma), suggesting derivation from Orosirian sources (Lacerda Filho et al., 2016). In a similar manner, the coupled $\varepsilon_{Nd(t)}$ values ranging mainly from +3.7 to −3.4 are consistent with short-lived mafic protoliths for the amphibolite rocks, formed essentially by juvenile material. From a petrogenetic point of view, rock shows transitional characteristics between MORB-type and island arc basalt chemical signatures, typical of tholeiitic basalts of back-arc settings, possibly associated to a continental arc setting (e.g., Lacerda Filho et al., 2016; Faleiros et al., 2016). Additional U—Pb provenance studies on two samples of garnet-muscovite schists with interlayered quartzite bands yielded maximum sedimentation ages between 1700 and 1730 Ma (Lacerda Filho et al.,

2016). In addition, Plens (2018) reported roughly similar ages for the youngest detrital population in a sillimanite-quartz schist. The available slightly positive $\varepsilon_{Nd(t)}$ values and the early Orosirian T_{DM} crustal residence ages suggested that the original sediments probably derived from crustal sources such as the basement rocks of the Eastern and Western terranes (see Table 2). One sample of a kyanite-garnet-biotite-muscovite schist yielded a U–Pb monazite Concordia age of 1308 ± 39 Ma, which was interpreted as the age of a metamorphic overprint (Lacerda Filho et al., 2016). This age agrees well with the documented K–Ar and $^{40}Ar–^{39}Ar$ mica ages of the basement rocks and Alto Tererê amphibolite, with ca. 1300 Ma (Table 2).

Finally, the rocks of the Alto Tererê Group in the Eastern Terrane (see Fig. 3) are dominated by Barrovian-type metamorphism, varying from upper greenschist to middle amphibolite facies. The metamorphic variation is consistent with the observed west verging of the stacked nappes in the Eastern Terrane, carrying the Alto Tererê rocks, the Caracol Gneiss and/or the Alumiador batholith, as observed along the boundary between the Eastern and Western Terranes (e.g., Faleiros et al., 2016; Lacerda Filho et al., 2016; Cabrera, 2015).

3.3. The Southeastern Terrane

Faleiros et al. (2016) suggested that the Southeastern Terrane could be a third tectonic compartment of the RAT. It is essentially composed of calc-alkaline mylonitic banded gneiss, augen gneisses and deformed leucogranites, intruded by alkaline monzogranitic rocks. The metaigneous rocks of the Southeastern Terrane show broadly similar deformation and metamorphic characteristics to the adjoining Caracol Gneiss, though limited by the Serra do Perdido dextral strike-slip shear zone which is regionally an uncommon feature over the RAT (Remédio and Faleiros, 2014; Faleiros et al., 2016). In a similar manner with the Eastern Terrane, relics of the Alto Tererê Group overlie in places the country rocks of the Southeastern Terrane, as depicted in Fig. 3. This terrane was the focus of very limited U–Pb zircon geochronological work and no Sm–Nd data are available about its rocks. One monzogranite intrusion gave a UPb zircon age of 1791 ± 19 Ma whereas one augen gneiss yielded a UPb zircon age U–Pb zircon age of 1820 ± 18 Ma (Faleiros et al., 2016). This latter age is very similar to that reported for an orthogneiss occurring in the Eastern Terrane (see Section 3.2.2 and Table 2).

4. Methodology

U–Pb measurements were made on zircon crystals extracted from rock samples by conventional methods (crushing, sieving and heavy liquid separation), cast in epoxy mounts, and polished. Zircon populations were photographed in reflected light and imaged using cathodoluminescence (CL) to reveal their internal structure. The spots considered more adequate for the isotopic analysis were selected. The dating was carried out using a Sensitive High-mass Resolution Ion MicroProbe (SHRIMP-II) and the Thermo-Fisher Neptune laser-ablation (LA) multi-collector inductively coupled plasma mass spectrometer (ICP-MS) at the Geochronological Research Center of the University of São Paulo (CPGeo-USP), Brazil. Table 3 shows the coordinates of the selected samples and the selection strategy used in our geochronological study. Table 4 and the Supplementary Material include the U–Pb analytical data acquired by the SHRIMP and LA-ICP-MS instruments.

The SHRIMP-II analysis was carried out on metaigneous rocks. The analytical procedures, acquisition, and data processing were reported by Sato et al. (2014). Zircon populations were mounted on adhesive tapes, cast in epoxy resin, and polished together with the TEMORA-2 zircon standard ($^{206}Pb/^{238}U$ age = 416.78 ± 0.33 Ma; Black et al., 2003). U abundance and U/Pb values were calibrated against the Sri Lanka SL13 (238 ppm) and the Temora 2 zircon standards, respectively. The individual SHRIMP ages were determined from five successive scans of the mass spectrum, and the average ages reported in the text are weighted–mean $^{207}Pb/^{206}Pb$ ages with 95% confidence interval. Correction for common Pb was made based on the measured ^{204}Pb, and the typical error component for the $^{206}Pb/^{238}U$ ratios is lesser than 2%. Data were reduced using SQUID 1.06 software, and Concordia age calculations were performed using the ISOPLOT 4 (Ludwig, 2009a, Ludwig, 2009b). Data-point error ellipses in the Concordia diagrams are at the 68.3% confidence level (1 sigma) and the analytical uncertainties of the isotopic ratios are reported at the 1-sigma level.

From selected siliciclastic rocks a large split of detrital zircon grains with all available shapes and sizes was recovered. U–Pb zircon geochronology was carried out using the LA-ICP-MS with a 193 μm ArF Excimer laser ablation system operating at 6 Hz and 5 mJ to produce a spot size of 39 μm (Sato et al., 2010) in order to acquire the U, Th and Pb isotopic data. Corrections for laser-induced elemental fractionation of the $^{206}Pb/^{238}U$ ratio and instrumental discrimination were calibrated against the GJ-1 zircon standard (U–Pb mean age of 601 ± 3.5 Ma; Elholou et al., 2006). The analytical data are divided into groups of 2–7 spreadsheets per site, and each spreadsheet was organized as follows: two blanks, three GJ-1 standard, 13 unknown zircon spots, two GJ-1 standards, and two blanks. For each blank, standard, and unknown, a series of 50 sequential readings (laser shots) was taken, covering all isotopes of interest. Using a hybrid software that combines the Python programming language and the R statistical/plotting package (Siqueira et al., 2014), the ^{204}Pb values were then corrected for ^{204}Hg interference (assuming a $^{202}Hg/^{204}Hg = 4.355$); the blank and common Pb (Stacey and Kramers, 1975) corrections were applied, and finally the $^{206}Pb^*/^{238}U$, $^{207}Pb^*/^{235}U$, Th/U and $^{206}Pb^*/^{207}Pb^*$ ratios (and their respective one-sigma errors) were calculated, preserving the full internal variability of each ratio in order to compute the correlation values. This software includes tools for removal of automatic outliers, fractioning compensation, and immediate visualization of all corrections, as well as an output fully compatible with ISOPLOT/Ex®3.00 software (Ludwig, 2003). Only isotopic data with total common Pb contents below 6% and concordance of 100 ± 10 were used for age calculations shown in the Concordia diagrams and combined probability density plots.

5. Results

New U–Pb zircon SHRIMP ages were determined for 13 granitoid rocks from the main tectonic units of the Western and Eastern Terranes: Porto Murtinho (RA-65A), Alumiador (RA-54A and RA-62F), Caracol (RA-44, RA-46, RA-48), Baía das Garças (RA-31) and Paso Bravo (RA-88B, RA-93A, RA-97B, RA-101 and RA-114, including one metavolcanic sample (RA-70B) from the Serra da Bocaina Formation. An additional age was carried out on a granitoid sample of the Corumbá Window (RA-08D).

Moreover, new U–Pb LA-ICP-MS detrital zircon analyses were performed on eight siliciclastic samples. For the sake of simplicity and because of the lack of systematic U–Pb provenance studies on these rocks at the regional scale, we use, in this study, the name “Alto Tererê Group” for all them, as supracrustal relicts of the RAT (see Section 3.1.3), no matter if they belong to different units in the Western or Eastern terranes. Fig. 3 shows the geographic distribution of the studied samples. One of them (FMR-200) was collected in the northern part of the area, four of them in the southern part (EAR-142, MP-82, RA-75A, RAT-99) and the others in the central part of the RAT (EAR-001, EAR-163, EAR- 161).

5.1. Western Terrane and Corumbá Window

For this region, six U–Pb zircon SHRIMP and five 5 LA-ICP-MS analyses were performed. One of the SHRIMP measurements was carried out on one metabasalt (FMR-200), which is supposed to be from the Rio Naitaca Formation, given the geographic distribution (see Table 3). On the LA-ICP-MS detrital zircon analyses for the provenance

Table 4
U–Pb SHRIMP analytical data for the studied metaigneous samples.

Sample Spot number	Ratios						err corr	% Com ^{206}Pb	Age (Ma)				Disc %	ppm		Th/U
	$^{207}Pb/^{235}U$	err %	$^{206}Pb/^{238}U$	err %	$^{207}Pb/^{206}Pb$	err %			$^{206}Pb/^{238}U$	1σ	$^{207}Pb/^{206}Pb$	1σ		U	Th	
Western Terrane and Corumbá window																
Porto Murtinho Complex																
RA-65A – Biotite Migmatitic Gneiss																
RA-65A-1.1	5.6223	1.3	0.3196	0.7	0.1276	1.1	0.527	0.73	1788	11	2065	20	15	242	194	0.83
RA-65A-2.1	7.4237	1.0	0.3927	0.7	0.1371	0.6	0.744	0.38	2135	13	2191	11	3	185	103	0.57
RA-65A-3.1	6.5338	1.3	0.3744	0.9	0.1266	1.0	0.643	0.44	2050	15	2051	18	0	92	60	0.67
RA-65A-4.1	6.0741	1.5	0.3423	0.7	0.1287	1.3	0.447	1.11	1897	11	2081	23	10	367	128	0.36
RA-65A-5.1	6.6582	1.0	0.3777	0.8	0.1278	0.6	0.794	0.05	2066	14	2069	11	0	109	68	0.64
RA-65A-6.1	6.6436	0.9	0.3764	0.7	0.1280	0.6	0.776	0.18	2059	13	2071	10	1	154	116	0.78
RA-65A-7.1	7.0644	1.0	0.3816	0.7	0.1343	0.6	0.749	0.31	2084	13	2154	11	3	175	98	0.58
RA-65A-8.1	7.0085	1.1	0.3861	0.8	0.1316	0.7	0.750	0.17	2105	14	2120	12	1	101	41	0.42
RA-65A-9.1	7.2971	0.8	0.4002	0.7	0.1322	0.4	0.872	0.00	2170	13	2128	7	−2	184	74	0.41
RA-65A-10.1	6.1916	1.3	0.3506	0.9	0.1281	1.0	0.648	0.53	1937	14	2072	18	7	168	114	0.70
RA-65A-11.1	6.7753	1.0	0.3840	0.8	0.1280	0.6	0.806	−0.06	2095	14	2070	10	−1	100	68	0.70
RA-65A-12.1	6.7001	0.8	0.3794	0.7	0.1281	0.4	0.860	0.13	2074	12	2072	7	0	303	159	0.54
Alumiador Suite																
RAPA-54A – Granitic Orthogneiss																
RAPA-54-1.1	5.6051	2.0	0.3486	1.6	0.1166	1.1	0.852	−0.16	1928	27	1905	20	−1	87	98	1.17
RAPA-54-2.1	4.7917	1.7	0.3255	1.6	0.1068	0.4	0.779	0.07	1816	26	1745	7	−4	1465	1612	1.14
RAPA-54-3.1	4.9971	2.1	0.3268	1.5	0.1109	1.4	0.778	0.52	1823	24	1814	26	0	350	285	0.84
RAPA-54-3.2	4.3369	7.2	0.2964	1.7	0.1061	7.0	0.273	4.38	1674	25	1734	128	4	170	92	0.56
RAPA-54-4.1	5.0250	2.0	0.3280	1.8	0.1111	0.8	0.903	0.00	1829	29	1818	15	−1	132	118	0.93
RAPA-54-5.1	4.9614	2.8	0.3204	1.6	0.1123	2.3	0.754	1.07	1792	25	1837	42	3	100	94	0.97
RAPA-54-6.1	7.0142	5.7	0.3908	1.8	0.1302	5.4	0.175	4.00	2126	32	2100	95	−1	86	59	0.71
RAPA-54-7.1	5.1167	4.4	0.3293	1.7	0.1127	4.1	0.523	2.43	1835	27	1843	74	0	85	62	0.75
RAPA-54-8.1	4.9830	2.4	0.3230	1.6	0.1119	1.7	0.838	0.39	1805	26	1830	32	1	92	57	0.65
RAPA-54-9.1	4.9269	1.9	0.3225	1.7	0.1108	0.9	0.928	0.15	1802	26	1813	15	1	199	180	0.94
RAPA-54-10.1	5.2895	14.5	0.2917	2.5	0.1315	14.3	0.141	11.53	1650	37	2118	251	28	109	97	0.92
RAPA-54-11.1	5.0693	17.8	0.3135	2.3	0.1173	17.6	0.126	11.69	1758	35	1915	316	9	144	113	0.81
RAPA-54-12.1	1.5499	10.9	0.0982	1.8	0.1145	10.7	0.091	8.31	604	10	1871	193	210	323	239	0.76
RA-62F – Monzogranite																
RA-62F.1.1	5.1990	2.0	0.3308	1.7	0.1140	1.1	0.840	0.19	1842	27	1864	20	1	201	296	1.52
RA-62F.2.1	3.4737	6.1	0.2192	1.8	0.1149	5.9	0.292	4.75	1278	21	1879	106	47	242	154	0.66
RA-62F.3.1	5.1656	2.5	0.3362	1.7	0.1114	1.9	0.680	0.27	1868	28	1823	34	−2	145	108	0.77
RA-62F.4.1	5.1016	2.5	0.3255	1.7	0.1137	1.8	0.691	0.61	1817	28	1859	33	2	125	134	1.10
RA-62F-5.1	5.2065	2.3	0.3354	1.7	0.1126	1.5	0.745	0.80	1865	28	1841	28	−1	138	110	0.83
RA-62F-6.1	4.9207	2.4	0.3127	1.8	0.1141	1.7	0.730	0.62	1754	27	1866	30	6	98	151	1.59
RA-62F-7.1	5.1947	1.9	0.3269	1.7	0.1152	0.8	0.901	0.15	1823	27	1884	15	3	186	221	1.22
RA-62F-8.1	4.2374	3.0	0.2706	1.7	0.1136	2.5	0.559	1.66	1544	23	1857	45	20	279	257	0.95
RA-62F-9.1	5.2151	2.0	0.3300	1.7	0.1146	1.0	0.875	0.16	1838	27	1874	17	2	128	95	0.77
RA-62F-10.1	4.5219	1.9	0.2884	1.6	0.1137	0.9	0.879	0.57	1634	24	1859	16	14	436	590	1.40
RA-62F-11.1	5.1729	1.9	0.3326	1.7	0.1128	0.7	0.916	0.09	1851	27	1845	14	0	139	182	1.36
RA-62F-12.1	2.0084	4.7	0.1686	1.8	0.0864	4.4	0.379	2.89	1005	17	1347	84	34	1238	1316	1.10
RA-62F-13.1	5.2359	2.8	0.3439	1.7	0.1104	2.2	0.613	1.35	1905	28	1806	40	−5	202	233	1.19
RA-70B – Volcaniclastic rock																
RA-70B-1.1	5.3083	1.0	0.3349	0.8	0.1150	0.6	0.769	0.11	1862	13	1879	12	1	98	99	1.04
RA-70B-2.1	5.4362	1.4	0.3408	0.9	0.1157	1.0	0.642	0.24	1891	14	1890	19	0	68	96	1.47
RA-70B-3.1	5.3162	1.0	0.3355	0.8	0.1149	0.7	0.735	0.11	1865	12	1879	13	1	104	176	1.75
RA-70B-4.1	5.2554	1.0	0.3362	0.7	0.1134	0.7	0.734	0.18	1868	12	1854	12	−1	124	136	1.14
RA-70B-5.1	5.3114	1.0	0.3355	0.7	0.1148	0.7	0.722	0.13	1865	12	1877	13	1	118	135	1.19
RA-70B-6.1	5.3055	1.3	0.3372	0.8	0.1141	1.0	0.651	0.17	1873	14	1866	18	0	71	109	1.59
RA-70B-7.1	5.3387	1.0	0.3363	0.7	0.1151	0.7	0.726	0.01	1869	12	1882	13	1	119	286	2.48
RA-70B-8.1	5.2167	1.1	0.3354	0.7	0.1128	0.8	0.661	0.24	1865	12	1845	15	−1	122	94	0.80
RA-70B-9.1	5.3056	1.0	0.3364	0.7	0.1144	0.6	0.749	0.09	1869	12	1870	12	0	123	207	1.74
RA-70B-10.1	5.2555	1.4	0.3303	0.9	0.1154	1.1	0.614	0.28	1840	14	1886	20	3	61	66	1.12
RA-70B-11.1	5.2458	1.0	0.3327	0.8	0.1144	0.7	0.738	0.09	1852	12	1870	12	1	109	113	1.07
RA-70B-12.1	5.3324	1.8	0.3382	1.3	0.1144	1.2	0.739	0.17	1878	21	1870	21	0	57	57	1.03
Corumbá Window																
RA-08D – Granitic Gneiss																
RAPA-08D-1.1	5.0368	2.4	0.3056	1.6	0.1195	1.7	0.366	0.48	1719	24	1949	31	13	110	141	1.33
RAPA-08D-2.1	5.1662	1.8	0.3330	1.6	0.1125	0.9	0.874	−0.11	1853	25	1841	17	−1	164	92	0.58
RAPA-08D-3.1	5.2401	1.9	0.3338	1.6	0.1139	1.0	0.866	−0.09	1857	26	1862	18	0	129	107	0.85
RAPA-08D-4.1	5.3175	2.0	0.3335	1.6	0.1156	1.2	0.839	0.07	1855	26	1890	22	2	99	171	1.79
RAPA-08D-5.1	4.8687	2.1	0.3166	1.8	0.1115	1.1	0.892	0.02	1773	28	1825	20	3	208	237	1.18
RAPA-08D-6.1	5.3466	1.8	0.3397	1.6	0.1141	0.8	0.890	−0.07	1885	26	1866	14	−1	183	357	2.02
RAPA-08D-7.1	5.3946	1.9	0.3416	1.6	0.1145	1.0	0.886	−0.20	1894	26	1873	18	−1	153	128	0.87
RAPA-08D-8.1	4.2950	2.8	0.2627	1.5	0.1186	2.3	0.429	0.45	1503	21	1935	41	29	543	591	1.13
RAPA-08D-9.1	5.4090	2.0	0.3302	1.6	0.1188	1.2	0.700	0.19	1839	25	1938	22	5	187	164	0.91
RAPA-08D-10.1	3.8325	3.1	0.2279	1.6	0.1220	2.6	0.778	0.82	1324	19	1985	47	50	196	178	0.94
RAPA-08D-11.1	5.9627	1.8	0.3324	1.6	0.1301	0.9	0.868	−0.09	1850	25	2099	16	13	131	150	1.19
RAPA-08D-12.1	5.2630	1.7	0.3368	1.5	0.1133	0.8	0.903	0.01	1871	25	1854	14	−1	168	170	1.04

(*continued on next page*)

Table 4 (*continued*)

Sample Spot number	Ratios						err corr	% Com ^{206}Pb	Age (Ma)				Disc %	ppm		Th/U
	$^{207}Pb/^{235}U$	err %	$^{206}Pb/^{238}U$	err %	$^{207}Pb/^{206}Pb$	err %			$^{206}Pb/^{238}U$	1σ	$^{207}Pb/^{206}Pb$	1σ		U	Th	
RAPA-08D-13.1	5.4418	1.9	0.3445	1.6	0.1146	0.9	0.873	0.03	1908	27	1873	17	−2	105	91	0.90
RAPA-08D-14.1	5.3879	1.7	0.3423	1.5	0.1142	0.7	0.793	0.00	1898	25	1867	13	−2	165	114	0.71
Serra da Bocaina Formation																
FMR-200 – Metavolcanic rock																
VOL-01-1.1	5.1167	0.8	0.3313	0.5	0.5380	0.1	0.709	0.22	1845	7	1832	13	−1	182	175	0.99
VOL-01-1.2	4.7838	1.3	0.3138	0.4	0.3211	0.1	1.197	0.77	1760	6	1809	22	3	237	118	0.52
VOL-01-2.1	4.4423	2.4	0.2933	0.4	0.1548	0.1	2.382	1.86	1658	5	1797	43	8	351	314	0.92
VOL-01-3.1	5.8023	8.3	0.3515	1.7	0.2049	0.1	8.110	3.05	1942	28	1952	145	1	177	98	0.57
VOL-01-4.1	6.9931	0.8	0.4201	0.7	0.8112	0.1	0.469	0.02	2261	12	1967	8	−13	231	128	0.57
VOL-01-5.1	5.5842	0.6	0.3351	0.3	0.4873	0.1	0.526	0.15	1863	5	1969	9	6	565	42	0.08
VOL-01-6.1	6.3971	0.7	0.3549	0.3	0.4856	0.1	0.577	0.37	1958	5	2108	10	8	437	72	0.17
VOL-01-7.1	3.6656	4.2	0.2426	0.4	0.1058	0.1	4.182	3.39	1400	6	1792	76	28	464	740	1.65
VOL-01-8.1	4.9577	0.9	0.3232	0.6	0.6042	0.1	0.742	0.26	1805	9	1820	13	1	246	240	1.01
VOL-01-9.1	4.8404	1.0	0.3168	0.5	0.5352	0.1	0.805	0.16	1774	8	1813	15	2	151	161	1.10
VOL-01-10.1	4.8286	0.8	0.3201	0.5	0.5942	0.1	0.616	0.14	1790	7	1789	11	0	190	227	1.24
VOL-01-11.1	5.7856	0.4	0.3458	0.2	0.6518	0.1	0.271	0.09	1915	4	1976	5	3	1010	375	0.38
VOL-01.12.1	6.8840	1.9	0.4347	1.3	0.1149	1.3	0.714	0.70	2327	26	1878	24	−19	271	243	0.93
VOL-01.10.2	4.9007	1.2	0.3219	1.0	0.1104	0.6	0.862	0.15	1799	16	1806	11	0	178	230	1.33
VOL-01.1.3	5.3783	1.1	0.3473	1.0	0.1123	0.5	0.894	0.12	1921	17	1837	9	−4	242	75	0.32
VOL-01.13.1	6.1739	1.1	0.3700	1.0	0.1210	0.4	0.919	0.13	2030	17	1971	8	−3	318	201	0.65
The Eastern Terrane																
The Caracol Gneiss and Baía dos Garças suite																
RA-44 – Biotite Gneiss																
RA-44.1.1	4.9186	2.0	0.3266	1.8	0.1092	0.9	0.891	−0.01	1822	29	1786	17	−2	86	77	0.92
RA-44.2.1	3.9800	2.3	0.2643	2.1	0.1092	0.9	0.919	−0.01	1512	29	1786	17	18	86	77	0.92
RA-44.3.1	4.5184	3.4	0.3178	1.9	0.1031	2.9	0.543	0.99	1779	29	1681	53	−6	85	66	0.80
RA-44.4.1	4.6369	4.0	0.3199	1.9	0.1051	3.6	0.462	1.26	1789	29	1717	66	−4	81	64	0.82
RA-44.5.1	4.6871	5.3	0.3068	1.9	0.1108	5.0	0.360	2.70	1725	29	1813	90	5	77	76	1.01
RA-44.6.1	1.1113	4.8	0.1002	1.9	0.0805	4.4	0.392	1.09	615	11	1208	87	96	127	49	0.40
RA-44.6.2	5.1895	4.1	0.3262	2.0	0.1154	3.6	0.485	0.94	1820	32	1886	65	4	61	73	1.23
RA-44.6.3	5.4208	3.1	0.3324	2.7	0.1183	1.7	0.848	−0.09	1850	43	1930	30	4	27	42	1.63
RA-44-10.1	2.7004	2.5	0.2216	2.3	0.0884	0.9	0.922	0.27	1290	27	1391	18	8	256	28	0.11
RA-44-11.1	4.3337	2.8	0.2896	2.4	0.1085	1.5	0.853	0.17	1639	35	1775	27	8	43	37	0.89
RA-44-12.1	4.7962	2.5	0.3202	2.3	0.1086	1.0	0.921	0.21	1791	36	1776	18	−1	81	75	0.96
RA-46 – Leucocratic Gneiss																
RAPA-46-1.1	4.7644	2.1	0.3166	1.6	0.1091	1.3	0.805	0.11	1773	25	1785	24	1	94	67	0.73
RAPA-46-2.1	4.7529	2.0	0.3205	1.6	0.1076	1.2	0.893	0.21	1792	24	1758	22	−2	134	70	0.54
RAPA-46-3.1	4.5040	1.8	0.3080	1.5	0.1061	0.9	0.839	0.21	1731	23	1733	16	0	225	241	1.11
RAPA-46-4.1	3.8605	2.5	0.2601	1.7	0.1077	1.8	0.943	1.06	1490	22	1760	33	18	259	217	0.87
RAPA-46-5.1	4.8140	1.7	0.3200	1.6	0.1091	0.6	0.920	0.03	1790	24	1785	11	0	288	210	0.75
RAPA-46-6.1	4.0289	2.0	0.2710	1.5	0.1078	1.3	0.480	0.35	1546	21	1763	24	14	172	173	1.04
RAPA-46-7.1	4.6274	2.1	0.3120	1.5	0.1076	1.4	0.831	0.45	1750	23	1759	26	0	233	140	0.62
RAPA-46-8.1	4.7246	2.0	0.3174	1.6	0.1080	1.2	0.874	0.21	1777	24	1765	22	−1	133	120	0.93
RAPA-46-9.1	4.7210	1.8	0.3159	1.6	0.1084	0.9	0.772	0.08	1770	24	1772	17	0	150	113	0.78
RAPA-46-10.1	4.6916	1.9	0.3159	1.6	0.1077	1.2	0.894	0.34	1770	24	1761	21	−1	145	116	0.83
RAPA-46-11.1	3.6812	3.8	0.2495	1.6	0.1070	3.4	0.803	1.97	1436	20	1749	63	22	305	299	1.01
RAPA-46-12.1	4.3218	1.7	0.2964	1.6	0.1057	0.6	0.958	0.17	1673	23	1727	11	3	419	250	0.62
RA-48 – Leucocratic Orthogneiss																
RAPA-48-1.1	2.4371	2.0	0.2109	1.5	0.0838	1.3	0.836	0.75	1234	17	1288	26	4	1292	59	0.05
RAPA-48-1.2	2.3919	2.1	0.2089	1.5	0.0831	1.5	0.918	0.80	1223	16	1271	30	4	1122	83	0.08
RAPA-48-2.1	0.4672	30.0	0.0329	2.6	0.1030	29.9	0.034	20.81	209	5	1678	552	704	7282	791	0.11
RAPA-48-3.1	3.5760	3.0	0.2600	1.5	0.0998	2.6	0.408	1.81	1490	20	1619	48	9	1822	1270	0.72
RAPA-48-4.1	2.2429	8.2	0.1847	1.6	0.0881	8.0	0.118	5.23	1093	16	1384	154	27	907	281	0.32
RAPA-48-5.1	4.4983	2.1	0.3086	1.6	0.1057	1.3	0.691	0.25	1734	24	1727	24	0	151	166	1.14
RAPA-48-5.2	4.6639	1.9	0.3141	1.6	0.1077	1.1	0.841	0.16	1761	24	1761	20	0	136	110	0.83
RAPA-48-6.1	0.7401	36.4	0.0603	2.4	0.0890	36.3	0.029	21.78	378	9	1403	696	272	3422	586	0.18
RAPA-48-7.1	1.4108	9.9	0.1190	1.5	0.0860	9.8	0.140	4.80	725	11	1337	190	84	1651	150	0.09
RAPA-48-8.1	3.9085	2.2	0.2701	1.5	0.1049	1.6	0.797	1.13	1541	20	1713	29	11	772	278	0.37
RAPA-48-8.2	2.8720	33.0	0.1645	3.8	0.1266	32.7	0.069	13.74	982	35	2052	578	109	1747	1139	0.67
RAPA-48-9.1	1.2876	37.2	0.0999	2.4	0.0935	37.2	0.018	22.80	614	14	1497	703	144	6001	534	0.09
RAPA-48-10.1	2.4433	2.3	0.1974	1.5	0.0898	1.7	0.710	0.75	1161	16	1421	33	22	2475	1894	0.79
RAPA-48-10.2	2.5266	1.7	0.1999	1.5	0.0917	0.8	0.957	0.40	1175	16	1460	15	24	2225	2066	0.96
RA-101 – Augen Gneiss																
RA-101-2.1	4.2836	1.4	0.2861	0.8	0.1086	1.1	0.563	0.53	1622	11	1776	21	9	124	74	0.62
RA-101-3.1	3.9302	3.3	0.2693	0.7	0.1058	3.3	0.214	2.43	1537	10	1729	60	12	237	159	0.69
RA-101-4.1	1.6521	1.4	0.1135	0.7	0.1056	1.2	0.506	0.55	693	5	1724	22	149	312	468	1.55
RA-101-5.1	4.4352	0.9	0.2992	0.7	0.1075	0.6	0.764	0.17	1687	10	1758	10	4	252	134	0.55
RA-101-6.1	4.8211	1.1	0.3221	0.8	0.1086	0.8	0.687	0.22	1800	12	1775	15	−1	152	93	0.63
RA-101-7.1	3.1110	1.3	0.2132	0.9	0.1059	1.0	0.656	0.48	1246	10	1729	18	39	222	320	1.49
RA-101-8.1	3.8611	1.0	0.2611	0.6	0.1073	0.8	0.617	0.48	1495	9	1753	15	17	355	272	0.79
RA-101-9.1	4.6492	0.9	0.3116	0.7	0.1082	0.6	0.750	0.11	1748	11	1770	11	1	191	142	0.76

(*continued on next page*)

Table 4 (*continued*)

Sample Spot number	Ratios						err corr	% Com ^{206}Pb	Age (Ma)				Disc %	ppm		Th/U
	$^{207}Pb/^{235}U$	err %	$^{206}Pb/^{238}U$	err %	$^{207}Pb/^{206}Pb$	err %			$^{206}Pb/^{238}U$	1σ	$^{207}Pb/^{206}Pb$	1σ		U	Th	
RA-101-10.1	4.0852	0.9	0.2763	0.7	0.1072	0.5	0.776	0.11	1573	9	1753	10	11	241	181	0.78
RA-101-11.1	4.5661	0.9	0.3077	0.7	0.1076	0.6	0.759	0.18	1729	10	1760	11	2	285	301	1.09
RA-101-12.1	3.4423	1.8	0.2321	1.2	0.1076	1.3	0.657	0.63	1346	14	1758	25	31	113	126	1.15
RA-101-13.1	4.1946	0.9	0.2822	0.7	0.1078	0.4	0.875	0.10	1602	11	1763	8	10	421	329	0.81
RA-88B – Quartz Gneiss																
RA-88B-1.1	4.3973	1.0	0.3015	0.7	0.1058	0.8	0.689	0.20	1699	11	1728	14	2	200	179	0.93
RA-88B-2.1	4.4739	1.8	0.3038	1.3	0.1068	1.2	0.726	0.21	1710	20	1746	23	2	69	50	0.75
RA-88B-3.1	4.5890	1.6	0.3096	0.9	0.1075	1.3	0.574	0.36	1739	14	1758	24	1	70	60	0.89
RA-88B-4.1	4.5729	0.9	0.3083	0.7	0.1076	0.6	0.758	0.12	1732	11	1759	11	2	202	186	0.95
RA-88B-5.1	3.6746	1.1	0.2524	0.8	0.1056	0.8	0.703	0.12	1451	10	1724	14	19	144	88	0.63
RA-88B-6.1	4.6211	1.2	0.3127	0.8	0.1072	0.9	0.656	0.22	1754	12	1752	16	0	119	126	1.10
RA-88B-7.1	4.5669	1.2	0.3083	1.0	0.1074	0.7	0.817	0.07	1732	15	1757	12	1	137	117	0.88
RA-88B-8.1	4.6886	0.9	0.3133	0.8	0.1085	0.5	0.815	0.09	1757	12	1775	10	1	147	142	1.00
RA-88B-9.1	4.7674	1.0	0.3152	0.8	0.1097	0.7	0.740	−0.09	1766	12	1795	13	2	121	107	0.91
RA-88B-10.1	4.6247	1.2	0.3141	0.8	0.1068	0.9	0.683	0.14	1761	12	1746	16	−1	104	114	1.14
RA-88B-11.1	4.3660	1.4	0.3039	0.8	0.1042	1.1	0.583	0.41	1710	12	1700	20	−1	108	131	1.25
RA-88B-12.1	4.6095	1.4	0.3117	0.8	0.1073	1.2	0.591	0.17	1749	13	1753	21	0	91	85	0.96
RA-31 – Biotite Gneiss																
RA-31.1.1	4.8804	2.3	0.3206	1.8	0.1104	1.3	0.798	−0.31	1793	28	1806	25	1	79	71	0.92
RA-31.2.1	4.6785	1.9	0.3200	1.7	0.1060	0.9	0.889	0.13	1790	26	1732	16	−3	218	241	1.14
RA-31.3.1	4.3058	1.8	0.2929	1.7	0.1066	0.7	0.923	0.11	1656	24	1742	13	5	268	207	0.80
RA-31.3.2	4.2120	2.4	0.2846	1.7	0.1073	1.7	0.700	0.78	1614	24	1755	32	9	181	139	0.79
RA-31-4.1	3.9490	3.0	0.2613	1.7	0.1096	2.4	0.551	1.77	1497	22	1793	46	20	266	306	1.19
RA-31-5.1	3.9799	1.8	0.2702	1.7	0.1068	0.8	0.908	0.21	1542	23	1746	14	13	306	322	1.09
RA-31-6.1	3.3921	2.3	0.2315	1.7	0.1062	1.5	0.715	1.02	1342	20	1736	30	29	321	321	1.03
RA-31-7.1	3.6731	2.2	0.2520	1.8	0.1057	1.3	0.815	0.50	1449	23	1726	24	19	205	153	0.77
RA-31-8.1	2.3377	2.4	0.1781	1.6	0.0952	1.7	0.678	1.16	1057	16	1532	33	45	1375	1996	1.50
RA-31-9.1	3.9868	1.7	0.2747	1.6	0.1052	0.6	0.934	0.24	1565	23	1719	11	10	566	702	1.28
RA-31-10.1	4.4164	1.8	0.3033	1.7	0.1056	0.7	0.925	0.15	1708	25	1725	12	1	290	471	1.68
RA-31-11.1	3.8060	2.3	0.2571	1.7	0.1074	1.5	0.740	0.90	1475	23	1755	29	19	267	295	1.14
RA-31-12.1	3.1341	1.9	0.2281	1.6	0.0996	0.9	0.858	0.62	1325	19	1617	18	22	975	894	0.95
RA-31-13.1	3.4996	2.8	0.2380	1.7	0.1066	2.2	0.592	1.49	1376	21	1743	42	27	232	194	0.86
Paso Bravo Province																
RA-93A – Orthogneiss																
RAPA-93A-1.1	4.1658	1.5	0.2802	1.4	0.1078	0.4	0.970	0.02	1592	20	1763	7	11	436	273	0.65
RAPA-93A-2.1	2.9673	3.1	0.2130	1.7	0.1010	2.5	0.553	1.44	1245	19	1643	48	32	147	522	3.68
RAPA-93A-3.1	4.1167	1.5	0.2842	1.4	0.1050	0.6	0.914	0.19	1613	20	1715	11	6	274	390	1.47
RAPA-93A-4.1	4.3962	1.6	0.3012	1.4	0.1059	0.6	0.916	0.08	1697	22	1729	12	2	205	167	0.84
RAPA-93A-5.1	3.8779	1.7	0.2619	1.4	0.1074	0.8	0.854	0.42	1499	19	1756	16	17	262	245	0.96
RAPA-93A-6.1	4.6279	1.5	0.3135	1.4	0.1070	0.5	0.935	0.07	1758	22	1750	10	0	232	220	0.98
RAPA-93A-7.1	4.5883	1.5	0.3106	1.4	0.1071	0.5	0.939	0.10	1744	21	1751	9	0	257	216	0.87
RAPA-93A-8.1	4.4399	1.5	0.3028	1.4	0.1063	0.5	0.939	0.11	1705	22	1737	10	2	230	182	0.82
RAPA-93A-9.1	4.1707	1.7	0.2917	1.6	0.1037	0.7	0.906	0.20	1650	23	1691	13	2	241	186	0.80
RAPA-93A-10.1	4.6288	1.5	0.3132	1.4	0.1072	0.4	0.959	0.00	1757	22	1752	8	0	293	265	0.93
RAPA-93A-11.1	4.5478	1.5	0.3063	1.4	0.1077	0.5	0.937	0.13	1722	21	1761	10	2	312	211	0.70
RAPA-93A-12.1	4.6555	1.5	0.3137	1.4	0.1076	0.5	0.944	0.04	1759	22	1760	9	0	203	204	1.03
RAPA-93A-13.1	4.4161	1.5	0.2964	1.4	0.1081	0.5	0.936	0.15	1673	21	1767	10	6	324	305	0.97
RAPA-93A-14.1	4.5746	1.6	0.3085	1.4	0.1075	0.6	0.910	0.12	1733	22	1758	12	1	217	222	1.06
RAPA-93A-15.1	4.7254	1.6	0.3193	1.4	0.1073	0.6	0.914	0.09	1786	23	1755	12	−2	157	83	0.55
RA-114 – Granite																
RAPA-114-1.1	4.5228	1.5	0.3035	1.4	0.1081	0.5	0.937	−0.03	1709	21	1767	10	3	186	89	0.50
RAPA-114-2.1	4.8038	1.8	0.3173	1.6	0.1098	0.9	0.882	−0.10	1776	25	1796	16	1	114	91	0.83
RAPA-114-2.2	4.8408	1.6	0.3153	1.5	0.1113	0.5	0.956	0.03	1767	23	1821	8	3	241	170	0.73
RAPA-114-3.1	4.7562	1.4	0.3199	1.4	0.1078	0.4	0.968	0.02	1789	22	1763	7	−1	436	273	0.65
RAPA-114-4.1	4.6439	1.6	0.3115	1.5	0.1081	0.6	0.919	−0.04	1748	22	1768	11	1	135	106	0.81
RAPA-114-5.1	4.7193	1.6	0.3195	1.4	0.1071	0.7	0.902	0.11	1787	23	1751	13	−2	150	126	0.87
RAPA-114-6.1	4.7011	1.5	0.3175	1.4	0.1074	0.5	0.945	0.01	1778	22	1755	9	−1	234	208	0.92
RAPA-114-7.1	4.6349	1.5	0.3117	1.4	0.1078	0.4	0.957	0.01	1749	22	1763	8	1	434	329	0.78
RAPA-114-8.1	4.6309	1.6	0.3115	1.5	0.1078	0.6	0.915	0.12	1748	22	1763	12	1	186	171	0.95
RAPA-114-9.1	4.7502	1.5	0.3213	1.4	0.1072	0.6	0.923	0.05	1796	22	1753	11	−2	174	136	0.81
RAPA-114-10.1	4.6118	1.5	0.3117	1.4	0.1073	0.6	0.931	0.07	1749	22	1754	10	0	236	182	0.80
RAPA-114-11.1	4.7830	1.5	0.3224	1.4	0.1076	0.6	0.924	0.13	1801	22	1759	11	−2	228	177	0.80
RA-97B – Aplite																
RA-97B-1.1	4.5576	1.4	0.3077	0.9	0.1074	1.1	0.632	0.27	1729	13	1756	19	2	113	163	1.49
RA-97B-2.1	4.7381	1.1	0.3105	0.8	0.1107	0.7	0.744	0.03	1743	13	1811	14	4	98	115	1.21
RA-97B-3.1	4.7527	1.4	0.3146	1.1	0.1096	1.0	0.731	0.09	1763	16	1792	18	2	55	40	0.75
RA-97B-4.1	4.3810	2.2	0.2923	0.9	0.1087	2.0	0.434	0.56	1653	14	1778	36	8	71	59	0.85
RA-97B-5.1	4.4203	0.8	0.3003	0.6	0.1067	0.6	0.737	0.08	1693	9	1745	10	3	352	288	0.85
RA-97B-6.1	4.6853	0.8	0.3132	0.7	0.1085	0.5	0.812	0.03	1756	10	1775	9	1	200	76	0.39
RA-97B-7.1	4.4976	1.0	0.3034	0.7	0.1075	0.6	0.762	0.09	1708	11	1758	11	3	154	116	0.78
RA-97B-8.1	4.3512	0.8	0.2936	0.6	0.1075	0.4	0.822	0.10	1659	9	1757	8	6	334	291	0.90
RA-97B-9.1	4.6902	0.9	0.3135	0.7	0.1085	0.6	0.769	0.09	1758	11	1774	11	1	149	103	0.72
RA-97B-10.1	3.4859	1.3	0.2381	0.7	0.1062	1.0	0.583	0.37	1377	9	1735	19	26	133	125	0.97

(*continued on next page*)

Table 4 (*continued*)

Sample Spot number	Ratios						err corr	% Com ^{206}Pb	Age (Ma)				Disc %	ppm		Th/U
	^{207}Pb/^{235}U	err %	^{206}Pb/^{238}U	err %	^{207}Pb/^{206}Pb	err %			^{206}Pb/^{238}U	1σ	^{207}Pb/^{206}Pb	1σ		U	Th	
RA-97B-11.1	4.6569	0.8	0.3109	0.7	0.1086	0.5	0.823	0.08	1745	10	1777	9	2	317	316	1.03
RA-97B-12.1	3.2494	0.8	0.2237	0.6	0.1054	0.5	0.756	0.14	1301	7	1721	10	32	277	210	0.78

studies, they were performed on low-grade metamorphic equivalents of the Alto Tererê Group.

5.1.1. Porto Murtinho complex

We collected sample RA-65A along the BR-267 highway (see Fig. 3). The outcrop is made up of migmatitic gneiss, from which the neosome band was selected for SHRIMP dating. The studied sample shows a granolepidoblastic texture, and consists of quartz, plagioclase, muscovite, biotite, chlorite, plus opaque minerals, apatite, zircon and titanite. The zircon grains vary in size from 90 to 370 μm (most up to 210 μm) and exhibit heterogeneous morphology (e.g., 1:2 to 1:4 elongation ratios, and prismatic to pyramidal habits with well-defined faces). In the CL images (Fig. 4), zircon crystals show bright luminescence, a prismatic habit with well-defined faces, and oscillatory zoning. Few grains show recrystallized sites.

Seventeen analyses were made, but four of them do not meet the analytical criteria (Table 4). Five points cluster on the Concordia, defining an age of 2069.5 ± 3.9 (MSWD = 0.001) – Fig. 5A. Different contents of U (varying from 92 to 150 ppm, except for spot #12.1, with 303 ppm) were obtained for a group of analyses (# 3.1, 5.1, 6.1, 11.1 and 12.1). These spots regress to yield an upper intercept age of 2154 ± 52 Ma, which may be related to a distinct old component in the progenitor magma.

5.1.2. Alumiador suite and Serra da Bocaina Formation

Sample RA-54A is a slightly foliated granitic orthogneiss, collected in the southern portion of the Alumiador suite (see Fig. 3). This sample consists of plagioclase, microcline, quartz, hornblende and minor biotite, and has a granoblastic texture. Titanite, zircon, epidote, apatite and opaque minerals are the accessories. Most zircon grains show growth zoning in CL images (Fig. 4). Six out of thirteen SHRIMP spot analyses yielded unacceptably high ^{204}Pb or U/Th values, including one single analysis that yielded a ^{207}Pb/^{206}Pb concordant age as old as 2100 Ma (see Table 4). They were not used in the age calculation. The reminder points cluster on the Concordia at 1816 ± 6.9 Ma (MSWD = 0.061), which is inferred as the crystallization age (Fig. 5B).

Sample RA-62F is a monzogranite collected from a large outcrop in the intersection of the BR-267 highway and the MS-384 state road (see Fig. 3). The outcrop is composed of medium- to coarse-grained pink granite with fresh biotite. In thin section, the sample consists of quartz, plagioclase, microcline, opaque minerals, biotite and muscovite, epidote + allanite, garnet, apatite and titanite. The texture is hypidiomorphic. The zircon grains have a length that varies from 120 to 320 μm (average 200 μm) with elongation ratios ranging from 1:2 to 1:4. Most crystals are euhedral with pronounced prismatic shapes; some are fractured and with homogeneous texture. CL images did not show inherited cores. Most crystals exhibit oscillatory zoning although sector zoning is also common (Fig. 4). Four isotopic analyses showed high U contents and were not used in the age calculation (see Table 4). Concordia age of 1857 ± 5.9 Ma (MSWD = 0.39) defined the crystallization age (Fig. 5C). In addition, eight spots with U contents between 125 and 202 ppm regressed to yield a very similar upper intercept age of 1860 ± 12 Ma.

Sample RA-70B was collected along the MS-467 road, ca. 25 km west of sample RA-62F (see Fig. 3). This outcrop is associated with a local NE-trending quartzite body with volcanic clasts. The studied sample is a non-foliated, dark-green volcaniclastic rock, mainly composed of volcanic material with subordinate feldspathic material. Most zircon grains are euhedral to subhedral, but fragmented grains are also common. Their length varies from 90 to 290 μm; the largest ones have pyramidal edges (elongations 1:2). Growth zoned and/or unzoned zircon is present in CL images and few grains have inclusions (Fig. 4). We performed twelve SHRIMP analyses, in which U contents range from 57 to 124 ppm (see Table 4). Concordia age of 1867.8 ± 3.0 Ma (MSWD = 0.93) – Fig. 5D - is identical within the analytical error with that of the monzogranite RA-62F.

Sample FMR-200 was described as a low-grade metabasalt, tentatively attributed to the Serra da Bocaina Formation. It was collected close to the Serra da Alegria (Fig. 3). The outcrop is not far from a pyroclastic rock (1813 ± 18 Ma), ascribed to Rio Naitaca Formation by Faleiros et al. (2016), and is close to a metasandstone which yielded a maximum depositional age of 1802 ± 49 Ma (Cabrera, 2015). The studied sample is a plagioclase-carbonate-chlorite schist, which shows compositional banding and has granoblastic and lepidoblastic textures in carbonate-rich and chlorite-rich layers, respectively. Accessory minerals are albite, titanite, quartz, epidote and opaque minerals. In particular, the chlorite-rich bands show relict microporphyritic igneous texture, highlighted by euhedral to subhedral plagioclase phenocrysts in a fine-grained matrix.

The zircon grains are subhedral with pyramidal and prismatic habits, ranging from 60 to 120 μm in length. In CL images (see Fig. 4), the grains showed internal oscillatory zoning and dark, thin edges. Twelve SHRIMP analyses were carried out, and seven of them (with U contents between 190 and 464 ppm; Table 4), including three concordant analyses, yielded an upper intercept age of 1818.9 ± 9.9 Ma (MSWD = 1.9), which was interpreted as the crystallization age (Fig. 5E). This age is identical within error with that reported for a rhyolite of the Serra da Bocaina Formation occurring in the southern portion of the Western Terrane (Brittes et al., 2016). A few slightly discordant spots (e.g., #6.1), possible xenocrysts, indicated apparent ages up to 2100 Ma. These oldest dates point to a protracted history for the Porto Murtinho crust.

5.1.3. Corumbá Window

The RA-08D granitic gneiss was collected from a railway cut ca. 30 km to the west of the city of Corumbá (see Fig. 3 inset). The outcrop exhibits extensive weathering and fracturing. In the thin section, the sample comprises quartz, plagioclase, microcline, opaque minerals, garnet and muscovite in a granoblastic matrix. The zircon population comprises large crystals with lengths from 100 to 400 μm. Subhedral habits (elongation ratios up to 1:4) with pronounced oscillatory zoning predominate in CL images (Fig. 4).

Nine out of 14 analyses yielded a Concordia age of 1869 ± 5 Ma (MSWD = 0.14), interpreted as the crystallization age (Fig. 5F). In these analyses, U contents range from 99 to 187 ppm. Additional discordant spots yielded a roughly similar upper intercept age. The only exception (spot #11.1; Table 4) yielded ^{207}Pb/^{206}Pb age of ca. 2100 Ma (13% disc.), which may indicate a distinct component in the original magma.

5.1.4. Alto Tererê samples in the Western Terrane

Sample EAR-082 was collected from a major N-S trending tectonic slice (see Fig. 3), which is interlayered with metasedimentary rocks and amphibolites, as well as the Alumiador batholith. The whole package

Fig. 4. Cathodoluminescence images of zircon grains from selected meta igneous rocks of the RAT, dated by the SHRIMP.

shows tectonic vergence to the west, with reverse faults towards the batholith. This sample was classified as a mylonitic muscovite quartzite with garnet porphyroblasts. The zircon population is composed of fractured, prismatic zircons (some metamict) and subangular fragments with lengths from 70 to 270 μm. In CL images, detrital crystals show bright oscillatory zoned cores with dark and thin luminescent rims (see Fig. 6). Dark engulfments are also present in few bright cores.

Most analytical points were concordant, and 59 out of 74 analyses (LA-ICP-MS) yielded an age spread between 1.98 and 1.63 Ga on the Concordia (Fig. 7A). All grains have high Th/U values (see Supplementary Material). In the histogram, a unimodal spectrum that peaked at 1.78 Ga, with most ages between 1.73 and 1.85 Ga, was present

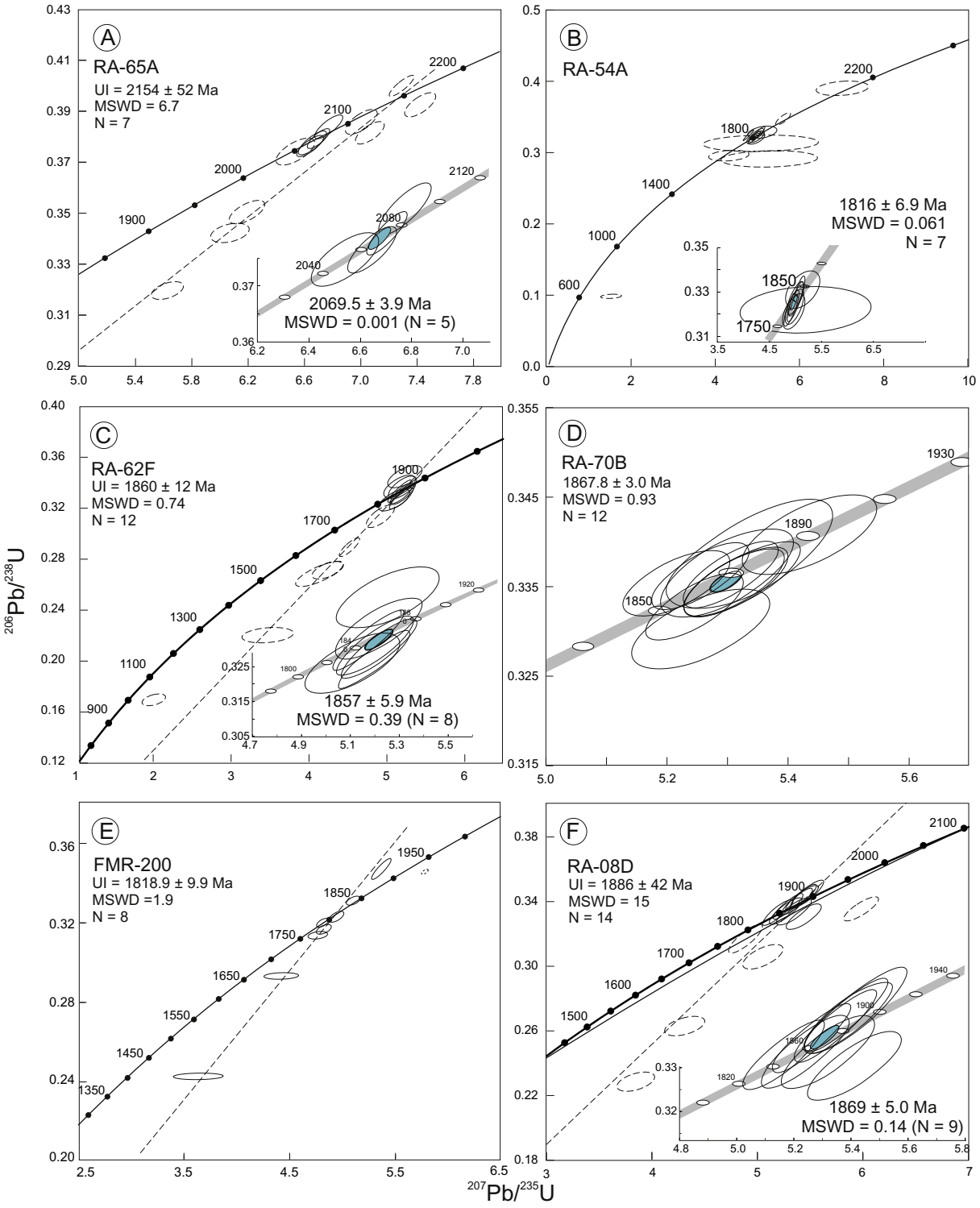

Fig. 5. SHRIMP diagrams for selected rocks of the Porto Murtinho complex and Alumiador batholith (Western Terrane).

(Fig. 7B). This age matches those of the Alumiador and basement rocks as well as the age of Caracol Gneiss to be dealt with later (see Table 2 and Sections 3.1.2 and 3.2.2). We estimated the maximum deposition age of quartzite EAR-082 based on several isotopic analyses of bright cores, which yielded roughly identical ages within the error, such as 1777 ± 50 Ma (#1.1, 98% conc.), 1747 ± 59 Ma (#62.1; 103% conc.) and 1734 ± 57 Ma (# 8.1; 103% conc.). Grain #71.1 yielded a significantly younger $^{207}Pb/^{206}Pb$ age of 987 ± 11 Ma (103% conc.; see Supplementary Material and Fig. 7B). This dark (i.e., metamict) and ghost oscillatory zoned, prismatic zircon gave the highest U content (721 ppm) among the analyses. We interpret that the isotopic systematics of this particular zircon was probably disturbed, including the effects of ancient Pb loss between the internal and rim zones (e.g., Vervoot and Kemp, 2016). No similar ages were found in the population. Therefore this anomalous result which is not statistically significant will not be considered in this study. Finally, spot analysis #35.1 yielded an age of 1626 ± 37 Ma (109% conc.). It is an oscillatory zoned prismatic zircon with thin dark metamorphic rims, and with

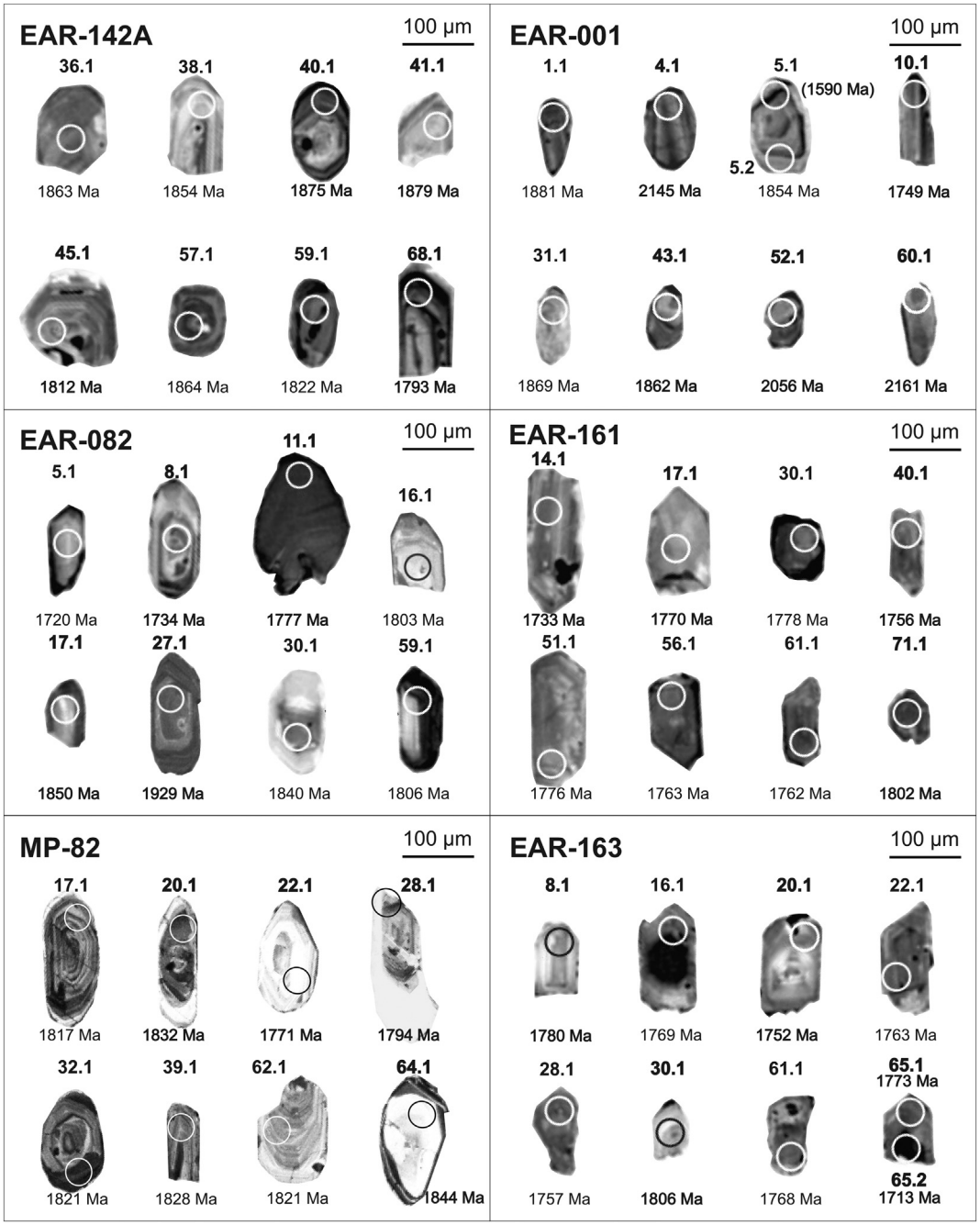

Fig. 6. Cathodoluminescence images of zircon grains from selected metasedimentary rocks, dated by the LA-ICPMS.

fractures. We consider that the result may not represent a true population, given the absence of similar ages in the population - see Supplementary Material.

5.2. Eastern Terrane

We conducted nine new SHRIMP U—Pb age determinations on selected samples from the Caracol Gneiss, which is the most widespread unit in the Eastern Terrane. Three samples were located along a transect in the vicinity of the Perdido River, not > 10–15 km apart from each other (see Fig. 3), and five other in Paraguay, in the southern portion of the RAT, referred to the Paso Bravo Province. We also collected a sample from the Baía das Garças suite in the northern portion of the Eastern Terrane. In addition, we present the LA-ICPMS results of three samples from the Alto Tererê Group. Fig. 3 presents the location of the sample.

5.2.1. The Caracol Gneiss along the Perdido River, in Brazil

Biotite gneiss RA-44 is composed of quartz, plagioclase, and biotite, and has a granolepidoblastic texture. Apatite, allanite, opaque minerals and garnet are accessory phases. Most zircon crystals have subhedral and homogeneous shapes and range from 90 to 190 μm in length. In CL images, they are bright luminescent, and some of them show oscillatory zoning and thin dark rims. Fractures are also common (Fig. 4).

Eleven SHRIMP analyses regress to yield an upper intercept U—Pb age of 1803 ± 90 Ma with a very high MSWD (not shown). Five of these analyses (U contents from 61 to 86 ppm) cluster on the Concordia at 1803 ± 33 Ma (MSWD = 0.25), defining the best-fit crystallization age (Fig. 8A). Two slightly discordant (4%) spots (# 6.2, 6.3) yielded $^{207}Pb/^{206}Pb$ apparent ages of 1930 ± 30 and 1886 ± 65 Ma,

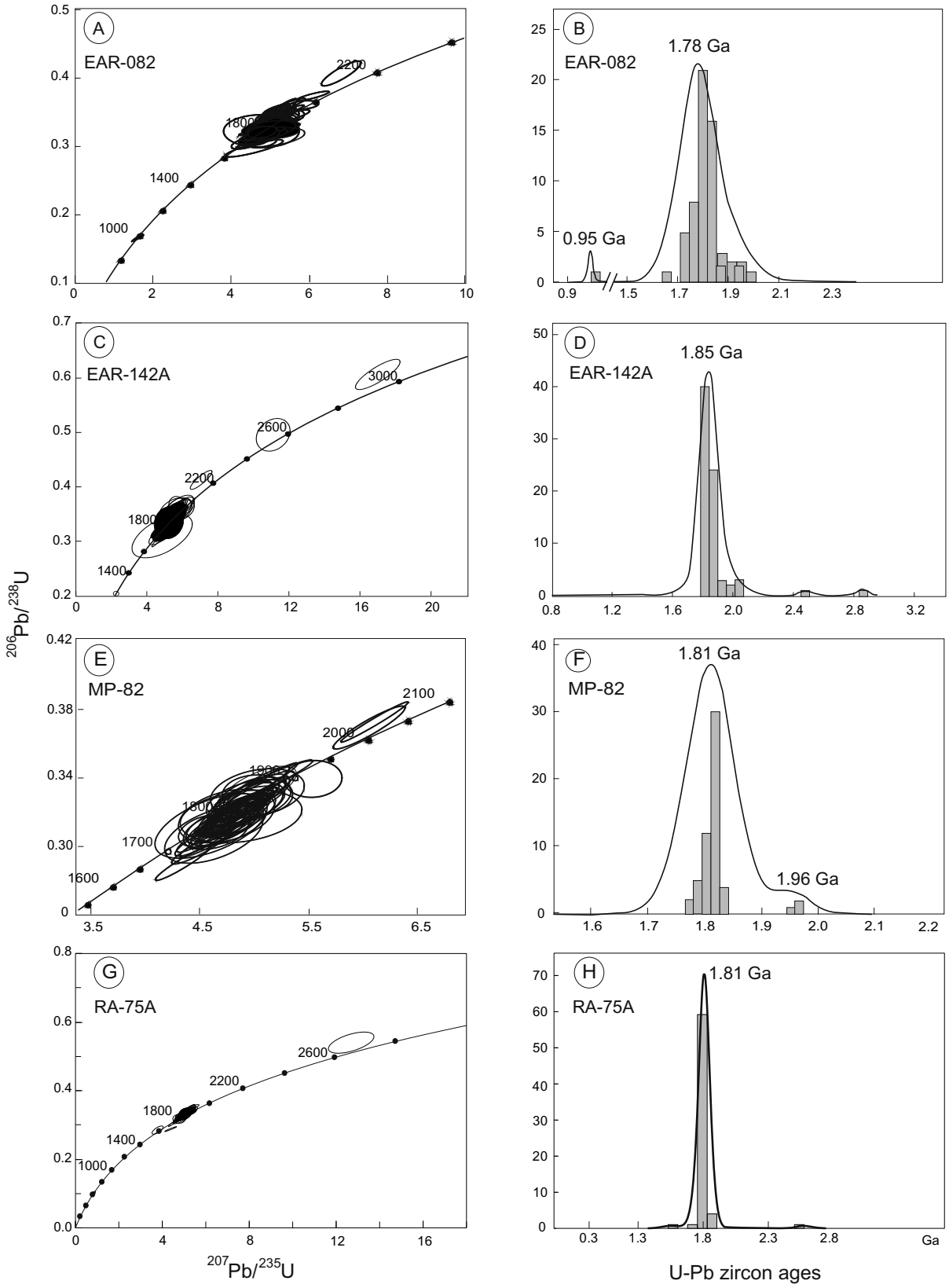

Fig. 7. Concordia and coupled Relative Probability Plots for selected supracrustal rocks (Alto Tererê correlatives) in the Western and Eastern terranes.

respectively, and may be inherited grains. In addition, one single zircon (# 10.1: see Table 4) yielded a distinct age of 1391 ± 18 Ma (8% disc.), suggesting this sample underwent a significantly younger partial isotopic reset after the crystallization.

Sample RA-46 is a foliated leucocratic gneiss, composed of quartz, microcline, plagioclase, chlorite (biotite alteration), garnet, opaque minerals, and zircon. The texture is granoblastic to granolepidoblastic. Zircon population is homogeneous, and some crystals show oscillatory

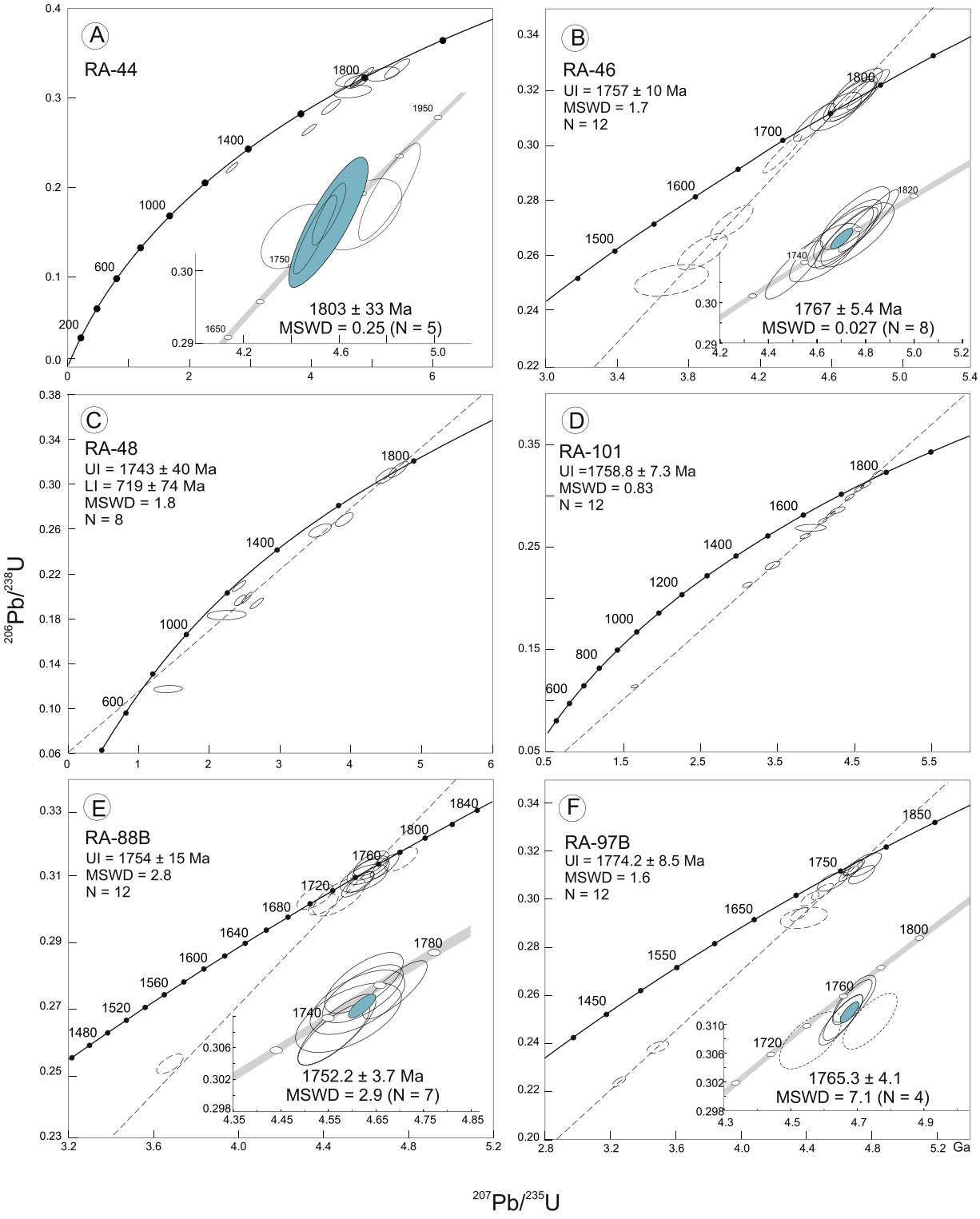

Fig. 8. SHRIMP diagrams for studied rocks in the Eastern Terrane.

zoning with thin dark rims in CL image (Fig. 4). Their length varies from 100 μm to 290 μm. Most crystals are subrounded to euhedral with more pronounced pyramidal shapes, and inherited cores are also present (see Fig. 3). Twelve zircon SHRIMP analyses were performed, some of those were discordant. Eight analyses (U contents from 94 to 288 ppm but mostly lower than 200 ppm) cluster on the Concordia (Fig. 8B) at 1767 ± 5.4 Ma (MSWD = 0.027), which is interpreted as the crystallization age.

Sample RA-48 is a coarse-grained leucocratic orthogneiss, with a mineral assemblage very similar to that of sample RA-46. Most zircons from this sample are prismatic with lengths varying from 100 to 260 μm. Many grains are metamict, but few grains are oscillatory zoned in CL images (Fig. 4). Table 4 shows the U contents of the analyses, which can be up to 2500 ppm in some grains. Fourteen SHRIMP analyses were carried out and most data were highly discordant in the Concordia diagram. Eight out of 13 analytical points could be regressed,

yielding an upper intercept age of 1743 ± 40 Ma with MSWD = 1.8 (Fig. 8C). Two coupled spot analyses from a single zircon (# 5.1 and 5.2) plotted right on the Concordia at 1727 ± 24 and 1761 ± 20 Ma (see Table 4). Two analyses of metamict grain #10.2 (see Fig. 4) yielded significantly younger $^{207}Pb/^{207}Pb$ ages (4% of disc.) of 1271 ± 30 and 1288 ± 26 Ma. These ages, despite the poor quality of the zircon, suggest that the orthogneiss underwent a regional metamorphic overprint long after the crystallization.

5.2.2. The Caracol Gneiss in the Paso Bravo province of Paraguay

Sample RA-101 (see Fig. 3) is an augen gneiss, which has a monzogranitic composition. In thin section, the sample is composed of quartz, microcline and plagioclase (phenocrysts), and has a (blastoporphyritic) granular texture, where the strong deformation is defined by recrystallized quartz. The length and U content of the zircon population range from 100 to 210 μm and from 113 to 421 ppm, respectively. Well-formed prismatic grains with oscillatory zoning predominate in CL images. Fractures and inclusions are also common (see Fig. 4), as expected in the local tectonic setting. Twelve zircon SHRIMP analyses were performed, and most grains plotted along a Discordia array (Fig. 8D). One of the points was right on the Concordia at the upper intercept, and the regression yielded an age (with the lower intercept forced to zero) of 1758.8 ± 7.3 Ma (MSWD = 0.83), interpreted as the best estimate for the crystallization age.

Sample RA-88B is a gneiss with feldspathic and quartz-rich bands, collected about 15 km west of Felix Lopes in Paraguay (Fig. 3). It is composed of plagioclase, quartz, microcline, hornblende, diopside, titanite, epidote, allanite, apatite, opaque minerals and zircon in a granoblastic matrix. In CL images, zircon grains are euhedral, prismatic, and oscillatory zoned. Dark engulfments are also common and were not used for analyses (Fig. 4). Zircon length varies between 100 and 300 μm, and most grains have U contents between 70 and 202 ppm. Twelve SHRIMP analyses were carried out. The data regressed to yield an upper intercept of 1754 ± 15 Ma. Alternatively, a Concordia age of 1752.2 ± 3.7 Ma (MSWD = 2.9) was calculated (Fig. 8E) disregarding two analyses with high U and/or high ^{204}Pb contents (# 1.1, 2.1). This age is considered to be the crystallization age of the rock.

Sample RA-97B is a (1 m-thick) aplite intrusive into gneiss located close to the Apa River, ca. 14 km east of San Carlos in Paraguay (Fig. 3). This aplite consists of alkali feldspar, muscovite and quartz. In CL images, zircon crystals are prismatic, with a pyramidal shape and oscillatory zoning (Fig. 4). Their length varies between 100 and 270 μm, and their U content varies from 55 to 352 ppm. Twelve SHRIMP analyses were performed (Fig. 8F). Part of the data was discordant along a Discordia line yielding an upper intercept age of 1774.2 ± 8.5 (MSWD = 1.6). Four of them yielded a similar age of 1765.3 ± 4.1 Ma within the errors, but with MSWD = 7.1. Therefore we consider that the 1774 Ma value as the best statistically estimation for the crystallization age.

Sample RA-93A is an amphibolite facies mafic orthogneiss collected a few kilometers west of Felix Lopes (Fig. 3). It has a nematoblastic texture and is essentially composed of hornblende, microcline, and plagioclase, and apatite and titanite are the main accessory minerals. The rock is interlayered with leucocratic bands and crosscut by pegmatitic bodies. The zircon population consists of sub-prismatic grains with cores and bright luminescent overgrowths in CL images (Fig. 4). The U contents ranged from 154 to 312 ppm. Fifteen SHRIMP analyses were conducted, and few grains were discordant (Fig. 9A) but reasonably aligned. Four of them plotted on the Concordia at the upper intercept, defining an age of 1753.9 ± 4.0 Ma (MSWD = 0.18), which is interpreted as the time of crystallization.

Finally, the porphyritic granite RA-114 was collected in the southernmost portion of the study area (Fig. 3). This sample is composed of quartz, plagioclase and microcline, and biotite, chlorite, opaque minerals and hornblende as secondary minerals. The zircons have well-preserved prismatic habits. In CL images, they are oscillatory zoned with dark cores (Fig. 4). Twelve SHRIMP analyses on the oscillatory domains are concordant to slightly discordant (Fig. 9B), and yielded altogether an age of 1768 ± 13 Ma (not shown). We selected ten of these analyses with U contents between 114 and 436 ppm (see Table 4) to calculate a Concordia age of 1763.9 ± 3.6 Ma (MSWD = 1.6), which is interpreted as the time of crystallization.

5.2.3. The Baía das Garças suite

Sample RA-31 is a foliated granitic rock, collected along the MS-382 state road, ca. 80 km away from Bonito (see Fig. 3). The outcrop is a biotite gneiss (granitoid composition) crosscut by quartz veins and formed by microcline, quartz, plagioclase and minor biotite. Zircon, apatite, allanite, epidote and opaque minerals are common accessories. In CL images, zircon crystals show oscillatory zoning, and most of them are prismatic, such as grain #1.1 (Fig. 4). They have variable lengths, between 140 and 350 μm, and U contents between 79 and 1275 ppm, with most grains below 350 ppm. In the Concordia diagram of Fig. 9C, most points were well-aligned along a Discordia line, yielding an age of 1776 ± 39 Ma (MSWD = 2.9), and one grain yielded a concordant age at 1725 ± 12 Ma (#3.1; Table 4).

5.2.4. The Alto Tererê Group in the Eastern Terrane

Sample collection was conducted along tectonic slices of the Alto Tererê rocks within the Caracol Gneiss. U–Pb dating (LA-ICP-MS) was carried out on detrital zircon for sediment provenance studies. Sample EAR-142A represents a NE-SW trending metasedimentary strata with interlayered amphibolite, occurring ca. 10 km northward from Serra da Esperança. The outcrop is tectonically aligned by the thrust fault. The sample is a muscovite quartzite with granoblastic texture and lepidoblastic layers.

The detrital zircon population exhibits euhedral, subhedral and rounded shapes, as well as fragments ranging from 80 to 250 μm in length. In CL images (Fig. 6), the zircon grains show bright, oscillatory zoned cores, and dark overgrowths, as well as weakly zones. Few metamict grains are also present. Coupled analyses were carried out on few grains. Seventy out of 74 analyses show a nearly continuous spread along the Concordia curve, mostly between 1.81 and 2.0 Ga (Fig. 7C). All spots showed high Th/U ratios, and a few analyses yielded reverse-concordant ages. In any case, the time interval along the Concordia reflects the distinct magmatic sources from which detrital zircon population derived. In the age probability histogram, a unimodal spectrum is observed with a peak at ca. 1.85 Ga (Fig. 7D). The major zircon population yielded ages between 1.90 and 1.80 Ga, roughly matching the ages of the rocks of the Alumiador suite (see Section 4.1.2).

The coupled spot analyses of grain #2 estimated the maximum depositional age of this quartzite to be 1821 ± 50 Ma (oscillatory zoned core, Th/U = 0.94; 101% conc.), and the weakly zoned rim yielded an age of 1790 ± 51 Ma (Th/U = 0.97; 99% conc.). These values are identical, within error, to ages of several other spots: #63.1 (1816 ± 53 Ma; 97% conc.), #35.1 (1813 ± 60 Ma; 98% conc.) and #68.1 (1793 ± 49 Ma; 103% conc.) – see Supplementary Material. Finally, three grains yielded older, reverse-concordant $^{207}Pb/^{206}Pb$ ages, indicating a distinct sedimentary provenance: 2034 ± 43 Ma (#51.1), 2483 ± 48 Ma (#30.2), and 2854 ± 39 Ma (# 1.1) – see Supplementary Material.

Sample MP-82, which is a quartz-muscovite schist, was collected from the southern flank of the Serra da Esperança (Fig. 3). The outcrop is in tectonic contact with the Cerro Porã Granite (1.78–1.72 Ga) and is severely affected by shear zones. This low-metamorphic package extends towards Paraguay, where the metasedimentary rocks were originally called “San Luiz Group” (Wiens, 1986). In thin section, sample MP-82 is essentially composed of quartz, muscovite and sericite, and the sericite content increases near the shear zones. The zircon population usually exhibits fractures and inclusions. High-U, metamict zircon is very subordinate. In CL images, most grains are sub-rounded, subpyramidal or prismatic fragments. They have bright cores (oscillatory

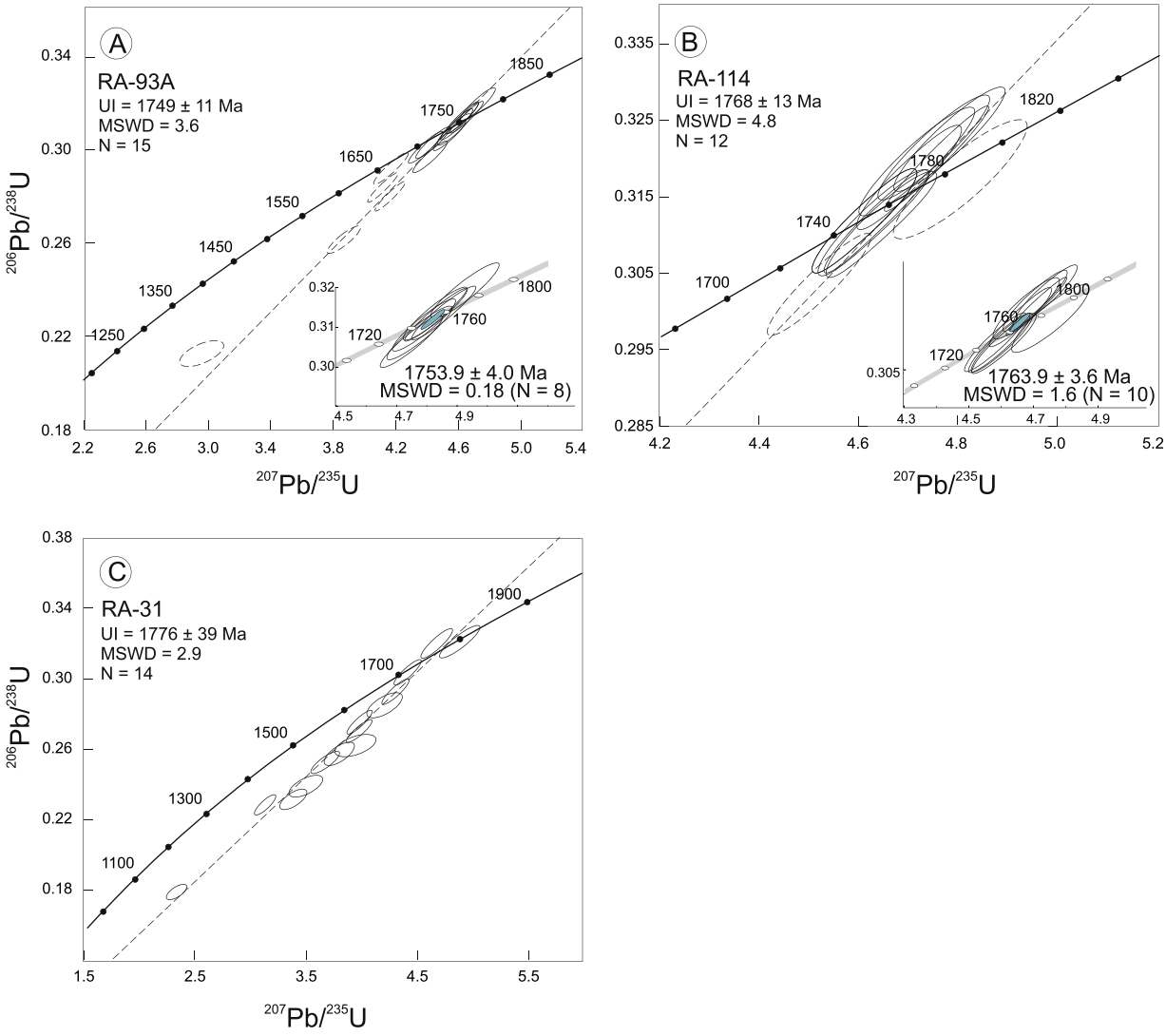

Fig. 9. SHRIMP diagrams for studied rocks in the Eastern Terrane.

or weakly zoned) and thin (dark) rims; some of them show complex internal zoning (see Fig. 6).

Most analytical points were concordant, and 45 out of 64 isotopic analyses on cores yielded $^{207}Pb/^{206}Pb$ ages (concordance 100 ± 10%) that plot on the Concordia from 1.77 to 1.95 Ga (Fig. 7E). Their Th/U values range between 0.17 and 1.90. One grain #48.1 (See Supplementary Material) yielded an age of 1955 ± 29 Ma (97% conc. $^{207}Pb/^{206}Pb$ age), which was identical, within error, to two reverse-concordant spots (# 51.1; #23.1) with $^{207}Pb/^{206}Pb$ ages of 1965 ± 31 and 1966 ± 34 Ma (104% and 103% of conc., respectively; (see Supplementary Material). In the age probability histogram, a unimodal spectrum that peaked at 1.81 Ga was observed (Fig. 7F), with main provenance sources with ages of 1.78 and 1.83 Ga, such as the Alumiador batholith and the Caracol Gneiss (see Sections 3.1.2 and 3.2.2). The youngest grains in the population (e.g., #1.1; #19.1, #22.1) yielded $^{207}Pb/^{206}Pb$ ages of 1769 ± 38 Ma (99% conc.), 1775 ± 34 Ma (98% conc.) and 1771 ± 87 Ma (99% conc.), which were used to estimate the maximum sedimentary age of schist MP-82 (See Supplementary Material). The associated quartzite of Serra da Esperança yielded an identical maximum depositional age of 1777 ± 34 Ma (Cabrera, 2015) with roughly similar provenance sources.

Two quartzite samples (RA-75A and RA-99) were collected at the Cachoeira do Apa (Fig. 3), ca. 20 km to the south of Serra da Esperança. They were collected a few hundred meters apart from both sides of the river. The outcrops are crosscut by abundant quartz veins, and the rocks are folded and thrust over the country rocks. In thin section, the quartzite is composed of quartz, plagioclase, as well as interstitial sericite and epidote, and has a granoblastic texture. The zircon population has varied shapes and sizes, which is consistent with their detrital nature. They usually have bright luminescent cores with internal oscillatory zoning in CL images (not available).

Analytical data from both samples plot similarly on Concordia diagrams of Figs. 7G and 10A, showing a nearly continuous spread of ages, mainly between 1.90 and 1.80 Ga. This suggests a derivation from igneous sources, such as the Alumiador and Caracol rocks. All analyses (total of 144; see Supplementary Material) yielded Th/U ratios between 0.16 and 1.13. Spot # 7.1 of sample RA-75 yielded a significantly older, reverse-concordant age of 2562 ± 69 Ma (108% conc.; Th/U = 0.21). A similar unimodal spectrum was observed for both samples (Figs. 7H and 10B), with dominated provenance sources with ages between 1.93 and 1.73 Ga and age peak at 1.81 Ga. Some spot analyses of samples RA-75A and RA-99A yielded broadly comparable $^{207}Pb/^{206}Pb$ ages around 1750–1730 Ma (e.g., #71.1, #76.1, #26.1 and #53.1, #33.1 and #38,1, see Supplementary Material) that could be the maximum depositional age of the quartzites.

Sample EAR-001 (Fig. 3) is a mylonitic muscovite quartzite with biotite and garnet. In the thin section, it shows granoblastic texture

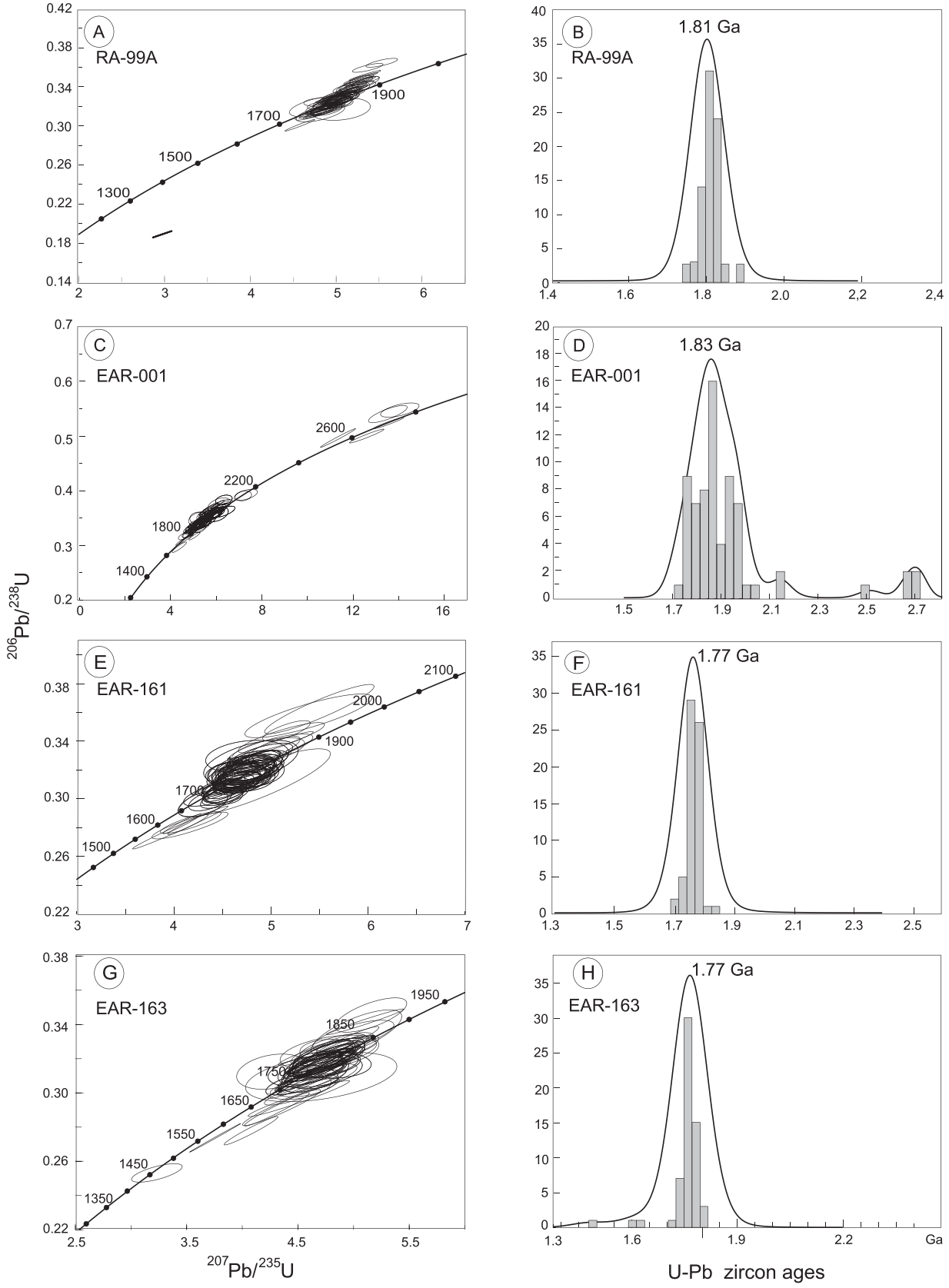

Fig. 10. Concordia and coupled Relative Probability Plots for selected supracrustal rocks of the Alto Tererê Group (Eastern Terrane).

with lepidoblastic layers, where muscovite and quartz are sigmoidal. Biotite-muscovite intergrowth is subordinate. The zircon population consists of prismatic, subprismatic, and/or subrounded grains and fragments, with lengths between 60 and 150 μm, indicating a detrital origin. CL images show both dark and bright luminescent zircons, some of the latter exhibiting sector zoning. A few crystals show metamorphic rims and/or are metamict (see Fig. 6).

Seventy-five out of 81 isotopic analyses plotted concordant and/or slightly discordant in the Concordia diagram (Fig. 10C), showing a nearly continuous spread of ages from 1.71 to 1.98 Ga. Grain (#5) yielded coupled ages of 1854 ± 51 (core; 100% conc.) and 1593 ± 73 (rim; 88%), as shown in Fig. 6, but the latter analysis did not meet the analytical criteria. Two concordant analyses yielded ages of ca. 2.15 Ga (#4.1 and #60.1), whereas four others yielded reverse-concordant Archean ages (e.g., 2514 ± 38 to 2723 ± 33 Ma). In any case, the large age spectra indicate that distinct meta-igneous material formed by different tectonic-magmatic events acted as source for this particular rock. Th/U values ranged from 0.15 to 2.68 (see Supplementary Material).

Fig. 10D shows the age probability histogram, which indicates again contrasting provenance sources with subordinate ages between ca. 2.0 and 1.7 Ga and peaked at 1.83 Ga. The distinct large age spread suggests sedimentary derivation from protoliths, which is similar for the Eastern and Western Terranes (e.g., Porto Murtinho, Morraria, Alumiador, Caracol; see Sections 4 and Table 2). The youngest population (e.g., #63.1, 29.1, 10.1, 8.1, 68.1, 26.1) yielded roughly comparable $^{207}Pb/^{206}Pb$ ages within the error, mostly from 1755 ± 56 to 1747 ± 45 Ma (see Supplementary Material). These ages were used to estimate the maximum depositional age of sample EAR-001.

Samples EAR-161 and EAR-163 were collected from the Serra do Alumiador, right on the Aldeia Tomázia Shear Zone, ca. 10 km away from sample EAR-001 (see Fig. 3). Sample EAR-161, in thin section, is a fine-grained garnet-biotite meta-arkose with garnet porphyroblasts, which has a lepidoblastic matrix texture. The zircons are mainly prismatic, subprismatic, and rounded, and range from 80 μm to 260 μm in length, indicating their detrital nature. In CL images, the population is very complex, including zircon with cores and fractures, as well as zircons with oscillatory zoning, metamorphic rims, engulfment of overgrowth material, and weakly-zoned textures (Fig. 6). Metamict grains and fragments are also observed.

Sixty-four out of 76 analyses of meta-arkose EAR-161 plot on the Concordia, showing a nearly continuous spread between 1.70 and 1.90 Ga (Fig. 10E). A few spots are slightly reverse-discordant. The apparent ages are roughly similar to those of the Alumiador and Caracol rocks. The Th/U ratios ranged from 0.39 to 0.89 (see Supplementary Material). The age probability histogram shows a unimodal spectrum with $^{207}Pb/^{206}Pb$ ages between 1.71 and 1.80 Ga and a peak at 1.77 Ga (Fig. 10F), in contrast with sample EAR-001. Several spot analyses (e.g., # 57.1, 2.1, 37.1, 60.1, 13.1, 21.1; see Supplementary Material) yielded individual $^{207}Pb/^{206}Pb$ ages between 1752 ± 51 and 1736 ± 42 Ma that overlap within the error. These ages defined the maximum depositional age for sample EAR-161.

Sample EAR-163 is located a few kilometers from sample EAR-161. It is a muscovite-quartz schist, which has a granoblastic texture and crenulated foliation. The zircon grains were mainly prismatic or subangular fragments, ranging from 70 μm to 320 μm in length. Most crystals showed dark cores and bright luminescent overgrowths, as well as weakly-zoned textures in CL images (Fig. 6). Metamict grains were subordinate. Analyses on zircon grains yielded Th/U ratios between 0.36 and 1.60 (see Supplementary Material).

Fifty five out of sixty-nine isotopic analyses were performed, and most showed a spread on the Concordia between 1.67 and 1.90 Ga (Fig. 10G). This age spread is roughly similar to that of sample EAR-161 and to the age of the likely sedimentary provenance. In a similar manner, the age probability histogram shows a unimodal distribution with a peak at 1.77 Ma (Fig. 10H). We chose spots #51.1 (1744 ± 51 Ma; 102% conc.) and # 37.1(1747 ± 44; 101% conc.) to estimate the maximum depositional age of sample EAR-161. These ages were similar to those of several others, such as spot #65.1 (oscillatory zone) that yielded an age of 1773 ± 56 (99% conc.), and spot #65.2 (dark core; 105% conc.) with a coupled analysis that yielded a similar age within the error (1713 ± 55 Ma) – see Fig. 6. Finally, two dark high-U cores gave anomalous $^{207}Pb/^{206}Pb$ ages considering the new and compiled data: #59.2 (Th/U = 1.60) with 1607 ± 63 Ma (109% conc.) and #60.2 (Th/U = 1.51) with 1480 ± 51 Ma (98% conc.), whereas their oscillatory magmatic rims (59.1, 60.1) yielded significantly older ages of 1751 ± 51 and 1773 ± 56 Ma, respectively. Therefore, these particular values were not considered in this study. In a similar manner, we did not use spot #45.1 with an age of 1615 ± 47 Ma (96% conc.), given the possible influence of the shear zone and/or fluid migration (see Supplementary Material).

6. Tectonic inferences

The new U–Pb SHRIMP and LA-ICPMS analyses, as well as the compiled geochronological and geochemical-isotopic information, provided new insights on the geodynamic evolution of the RAT. The working model considers the Eastern Terrane coeval with the Southeastern Terrane, given the roughly similar U–Pb crystallization ages within error, though the latter terrane has only two dates (Faleiros et al., 2016). The integrated geochronological interpretation indicates that three major late Paleoproterozoic orogenic events progressively formed the RAT, originating the Porto Murtinho Complex, as well as the Amoguijá and Caracol belts, and the associated supracrustal sequences. Moreover, the available K–Ar and $^{40}Ar–^{39}Ar$ dates show that the RAT underwent an Ectasian tectonic episode, which is consistent with the protracted paleotectonic link with the SW Amazonian Craton, as will be discussed later.

6.1. Porto Murtinho magmatic event

The new zircon SHRIMP U–Pb age of 2069.5 ± 3.9 Ma for a migmatite (see Fig. 4), together with the published ages of the Porto Murtinho Complex (see Table 2), indicates that the early magmatic event in the RAT lasted ca. 100 Myr, much longer than previously thought. There is restricted Nd isotopic evidence for the existence of a partial melting episode in the Porto Murtinho crust, which likely occurred between 2.07 and 1.99 Ga according to the available U–Pb zircon ages (see Section 3.1.1). Tentatively, the negative $\varepsilon_{Nd(t)}$ signatures could be associated with collisional dynamics akin to a continental arc setting, as also suggested by the calc-alkaline affinity of the country rocks of the Western Terrane.

A previous LA-ICP-MS provenance study on the Porto Murtinho Complex (Faleiros et al., 2016) yielded two age modes in the detrital zircon population (2220–1960 and 2980–2520 Ma), in addition to a few reworked zircon grains from Paleoarchean crust (see Sections 3.1 and Table 2). Therefore, these authors concluded that the formation of the Porto Murtinho Complex may have involved distinct sedimentary protoliths. The available T_{DM} ages varied between 2.1 and 3.1 Ga with positive $\varepsilon_{Nd(t)}$ values (+1.3 to +2.9) for rocks of ca. 2.07 Ga and mostly negative (down to −5.8) for rocks with age spanning 1.95–1.88 Ga (Fig. 11A; Table 2; Cordani et al., 2010; Lacerda Filho, 2015). These data suggested that much of the Western Terrane was built on or was adjacent to an ancient continental crust between 2.07 and 1.95 Ga ago, according to the U–Pb crystallization ages and coupled inherited zircon grains in the progenitor magma (e.g., sample RA-65A; see Section 5.1.1). Therefore this early magmatism was dominated by juvenile sources, while the late magmatic events exhibited a significant contribution of recycled crustal material.

The A-type Chatelodo Granite (1902 ± 12 Ma; Faleiros et al., 2016), the São Francisco Granite (1878 ± 7 Ma; Souza et al., 2016 and references therein) and the Fazenda Matão mafic-ultramafic suite

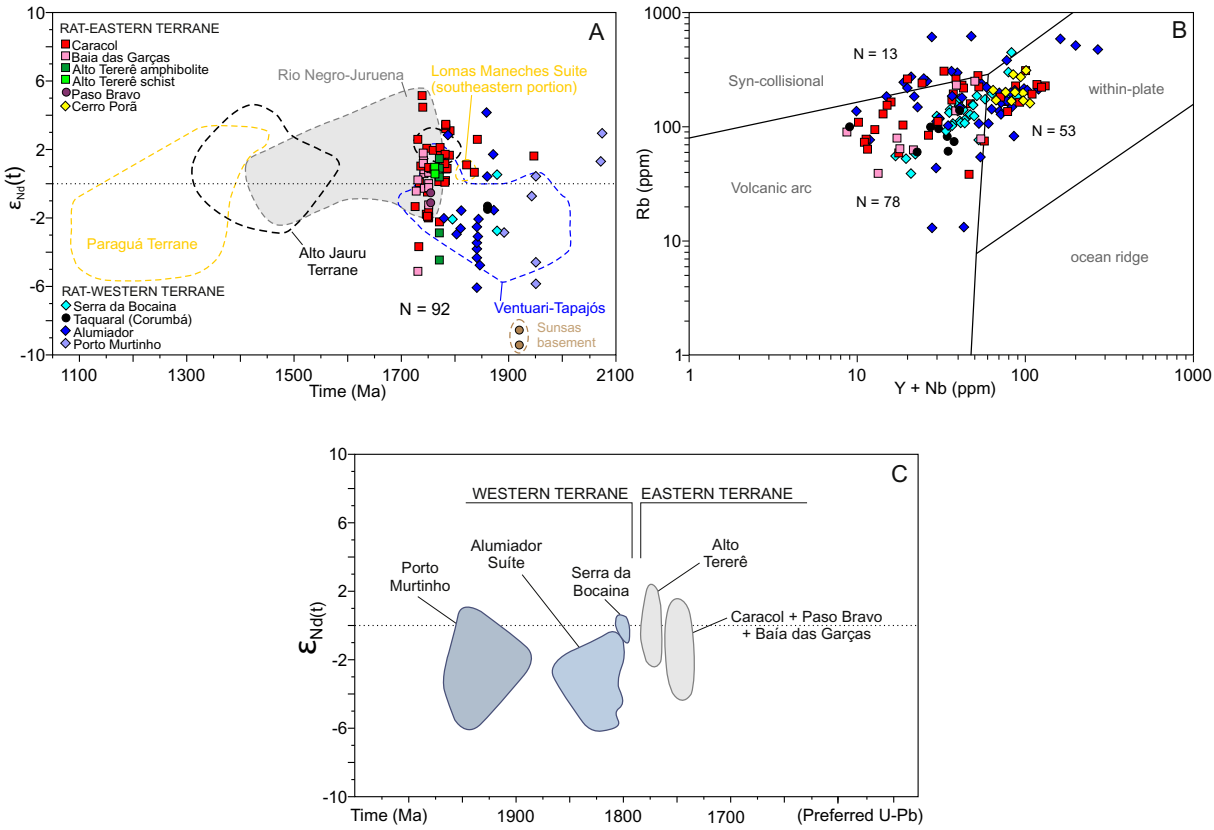

Fig. 11. A) Whole-rock Nd isotopic constraints for the Rio Apa Terrane and potential correlative tectonic units in Amazonia. Data compilation as follows: Rio Apa Terrane (Lacerda-Filho et al., 2006; Lacerda Filho et al., 2016; Cordani et al., 2010; Lacerda Filho, 2015; Redes et al., 2015; Faleiros et al., 2016); SW Amazonian Craton [Ventuari–Tapajós province (Dall' Agnol et al., 1999; Lamarão et al., 2002, 2005; Pinho et al., 2003; Santos et al., 2004), Rio Negro–Juruena province (Santos et al., 2000, 2008; Payolla et al., 2002), Paraguá Terrane (Santos et al., 2008; Matos et al., 2009), and Jauru Terrane (Geraldes et al., 2001; Santos et al., 2008)]; B) Whole-rock elemental geochemical data for granitoid rocks from the RAT (Lacerda-Filho et al., 2006; Godoy et al., 2010, 2014; Manzano et al., 2012; Brittes et al., 2013; Plens et al., 2013; Redes et al., 2015); C) $\varepsilon_{Nd(t)}$ compositional fields against time, showing the contrasting isotopic signatures among the Western and Eastern Terrane rocks. The isotopic values are referred to the U–Pb crystallization ages (data compiled from Cordani et al., 2010; Brittes et al., 2013; Redes et al., 2015; Lacerda Filho, 2015; Lacerda Filho et al., 2016; Costa, 2017). See text for details.

(1.95 Ga; Lacerda Filho, 2015; Costa, 2017) are likely extension-related rock associations (1.90–1.88 Ga). These magmatic episodes followed the tectonic stability of the Porto Murtinho crust. Two rhyolites previously correlated with the Serra da Bocaina Formation could be more likely associated to this specific tectonic setting (1.90–1.88 Ga), given their peculiar U–Pb crystallization ages of 1899 ± 9 Ma (Souza et al., 2016) and 1878 ± 9 Ma (Lacerda Filho, 2015), which are quite older than the typical rhyolites of the Serra da Bocaina Formation (Brittes et al., 2016).

6.2. Amoguijá continental arc

The Amoguijá continental arc activity (Manzano et al., 2012; Godoy et al., 2014; Lacerda Filho et al., 2016) produced voluminous plutonism (e.g., Alumiador granitoid suite) and genetically related volcanic-pyroclastic activity, highlighted by the Serra da Bocaina Formation, currently dated between 1860 and 1830 Ma (Brittes et al., 2016). According to these authors, the close spatial relationship between the plutonic and volcanic rocks, as well as their roughly similar ages and high-K calc-alkaline signatures, supports that their formation occurred during a single orogenic event, which lasted ca. 50 Myr according to the new and compiled ages.

The Alumiador batholith (i.e., Alumiador suite) is intrusive into the Porto Murtinho continental crust (Western Terrane). This batholith yielded new SHRIMP ages of 1857 ± 6 and 1816 ± 7 Ma (see Table 4) and previous U–Pb zircon ages varying from 1841 ± 15 to 1839 ± 33 Ma (Faleiros et al., 2016 and references therein). The nearby 1830 ± 12 Ma Santa Otília batholith and the penecontemporaneous Córrego do Cervo Granite (1841 ± 15 Ma; Faleiros et al., 2016) are also markers of the *syn-* to late-orogenic plutonism. This plutonism is coeval with the rhyolites of the Serra da Bocaina Formation which crystallized at 1831 ± 12 Ma (Brittes et al., 2016) – see Table 2. Trace element whole-rock chemical data (Godoy et al., 2010, 2014; Manzano et al., 2012; Brittes et al., 2013, 2016), coupled with available U–Pb zircon dates, indicate that the chemical signatures of 1860–1830 Ma-aged rocks from the Alumiador suite and Serra da Bocaina Formation are primarily similar to Phanerozoic arc-related granites (Fig. 11B). However, a significant number of samples from these two units present higher contents of Y + Nb, typical of post-collisional or anorogenic granites (Fig. 11B). Because of the complexity of the geochemical signature of the Alumiador suite, it is highly probable that it may have formed through more than one magmatic pulse.

The Alumiador granitic rocks yielded T_{DM} ages in the 2.6–2.4 Ga range, with primarily negative $\varepsilon_{Nd(t)}$ values from −1.4 to −5.9 and minor positive values between +0.5 and +4.2 (4 of 17 data) (Cordani et al., 2010; Lacerda Filho, 2015). The rhyolite from the Serra da Bocaina Formation yielded T_{DM} ages around 2.3 Ga with roughly similar negative $\varepsilon_{Nd(t)}$ values (−1.7 to −2.2). As such, these rocks probably derived from protoliths with a short crustal residence and with subordinate juvenile input (Cordani et al., 2010; Brittes et al., 2016). Elemental and Sm–Nd isotope geochemical data coupled with geological relationships are consistent with crustal contamination during slab subduction beneath a Paleoproterozoic active margin, represented by the newly established Porto Murtinho continental crust.

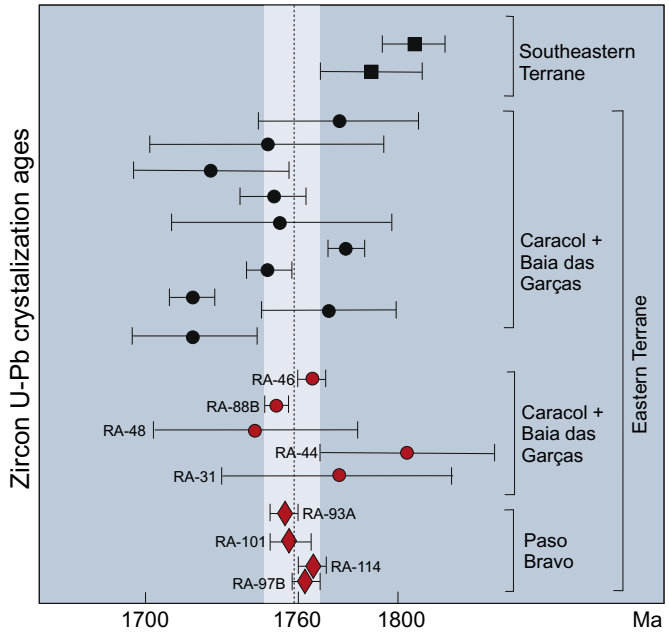

Fig. 12. New (red symbols) and compiled U–Pb ages for granitoid samples of the Eastern and Southeastern Terranes (dots) and Paso Bravo province (diamonds) - RAT. Black dots (published data). Gray zone represents the time interval of the magmatic activity (1780–1740 Ma), given by the most precise U–Pb SHRIMP analyses. The dashed line shows the possible magmatic peak at ca. 1760 Ma. See text for details. (For interpretation of the references to colour in this figure legend, the reader is referred to the web version of this article.)

The ages of the Alumiador suite are very similar to the ones of the granitoid rocks of the distal Corumbá Window, U–Pb zircon crystallization ages of 1869 ± 5 Ma (this work) and 1861 ± 5 Ma (Taquaral batholith; Redes et al., 2015). This fact indicates the possible extension of the Amoguijá continental belt to the region of Corumbá. The Taquaral pluton yielded slightly negative $\varepsilon_{Nd(t)}$ values (−1.5 and −1.3; Fig. 11A) and T_{DM} ages of 2.3 and 2.2 Ga (Redes et al., 2015), which are roughly similar to those of the Alumiador rocks. This pluton is composed of metaluminous to peraluminous high-K calc-alkaline rocks (Redes et al., 2015) with trace element signatures typical of arc-related granites (Fig. 11B), which are comparable to those of most of the Amoguijá granitic rocks.

The undeformed Aquidabã Granite (1811 ± 7 Ma; Brittes et al., 2016), as well as the Serra da Alegria suite (ca. 1790 Ma) and the Morro do Triunfo Gabbro that crosscut the Porto Murtinho belt could be related to the post-orogenic to anorogenic phases of the Amoguijá arc.

6.3. The Caracol arc and the Alto Tererê back-arc basin

The Caracol Gneiss and the associated weakly deformed leucogranites make up much of the Eastern Terrane, mostly derived from short-lived protoliths (Orosirian) given the available Nd and Hf isotopic constraints (Cordani et al., 2010; Plens, 2018). The new SHRIMP crystallization ages for three nearby samples of the Caracol Gneiss (1767.0 ± 5.4, 1758.8 ± 7.3 and 1765.3 ± 4.1 Ma) agree well within errors with the compiled data for this tectonic unit (e.g., Cordani et al., 2010; Faleiros et al., 2016). The Baía das Garças suite and the Paso Bravo granitoid rocks show roughly similar U–Pb zircon ages with those of the Caracol Gneiss - see Table 2. The new and compiled ages for the Eastern Terrane (1800–1740 Ma) indicate these rocks originated ca. 40 Myr after the tectonic stability of the Amoguijá arc (1870–1820 Ma). The northern portion of the Caracol Gneiss is roughly bounded by the Morraria Gneiss continental fragment (1950 ± 23 Ma; Cordani et al., 2010).

The Caracol Gneiss is overlain by or tectonically interleaved with the metavolcanic-sedimentary rocks of the Alto Tererê Group (< 1.77 Ga; Lacerda Filho et al., 2016). The basal amphibolite of the Alto Tererê Group was interpreted as linked to an extensional phase of a back-arc basin, dated at 1768 ± 6 Ma (Lacerda Filho et al., 2016). The chemical-isotopic signatures of the metabasic rocks showed mixed characteristics of MORB and island arc basalts, including depletion in high field strength elements, enrichment in large ion lithophile elements relative to normal MORB. The coexistence between positive and negative $\varepsilon_{Nd(t)}$ values (−5 to +3; Fig. 11A) is coherent with the effects of an original subducted component. (Lacerda Filho et al., 2016).

Fig. 12 presents the available ages for the Caracol Gneiss, the Baía das Garças suite, and the granitoid rocks located in the Paso Bravo Province (1753.9 ± 4.0 Ma and 1763.9 ± 3.6 Ma). We also note that two rocks of the Southeastern Terrane yielded U–Pb zircon ages similar to those of the rocks of the Eastern Terrane, suggesting that they could share the same evolutionary history. More precise U–Pb zircon crystallization ages fall between 1780 and 1740 Ma, with a possible peak at ca. 1760 Ma, as shown in Fig. 12. The Cerro Porã Granite, located in the southwestern portion of the study area, yielded roughly similar ages (1781 ± 7 to 1721 ± 25 Ma; Faleiros et al., 2016 and references therein).

The Caracol and Baía das Garças granitoid rocks present trace element contents similar to arc-related granites (e.g., Rb and Y + Nd contents; Fig. 11B). Rocks from both suites yielded roughly equivalent T_{DM} ages (2.0–2.2 Ga). The $\varepsilon_{Nd(t)}$ values were positive (up to +5.5) with subordinate negative values down to −5 (Fig. 11A). This bulk signature is consistent with a dominant input from a juvenile magma source with minor contamination from short-lived magmatic protoliths in an arc setting (Cordani et al., 2010). In a similar manner, two granitoid samples collected in the Paso Bravo province (see Fig. 3) yielded T_{DM} ages of 2.2 and 2.4 Ga, and $\varepsilon_{Nd(t)}$ values of −0.5 and − 1.1. Such particular signatures might have been influenced by metasomatic fluids, active during slab subduction, away from the Western Terrane, in agreement with the model of Cordani et al. (2010). In fact, the Nd isotopic constraints clearly contrast with that of the Western Terrane (Porto Murtinho and Amoguijá belts), whose rocks are widely dominated by negative $\varepsilon_{Nd(t)}$ values (Fig. 11A), and originated ca. 50 to 100 Myr earlier.

6.3.1. Tectonic model

New and compiled data (Table 2) confirmed that the Caracol accretionary arcs, which were active from 1780 to 1740 Ma, formed the Eastern Terrane, as envisaged by Cordani et al. (2010). The Baía das Garças suite, the country rocks of the Southeastern Terrane and the Paso Bravo granitoid rocks are considered to be genetically associated with the evolution of the Caracol magmatic arcs, given their age similarity and coherent isotopic constraints. The evolution of the Caracol arcs includes the Alto Tererê volcanic-sedimentary sequence, formed in a back-arc setting. The new and compiled zircon provenance studies indicated that the siliciclastic metasedimentary rocks were mainly derived from Orosirian to early Statherian magmatic sources.

The revised model proposed here for the Caracol arcs is primarily similar to the dynamic setting for the Solomon convergent margin following a collision with the Ontong Java Plateau, as envisaged by Stern (2004). According to this author, such a scenario could be distinguished in terms of induced nucleation of subduction zones (INSZ), developed in response to continuing plate convergence. Likewise that particular tectonic setting, we consider that the Caracol early subduction zones (present coordinates) were initially westward, whilst evolved away from the Amoguijá belt (i.e., Western Terrane). Continued oceanic closure and eventual collision with a microcontinent (e.g., Morraria Gneiss) resulted in new subduction zones (with reversal polarity) formed behind the magmatic arc. As a matter of fact, the Caracol products did not intrude the Western Terrane; instead, the eastward slab subduction was a causal relationship for the emplacement of the Baía

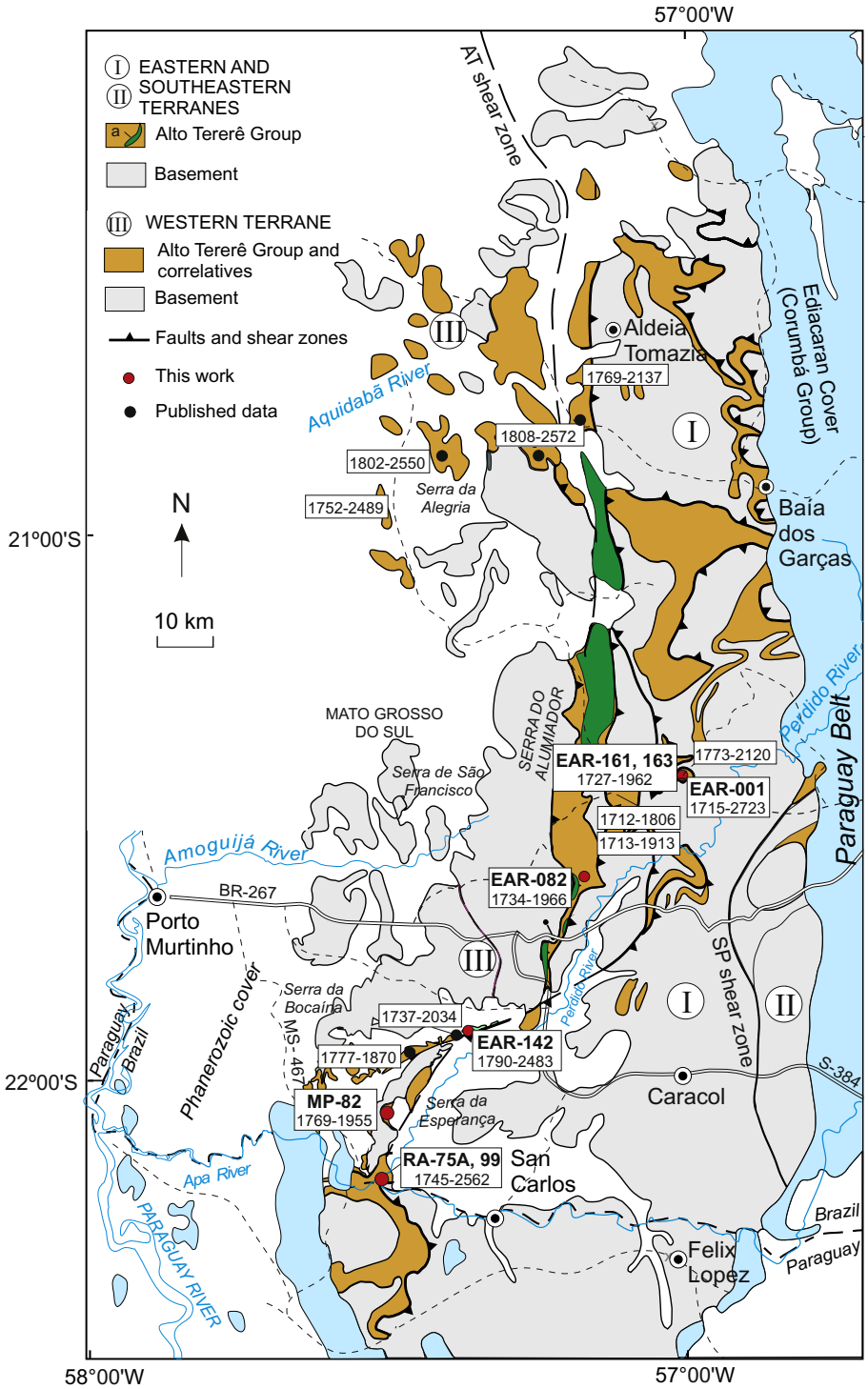

Fig. 13. Simplified geologic sketch of the Western and Eastern terranes with the geographic distribution of the Alto Tererê Group and correlative units, according to the working model. The range of the detrital zircon ages (new and compiled data) is shown in the boxes (samples in bold from this work).

das Garças granites into the foreland (Morraria Gneiss), affecting only part of a plate margin such as the case of INSZ (Stern, 2004).

This geodynamic process explains the dominant juvenile nature of the Caracol arcs, including the Alto Tererê magmatism, though influenced by metasomatic fluids associated to the subducted slabs. This hypothesis is consistent with the available positive and slightly negative $\varepsilon_{Nd(t)}$ values (see Fig. 11C). Small proportions of short-lived protoliths were also suggested during magma genesis, given by the more negative $\varepsilon_{Nd(t)}$ values, reflective of the subduction melts below the Morraria continental crust. The working model is also coherent with the variable positive and negative zircon $\varepsilon_{Hf(t)}$ values and coupled Lu−Hf T_{DM} model ages between 1.9 and 2.3 Ga for the Caracol rocks (Section 3.2.2). From the above, the isotopic characteristics of the Caracol belt differ from the Amoguijá continental belt (Western Terrane), whose rocks derived mainly from crustal-recycled material as indicated by the Nd isotopic constraints (Fig. 11C).

The progressive oceanic closure eventually docked the Eastern Terrane onto the continental margin of the Western Terrane (e.g.,

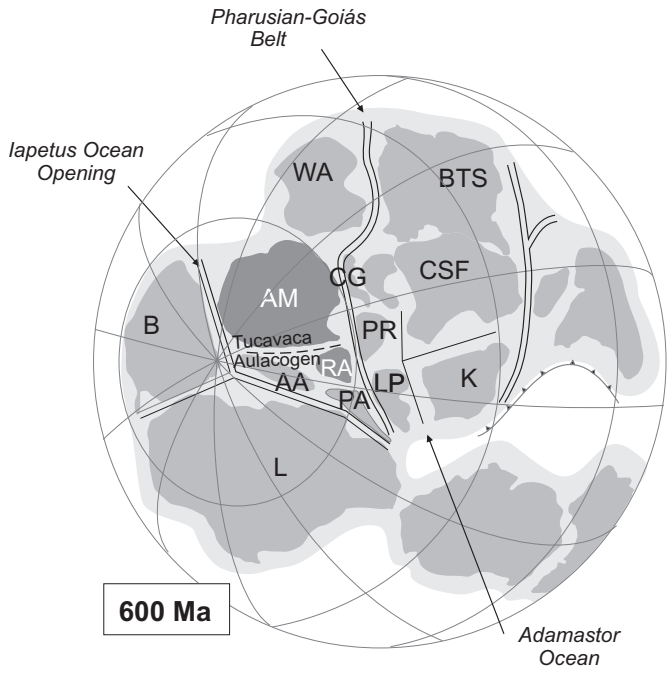

Fig. 14. Paleogeographic reconstruction of West Gondwana, showing the collisional Pharusian-Goiás Belt, related to the arrival of the Amazonia (AM) and West Africa (WA) at the Ediacaran as a result of the closure of a large ocean. The separation between Amazonia and Laurentia after 600 Ma marks the opening of the Iapetus Ocean (Cordani et al., 2009). See text for explanation. L: Laurentia; B: Baltica; K: Kalahari; CSF: Congo–São Francisco; LP: Rio de la Plata; RA: Rio Apa; AA: Arequipa-Antofalla; PR: Paraná; PA: Pampia. Pale gray represents the intervening Neoproterozoic belts.

Cordani et al., 2010) along the Aldeia Tomázia shear zone, leading to the RAT tectonic consolidation. Although the time of docking between the Western and Eastern Terranes is still uncertain, it may have occurred shortly after the tectonic stability of the Caracol arc. This thought derives from the model applied to the Amazonian Craton, whose growth is considered to be a result of continued soft collision and accretion processes through time and space (Cordani and Teixeira, 2007) – see Section 2. Our hypothesis contrasts therefore with other models that proposed that the juxtaposition of the Western and Eastern Terranes occurred much later.

Finally, in the Ectasian period, the RAT underwent crustal shortening and deformation. This process was responsible for the Barrovian-type metamorphism over the Alto Tererê Group, as well as the concomitant west-verging tectonic slices of the metavolcanic-sedimentary strata interleaved with inliers of the country rocks (Faleiros et al., 2016; Lacerda Filho et al., 2016) - see Figs. 2 and 3. This episode was also indicated by few $^{207}Pb/^{206}Pb$ ages in monazite from an amphibolite facies kyanite-garnet-biotite schist sample of the Alto Tererê Group (Lacerda Filho et al., 2016) and in a metamorphic zircon (Th/U < 0.08) from samples RA-44 (see Fig. 8A) and RA-48 that are attributed to the Caracol Gneiss (Fig. 8C). Crustal exhumation of the RAT occurred in the time interval 1370–1270 Ma, revealed by a large number of K−Ar and $^{40}Ar-^{39}Ar$ dating (Table 2).

7. Alto Tererê Group: detrital zircon constraints

All samples considered to be analogous to the metasedimentary rocks of the Alto Tererê Group have practically unimodal spectra with roughly similar maximum depositional ages across the RAT, ranging from 1.72 to 1.79 Ga. A restricted distributary sedimentary provenance with predominant Statherian age modes was obtained for most samples, which is consistent with the main age of the Eastern Terrane rocks, highlighted by the Caracol Gneiss. Such detrital zircon constraints agree well with the reported U−Pb zircon age (1768 ± 6 Ma), interpreted as the crystallization age of the amphibolitic layer interspersed within the basal sedimentary strata of the Alto Tererê Group (see Section 3.2.3). Therefore the basin infill was probably concomitant with the exhumation of the Caracol belt. In particular, the subordinate age mode of ca. 1.74 Ga of the detrital zircon population from samples RA-75A/RA-99 might suggest a fast exhumation of the Eastern Terrane.

We note that our youngest zircon population ages, given the typical errors of the LA-ICP-MS analyses, largely overlap with the maximum depositional ages reported for similar siliciclastic supracrustal rocks (i.e., Alto Tererê equivalents) that occur in the Western Terrane around the Serra da Alegria (e.g., Cabrera, 2015; Lacerda Filho, 2015). Some of these rocks located at the northwest portion have been interpreted to belong to the Rio Naitaca Formation, given that a basal lapilli tuff of the package yielded an age of 1813 ± 18 Ma (Faleiros et al., 2016). Nevertheless, based on the new and compiled detrital provenance data, we suggest that all the metavolcanic-sedimentary sequences across the RAT are roughly coeval, despite their contrasting metamorphic and deformation characteristics from place to place.

Fig. 13 shows the geographic distribution of the Alto Tererê Group and its probable correlatives across the RAT, in the light of the new and compiled detrital zircon constraints of the siliciclastic rocks. The variable age range shown in the boxes indicates again heterogeneous sources (mainly Paleoproterozoic), from which the precursor basin material was derived. Few samples (e.g., Figs. 7D, F and 10D) indicated sedimentary provenance shifts from place to place (Fig. 3). Recycled zircons from the Western Terrane (Porto Murtinho and Amoguijá tectonic units) were present, as indicated by Orosirian-type ages (see Figs. 7 and 10), although detritus from the passive margin of the Amoguijá belt predominate. The provenance history of the Alto Tererê precursor basin is consistent with active margin settings (trench, forearc, and back-arc basins), where the basins are dominated by detritus with ages roughly similar to the time of their sedimentation, as exemplified by Cawood et al. (2012). The detrital zircon age signatures, coupled with the chemical affinity of the Alto Tererê metabasic rocks, suggest a back-arc setting for the precursor basin (Lacerda Filho et al., 2016).

Finally, the Alto Tererê Group has a potential equivalent in the southern portion of the Ventuari-Tapajós province where a volcano-sedimentary sequence (rift-type) fills the Cachimbo tectonic basin (see Table 1). This sequence showed detrital provenance with significant proportion of 1.81–1.85 Ga zircon grains such as many of the Alto Tererê samples as depicted in Figs. 7 and 10. These samples also showed few Archean zircons, but up to the present, Archean crust was not observed in the RAT. These zircons may have been derived from sources like the oldest documented remnants in a cratonic block within the eastern portion of the Rio Negro-Juruena province (see Section 2) or even the distal Carajás region in the Amazonian Craton, and then recycled during the sedimentation of the Alto Tererê basin.

8. Tectonic correlations and paleogeographic inferences

In this section we will discuss the tectonic affinity among the RAT and the SW Amazonian Craton, using the most recent geochronologic information that is integrated with the geochemical-isotopic evidences and geophysical information. Pertinent aspects of the position of Amazonia and RAT in Columbia and Rodinia are also addressed, considering the coherent geometry among the roughly coeval accretionary orogens around the world and LIP barcode matches.

8.1. RAT affinity with SW Amazonian Craton

During the West Gondwana assembly, the RAT was already attached to the SW edge of the Amazonian Craton (e.g., Cordani et al., 2009), and was the stable foreland for the intervening Paraguay belt (Figs. 1

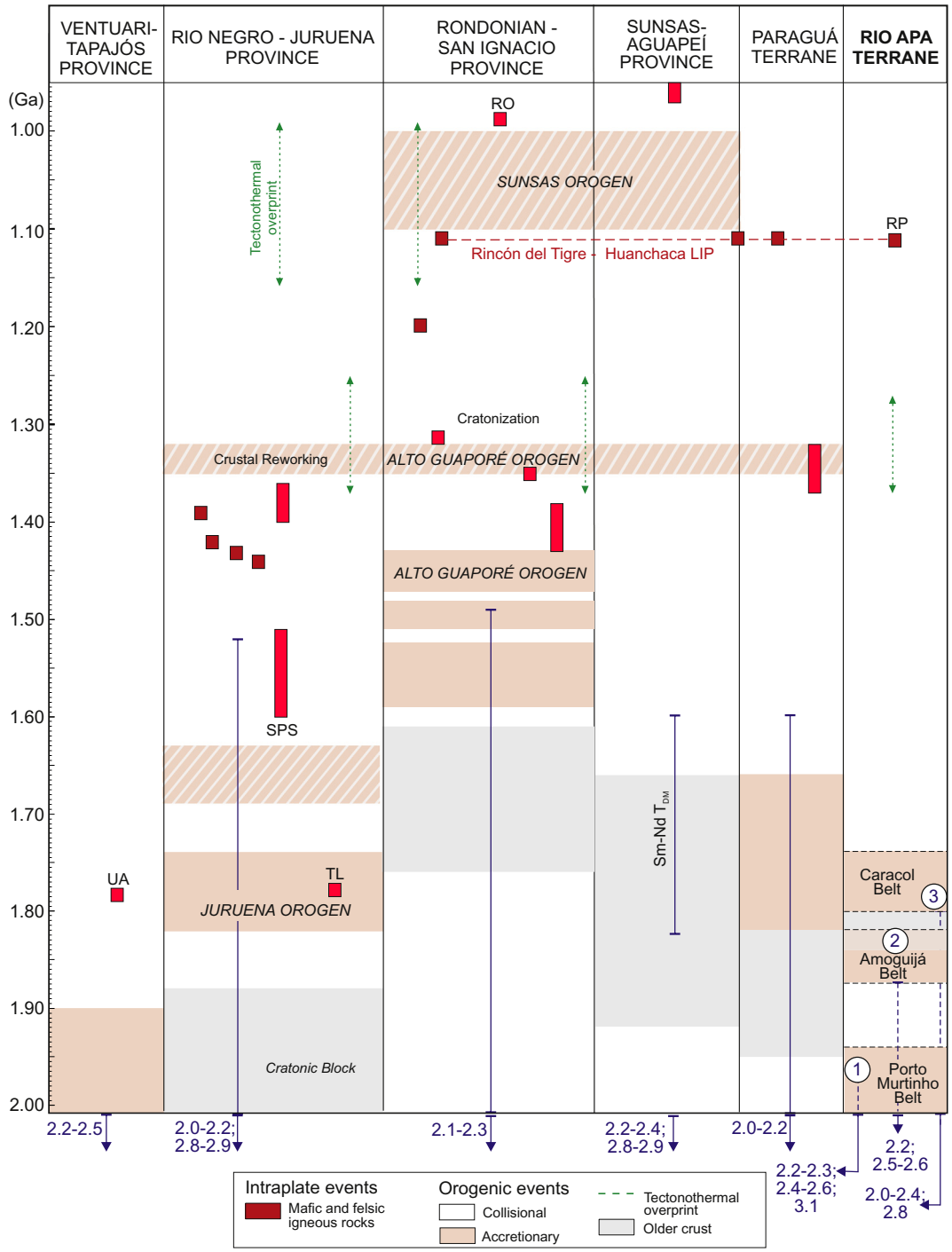

Fig. 15. Time-correlation tectonic chart for the Rio Apa Terrane and Paleo- to Mesoproterozoic provinces of the SW Amazonian Craton (adapted from Teixeira et al., 2019b), highlighted by the nominated orogenic events as discussed in the paper. Selected intraplate episodes (red symbols) are also shown: UA (Uatumã SLIP), TL (Teles Pires suite); SPS (Serra da Providência suite); RP (Rio Perdido Suite); RO (Rondônia Tin Granites). Dashed vertical bars (green) represent the range of K–Ar and ^{40}Ar–^{39}Ar ages. Vertical bars in blue show the range of the Sm–Nd T_{DM} ages (Ga). See text for explanation. (For interpretation of the references to colour in this figure legend, the reader is referred to the web version of this article.)

and 3). In such a perspective, the Tucavaca belt (see Fig. 1) - whose gently folded sedimentary units are correlative to the lithostratigraphic units of the Paraguay belt - would be an early aulacogen developed over the prolongation of the Amazonian Craton (present coordinates), though reflecting Ediacaran-aged deformation linked with the supercontinent assembly (Cordani et al., 2010 and references therein).

The position of the RAT to the west of the Transbrasiliano lineament (e.g., Curto et al., 2014; Cordani et al., 2016a) – the most significant continental-sized discontinuity in South America (Section 2) - also favors the protracted affinity of the RAT with the SW Amazonian Craton, rather with the Paranapanema block and the Rio de la Plata Craton (Fig. 14). This is an important contrast regarding other models (e.g., Gaucher et al., 2011 and references therein; Dragone et al., 2017). Indeed, these two latter cratonic units occur along the southern expression of the Transbrasiliano tectonic boundary in the opposite side of the Pampean Terrane (e.g., Peri et al., 2015; Cordani et al., 2016a; Ramos, 2018 and references therein). This fact determines that the Rio de la Plata Craton has a paleogeographic scenario coherent with the São

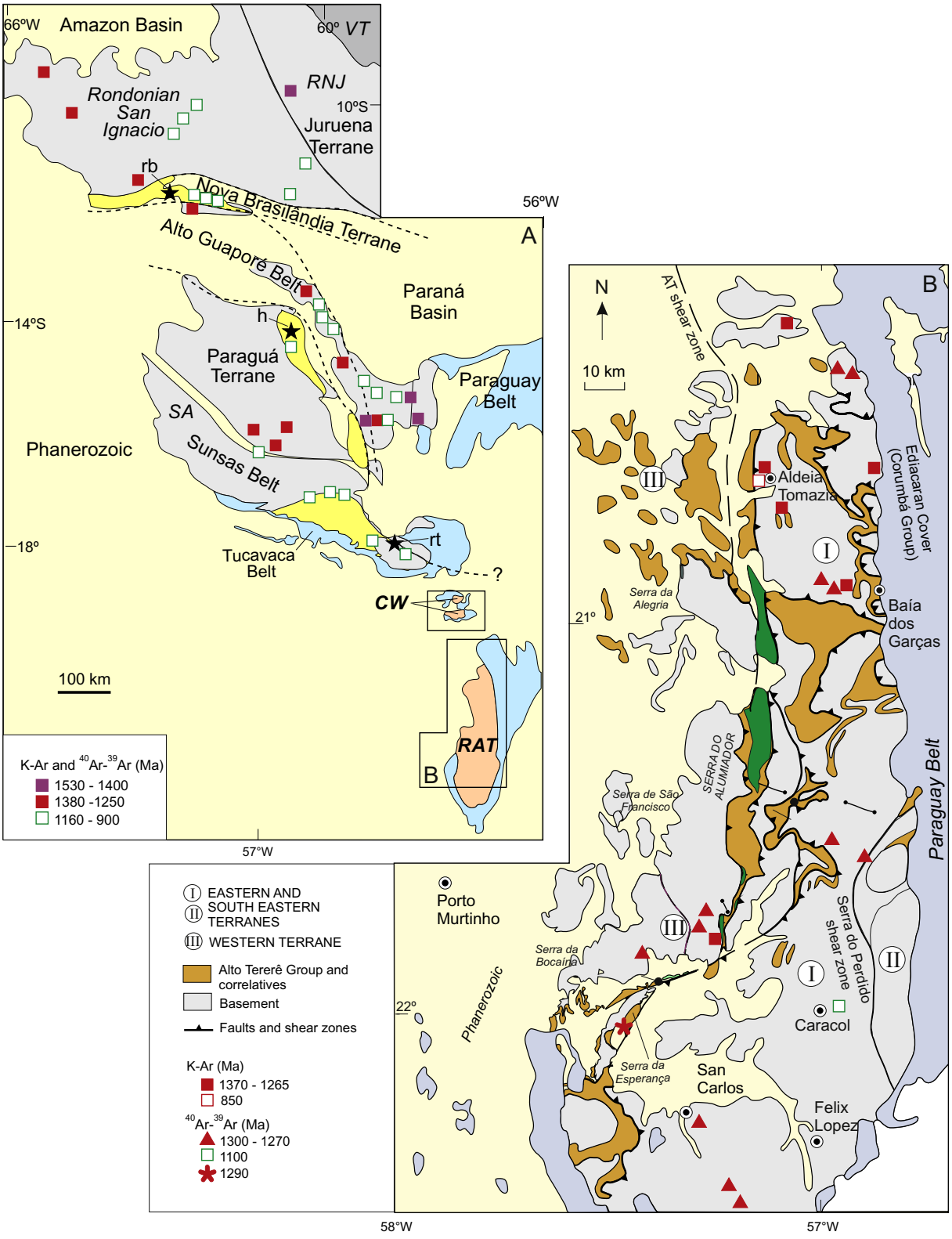

Fig. 16. Compilation of K–Ar and ^{40}Ar–^{39}Ar dates for the Rio Apa Terrane and the SW Amazonian Craton (data from Litherland et al., 1986, 1989; Cordani et al., 2010; Teixeira et al., 2010; Bettencourt et al., 2010, Tohver et al., 2004, 2006; Ruiz, 2005; Ruiz et al., 2014). The asterisk indicates the ^{40}Ar–^{39}Ar muscovite date in quartzite from the Alto Tererê Group. Geologic framework adapted from Figs. 1 and 3. See text for details.

Francisco Craton, the Paranapanema Block and other tectonic elements in the African counterpart within West Gondwana, which is also supported by the compelling paleomagnetic evidence (Halls et al., 2001; D'Agrella-Filho and Cordani, 2017; Rapalini, 2018; Teixeira et al., 2013). In any case, the RAT may have undergone some drift relative to Amazonia, as suggested by the NS-NNE tectonic architecture of the RAT that contrasts with the typical NW-SE trending provinces of the SW Amazonian Craton.

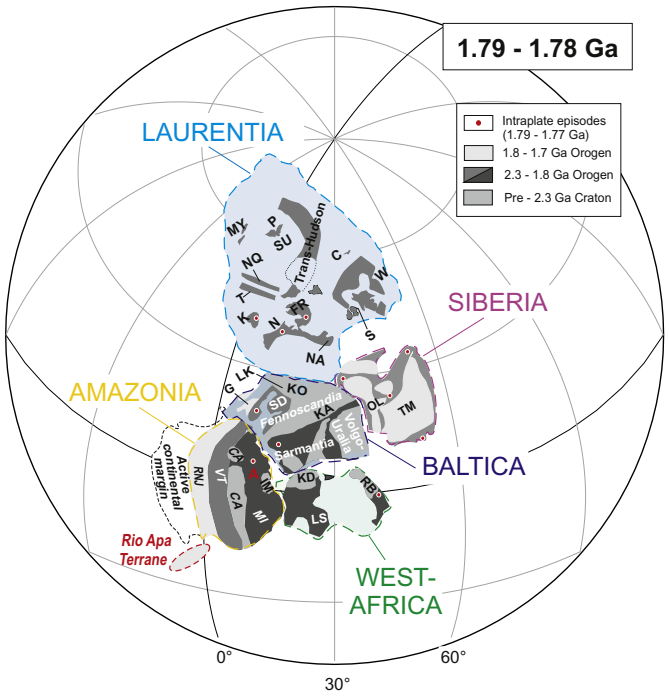

Fig. 17. The proto-Amazonian Craton (Amazonia) and the Rio Apa Terrane in Columbia at 1790–1780 Ma (adapted from Evans and Mitchell, 2011; Bispo-Santos et al., 2014 and Xu et al., 2014), based on geologic connections and quality-filtered paleomagnetic poles (not shown). The Avanavero (1.79 Ga) LIP and penecontemporaneous-like magmatism in the nearest crustal blocks are also shown (after Youbi et al., 2013). Keys: Amazonia and RAT in yellow; Laurentia in light blue; Baltica in dark blue, West Africa Craton in green, and Siberia in pink. Archean blocks and Paleoproterozoic belts (in gray): Laurentia (S–Slave; C–Churchill; SU–Superior; N–Nain, NQ–New Quebec; T–Torngat; W–Wopmay; P–Penokean; K–Ketilidian; NA–Nagssugtoqidian; FR–Foxe-Rinklan), Baltica (KO–Kola; KA–Karelia, LK–Lapland-Kola; SD–Svecofennian Domain; G–Gothian Province), Amazonia (CA–Central Amazonian, MI–Maroni-Itacaiunas;VT–Ventuari-Tapajos; RNJ–Rio Negro-Juruena), West Africa (LS–Leo shield, KD–Kenemanan Domain, RB–Requibat shield) and Siberia (TM–Tungus-Malan and OL-Olenek domains). See text for details. (For interpretation of the references to colour in this figure legend, the reader is referred to the web version of this article.)

In pre-Gondwana times, the position of the RAT in relation to other continental masses is debatable. It has been postulated that it was either allochthonous or autochthonous during the Paleo- to late Mesoproterozoic accretion of the Amazonian Craton. For example, paleo-reconstructions have been proposed between RAT and a continental mass called Pampia (Ramos et al., 2010), as well as with the Arequipa-Antofalla basement (also termed the Arequipa Terrane), both of them hidden below the sedimentary cover in central South America. In a similar manner, it has been suggested that several late Paleoproterozoic blocks like Pampia, Arequipa and the RAT, though largely overlain by the mentioned Phanerozoic sedimentary cover, may have formed a major continental mass (Mara Craton) which eventually collided with a growing Amazonia at ca. 1.3 Ga ago (e.g., Casquet et al., 2008, 2012).

If a correlation between the RAT and Pampia is rather possible, in our view the Arequipa Terrane - one of the allochthonous inliers in the Andes (e.g., Ramos, 2018 and references therein) – seems not to have a direct geologic-tectonic affinity with the RAT; it may have originated as a disrupted part of prior continental masses (e.g., Laurentia) and may have been trapped together with other crustal fragments, in the Stenian period, during the Grenville/Sunsas collage as part of the Rodinia formation (e.g., Cordani et al., 2000, 2009, 2010; Chew and Cardona, 2011; Tohver et al., 2006).

Among the autochthonous models for Amazonia, Cordani et al. (2010) considered a tectonic correlation between the RAT and the Rio Negro-Juruena province of the Amazonian Craton, given the roughly age-equivalent lithostratigraphic units and the contemporary events. Faleiros et al. (2016) suggested that the RAT could be a dispersed fragment of the southern sector of the Ventuari-Tapajós province in the light of the coherent U—Pb zircon ages with the Porto Murtinho and Amoguijá rocks, as well as the very similar $\varepsilon_{Nd(t)}$ signatures. An alternative correlation between the Porto Murtinho gneisses and the ca. 1.92 Ga crystalline basement in the Sunsas belt (Vargas-Matos et al., 2011) was also envisaged by Faleiros et al. (2016) - see Fig. 1 and Table 1.

8.2. RAT and growing Amazonia

Fig. 15 shows a comparative time-correlation chart of the documented orogenic events and intraplate magmatism in the RAT and the SW portion of the Amazonian Craton, providing the pertinent paleotectonic inferences for our review. From this perspective, we envisioned that the Ventuari-Tapajós province and the Rio Negro-Juruena province (Juruena orogen) are the best possibilities for a protracted link with the RAT. Another potential correlation could be with the possible protoliths of the Paraguá Terrane, given the age similarities (e.g., Cordani et al., 2010; Lacerda Filho et al., 2016).

In particular, the orogenic processes that formed the Ventuari-Tapajós and Rio Negro-Juruena provinces are remarkable contemporary with the Porto Murtinho (2.07–1.94 Ga), Amoguijá (1.87–1.82 Ga) and Caracol (1.80–1.74 Ga) belts (see Table 1). Specifically, the Porto Murtinho rocks are age-equivalent with calc-alkaline orthogneisses (2.05–2.03 Ga) and granitoid suites (1.97–1.93 Ga) of a cratonic block within the eastern portion of the Rio Negro-Juruena province (Central Brazil shield), correlative to the Tapajós crust (see Section 2). In a similar manner, the eastern portion of the Juruena Terrane includes the 1.78–1.76 Ga Teles Pires suite and the Colider and Roosevelt volcano-sedimentary sequences (1.78–1.74 Ga) that are roughly coeval with the granitoid rocks of the Caracol belt.

From the above pieces of evidence, the RAT seems to be genetically related to the accretionary edge of Amazonia during the late Rhyacian to early Statherian periods. Moreover, Fig. 11A shows that the entire Eastern Terrane (RAT) shares ages and Nd isotopic similarities with the Rio Negro-Juruena province. The rocks from the Porto Murtinho, Alumiador and Serra da Bocaina units predominantly disclose negative $\varepsilon_{Nd(t)}$ values that partial share the Ventuari-Tapajos isotopic field. However, in contrast, juvenile-like isotopic signatures are apparent for some rocks of the Western Terrane. Fig. 11A also shows the contrasting Nd compositional fields of the Sunsas basement, and the Alto Jauru and Paraguá terranes (except the Lomas Maneches protoliths) compared to the RAT. From the above, the tectonic affinity among the RAT and the Rio Negro-Juruena and Ventuari-Tapajós provinces is reinforced.

From a paleogeographic perspective, these two tectonic provinces in the SW part of the Amazonian Craton exhibit progressively younger lithostratigraphic units towards southwest within the Brazil Central shield with typical NW-SE trending structures (see Fig. 1). This framework contrasts with the NS-NNE tectonic architecture of RAT units, where the oldest ones make up the Western Terrane (Porto Murtinho and Amoguijá belts) while the youngest units comprise the Eastern Terrane (i.e., 1.80–1.74 Ga Caracol belt). In consequence, the RAT - if it was indeed once attached as a component of the Ventuari-Tapajós and Rio Negro-Juruena provinces, – should have separated and acted as a microplate shortly after its accretion onto Amazonia. From a geodynamic perspective, our working model for the Caracol magmatic arcs (Section 6.3.1) implies that plate motion of RAT occurred sometime after final docking of the Caracol belt onto the Western Terrane, though preserving the close affinity with the Amazonia.

Next, we evaluate the potential correlation among the RAT and Amazonia in the Ectasian. Fig. 16 displays a regional distribution of

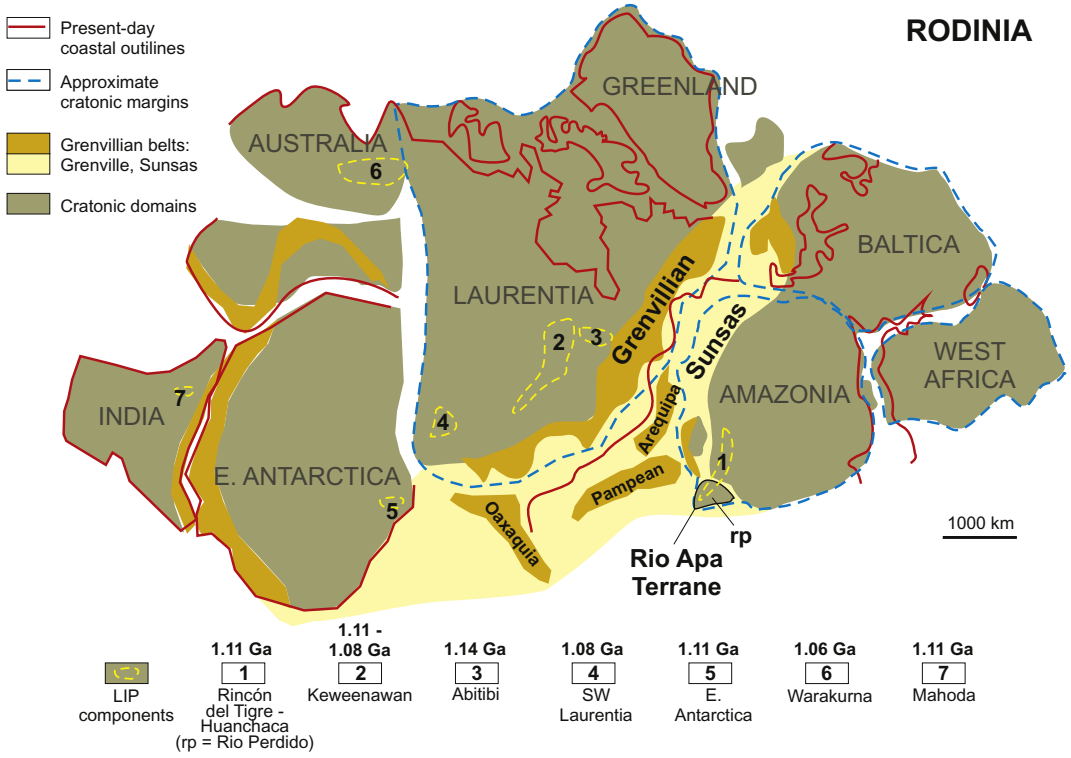

Fig. 18. Reconstruction of the core of supercontinent Rodinia (1.1–0.9 Ga), highlighted by the Grenvillian-Sunsas tectonic match between Laurentia and Amazonia (adapted from Li et al., 2008; Roberts, 2013; Johansson, 2014; D'Agrella-Filho and Cordani, 2017). The Rincón del Tigre-Huanchaca LIP (1.11 Ga) and its correlatives around Rodinia are also shown, highlighted by the Keweenawan plume (1.11–1.08 Ga) in Laurentia – considered a closest neighbor with Amazonia at the time (compiled data from Ernst, 2014).

K−Ar and $^{40}Ar-^{39}Ar$ mineral ages, indicating the important role of tectonothermal/exhumation processes in the Ectasian period (data compilation from Litherland et al., 1986, 1989, Tohver et al., 2004; Teixeira et al., 2010; Bettencourt et al., 2010; Cordani et al., 2010). In this sense, the Rondonian-San Ignacio province and the Paraguá Terrane have a remarkable age match with the RAT in the range 1370–1270 Ma. In addition, a few documented U−Pb monazite ages in the Eastern Terrane, as depicted in Fig. 16 (Lacerda Filho et al., 2016), confirm that affinity. Such a robust coherence from the tectonic point of view suggests that the RAT underwent the tectonic/metamorphic offshoots of the outboard Alto Central Brazil orogeny (e.g., Bettencourt et al., 2010; Rizzotto et al., 2013) – see Section 2. Therefore, at this time, the RAT was a very probable close neighbor of Amazonia.

Finally, we consider the case of the 1.11 Ga Rincón del Tigre-Huanchaca LIP (Teixeira et al., 2015) of SW Amazonia which allows a tight age match with the mafic dikes of the Rio Perdido suite in the RAT (see Fig. 3). Both blocks, most likely, were good neighbors also at 1.11 Ga ago. Noteworthy, the components of this LIP broadly follow the arcuate structural trend of the Alto Central Brazil and Sunsas belts (see Fig. 1), probably controlled by a large-scale crustal weakness along the active continental margin of Amazonia and penecontemporaneously to the onset of the Sunsas orogeny (Teixeira et al., 2019a). However, the RAT did not record the related collisional-like tectonothermal overprints akin to the outboard Sunsas orogeny (Fig. 16), and in this sense, it might have undergone a separation from Amazonia as a peripheral microplate. The hypothesis of a microplate is also consistent with the distinct gravity anomalies that characterize the SW edge of the Amazonian Craton and the RAT, respectively (Dragone et al., 2017). In any case, the paleogeography of RAT relative to Amazonia in Proterozoic times depends on further paleomagnetic studies.

8.3. Amazonia in Columbia and Rodinia

The relative positions of Amazonia in Columbia and Rodinia supercontinents are well-established by means of a coherent geometry of orogenic belts, key paleomagnetic constraints, as well as LIP barcode matches through time. Specifically for Columbia, different configurations have been debated, among other issues like the interconnectedness of the orogenic bounds and their tectonic settings (i.e. intra- or inter-cratonic in nature) (e.g., Zhao et al., 2002;Meert, 2012;Santosh and Zhao, 2009;Evans and Mitchell, 2011; Bispo-Santos et al., 2008, 2014; Johansson, 2009; Roberts, 2013; Xu et al., 2014; Pisarevsky et al., 2014; D'Agrella-Filho and Cordani, 2017; Meert and Santosh, 2017 and references therein). In this work, concerning Amazonia, we follow the paleogeographic model by Bispo-Santos et al. (2014) which is based on a wealth of reliable paleomagnetic poles and geochronological datings accumulated in the last decade in the Amazonian Craton, in agreement with the working model (Fig. 17).

The mid- to late Paleoproterozoic accretionary growth of Amazonia built the Ventuari-Tapajós (2.05–1.80 Ga) and the Rio Negro-Juruena (1.82–1.60 Ga) tectonic provinces, including the intervening Paraguá Terrane and the RAT (Cordani and Teixeira, 2007; this work) – see Tables 1 and 2. The stepwise growth was accompanied by inboard intraplate phenomena within the already established domains, such as the Uatumã (1.89–1.87 Ga) and Avanavero (1.79 Ga) LIP events (Teixeira et al., 2019b and references therein). The latter igneous activity, in particular, has a widespread distribution in Columbia, as documented by Youbi et al. (2013) – see Fig. 17. In this sense, D'Agrella-Filho et al. (2016) recently reassessed the available high-quality (1.79–1.78 Ga) paleomagnetic poles for the proto-Amazonian Craton compared to those of LIP episodes around the world. Their reconstruction favored a nearly equatorial paleogeography of Amazonia with the West Africa-Baltica connection, and a potential link with eastern Laurentia (Johansson, 2009; Bispo-Santos et al., 2014). Siberia

might also be the nearest block at that time in the light of its coherent tectonic structure with this fit (Fig. 17).

The Avanavero LIP in Amazonia is contemporary with the Teles Pires suite and Colider Group volcanics occurring in the Ventuari-Tapajós/Rio Negro-Juruena border (Alta Floresta domain; see Section 2). Altogether, these particular magmatic episodes are equivalent in age with the plutonic products of the Caracol magmatic arcs in the RAT, active from 1.78 to 1.74 Ga (Section 6.3.1 and Fig. 15). The Paleoproterozoic above-mentioned episodes in Amazonia were roughly coeval with the accretionary-collisional orogenic systems (2.1–1.7 Ga) that formed the building blocks of Columbia, such as the 1.81–1.76 Ga phase of the Transscandinavian belt (Baltica) and the 2.0–1.8 Ga Trans-Hudson orogen in Laurentia, whilst supported by paleomagnetic evidence (e.g., Zhao et al., 2002; Johansson, 2009; Evans and Mitchell, 2011; Xu et al., 2014; Bispo-Santos et al., 2014). The bulk geodynamic scenario is indicative of the westward younging zones of this supercontinent, assuming an Amazonia-West Africa-Baltica-Laurentia-Siberia fit.

Moreover, we also evaluate in the context of Rodinia the tectonic significance of the 1.11 Ga Rincón del Tigre-Huanchaca LIP that includes a component in the RAT (Rio Perdido suite) – see Fig. 15. The onset of this LIP was penecontemporaneous with the Grenville-Sunsas orogeny (Teixeira et al., 2015), which is part of the global orogenic cycle that eventually assembled the Rodinia supercontinent. The Rodinia reconstruction in Fig. 18 (adapted from Johansson, 2014) builds on many previous models with Baltica and Amazonia placed along the Grenville margin of Laurentia in a position with Baltica close to Labrador (e.g., Tohver et al., 2006; Li et al., 2008; Johansson, 2009, 2014; Roberts, 2013). According to this reconstruction, the orientation of Amazonia leaves a gap between the Sunsas orogen in SW Amazonia and the central Grenville orogen in Laurentia, following the SAMBA model of Johansson (2009).

In a broader sense, the 1.11 Ga LIP in SW Amazonia has a remarkable match with prominent intraplate activity around the world (Fig. 18), such as the Keweenawan plume (1.11–1.08 Ga) in Laurentia – considered a closest neighbor with Amazonia at that time (Ernst, 2014; Table 3 in Teixeira et al., 2019b). However, a discussion on issues like the longevity of this LIP and its possible number of nodes is beyond this review.

Declaration of competing interest

The authors declare that they have no known competing financial interests or personal relationships that could have appeared to influence the work reported in this paper.

Acknowledgments

Financial support was provided by grant 2013/12754-0 of the São Paulo Research Foundation (FAPESP), managed by UGC. WT, FMF, and ASR thank the National Council of Technological and Scientific Development (CNPq – Brazil) for the research productivity scholarship grants (303498/2014-5, 302884/2015-7 and 312811/2017-9 respectively). We acknowledge Editor Carlo Doglioni for his efficient handling of the manuscript. Very helpful comments on the manuscript by anonymous reviewers and Editor were greatly appreciated and helped to significantly improve the early drafts of this paper.

Appendix A. Supplementary data

Supplementary data to this article can be found online at https://doi.org/10.1016/j.earscirev.2020.103089.

References

Almeida, F.F.M., 1967. Origem e Evolução da Plataforma Brasileira: Boletim DNPM. Div. Geol. Mineral. 241, 1–36.
Araújo, H.J.T., Santos Neto, A., Trindade, C.A.H., Pinto, J.C.A., Montalvão, R.M.G., Dourado, T.D.C., Palmeira, R.C.B., Tassinari, C.C.G., 1982. Folha SF. 21 – Campo Grande. Projeto RADAMBRASIL; Geologia. Rio de Janeiro, Ministério das Minas e Energia 28, 23–109.
Bettencourt, J.S., Leite Jr., W., Payolla, B., Ruiz, A.S., Matos, R.S., Tosdal, R.M., 2010. The Rondonian-San Ignacio Province in the SW Amazonian Craton: an overview. J. S. Am. Earth Sci. 29, 28–46.
Bettencourt, J.S., Juliani, C., Xavier, R.P., Monteiro, L.V.S., Bastos Neto, A.C., Klein, E.L., Assis, R., Leite Jr., W.B., Moreto, C.P.N., Fernandes, C.M.D., Pereira, V.P., 2016. Metallogenetic systems associated with granitoid magmatism in the Amazonian Craton: an overview of the present level of understanding and exploration significance. J. S. Am. Earth Sci. 68, 22–49.
Bispo-Santos, F., D'Agrella-Filho, M.S., Pacca, I.I.G., Janikian, L., Trindade, R.I.F., Elming, S.-Å., Silva, J.A., Barros, M.A.S., Pinho, F.E.C., 2008. Columbia revisited: paleomagnetic results from the 1790 Ma Colíder volcanics (SW Amazonian Craton, Brazil). Precambrian Res. 164, 40–49.
Bispo-Santos, F., D'Agrella-Filho, M.S., Trindade, R.I.F., Janikian, L., Reis, N.J., 2014. Was there SAMBA in Columbia? Paleomagnetic evidence from 1790 Ma Avanavero mafic sills (Northern Amazonian craton). Precambrian Res. 244, 139–155.
Black, L.P., Kamo, S.L., Allen, C.M., Aleinikoff, J.N., Davis, D.W., Korsch, R.J., Foudoulis, C., 2003. TEMORA 1: a new zircon standard for Phanerozoic U–Pb geochronology. Chem. Geol. 200, 155–170.
Boger, S.D., Raetz, M., Giles, D., Etchart, E., Fanning, M.C., 2005. U–Pb age data from the Sunsas region of Eastern Bolivia, evidence for the allochtonous origin of the Paraguá Block. Precambrian Res. 139, 121–146.
Boggiani, P.C., Alvarenga, C.J.S., 2004. A faixa Paraguai. organizers In: Mantesso-Neto, V., Bartorelli, A., Carneiro, C.D.R., Brito-Neves, B.B. (Eds.), Geologia do continente sul-americano: evolução da obra de Fernando Flávio Marques de Almeida: São Paulo, Beca, Brazil, pp. 113–120.
Borghetti, C., Philipp, R.O., Mandetta, P., Hoffmann, I., 2018. Geochronology of the Archean Tumucumaque complex, Amapá Terrane, Amazonian Craton, Brazil. J. S. Am. Earth Sci. 88, 294–311.
Brittes, A.F.N., Sousa, M.Z.A., Ruiz, A.S., Batata, M.E.F., Lafon, J.-M., Plens, D.P., 2013. Geology, petrology and geochronology (Pb-Pb) of the Serra da Bocaina Formation: evidence of an Orosirian Amoguijá Magmatic Arc in the Rio Apa Terrane, south of the Amazonian Craton. Braz. J. Geol. 43, 48–69.
Brittes, A.F.N., Lafon, J.M., Souza, M.Z.A., Ruiz, A.S., Batata, M.E., Lima, G.A., 2016. Petrologia, geoquímica e geocronologia U-Pb (SHRIMP) em zircão das rochas piroclásticas e efusivas da Formação Serra da Bocaina – terreno Rio Apa – Sul do Craton Amazonico. In: 48° Congresso Brasileiro de Geologia. 8209.
Cabrera, R.F., 2015. Geologia, Deformação e Idade (U-Pb) do Grupo Campanário, Sequência Metassedimentar Mesoproterozoica no Terreno Rio Apa, Sul do Cráton Amazônico. Unpublished Master Thesis. Federal University of Mato Grosso, Cuiabá, MT, Brazil. 68 pp.
Casquet, C., Pankhurst, R.J., Rapela, C.W., Galindo, C.M., Fanning, C.M., Chiaradia, M., Baldo, E., González-Casado, J.M., Dahlquist, J.A., 2008. The Mesoproterozoic Maz Terrane in the Western Sierras Pampeanas, Argentina, equivalent to the Arequipa–Antofalla block of southern Peru? Implications for West Gondwana margin evolution. Gondwana Res. 13, 163–175.
Casquet, C., Rapela, C.W., Pankhurst, R.J., Baldo, E.G., Galindo, C., Fanning, C.M., Dahlquist, J.A., Saavedra, J., 2012. A history of Proterozoic terranes in southern South America: from Rodinia to Gondwana. Geosci. Front. 3, 137–145.
Cawood, P.A., Hawkesworth, C.J., Dhuime, B., 2012. Detrital zircon record and tectonic setting. Geology 40 (10), 875–878.
Chew, D.M., Cardona, A., Miškovic, A., 2011. Tectonic evolution of western Amazonia from the assembly of Rodinia to its break-up. Int. Geol. Rev. 53 (11 − 12), 1280–1296.
Cordani, U.G., Teixeira, W., 2007. Proterozoic Accretionary belts in the Amazonian Craton. org In: Hatcher Jr.R.D., Carlson, M.P., McBride, J.H., Martinez Catalán, J.R. (Eds.), The 4D Framework of Continental Crust: GSA Memoir, Boulder, Colorado. 200. pp. 297–320 Geological Society of America Book Editors.
Cordani, U.G., Sato, K., Teixeira, W., Tassinari, C.C.G., Basei, M.A.S., 2000. Crustal evolution of the South American platform. In: Cordani, U.G., Milani, E.J., Thomaz-Filho, A., Campos, D.A. (Eds.), Tectonic Evolution of South America: Rio de Janeiro, Brazil, 31st International Geological Congress, pp. 19–40.
Cordani, U.G., Teixeira, W., D'Agrella-Filho, M.S., Trindade, R., 2009. The position of the Amazonian Craton in supercontinents. Gondwana Res. 15, 396–407.
Cordani, U.G., Teixeira, W., Tassinari, C.C.G., Coutinho, J.M.V., Ruiz, A.S., 2010. The Rio Apa craton in Mato Grosso do Sul (Brazil) and northern Paraguay: geochronological evolution, correlations and tectonic implications. Am. J. Sci. 310, 981–1023.
Cordani, U.G., Ramos, V.A., Fraga, L.M., Cegarra, M., Delgado, I., de Souza, K.G., Gomes, F.E.M., Schobbenhaus, C., 2016a. Tectonic Map of South America. Scale: 1/5,900,000. Commission for the Geological Map of the World, Paris.
Cordani, U.G., Sato, K., Sproensser, W., Fernandes, F.S., 2016b. U-Pb zircon ages of rocks from the Amazonas Territory of Colombia and their bearing on the tectonic history of the NW sector of the Amazonian Craton. Braz. J. Geol. 46, 5–35.
Costa, J.T., 2017. Suíte Intrusiva Fazenda Matão: Complexo Máfico-Ultramáfico Orosiriano no Bloco Rio Apa – Sul do Cráton Amazônico. Unpublished Master Thesis, Federal University of Mato Grosso, Mato Grosso, Brazil. 117 p.
Curto, J.B., Vidotti, R.M., Fuck, R.A., Blakely, R.J., Alvarenga, C.J.S., Dantas, E.L., 2014. The tectonic evolution of the Transbrasiliano Lineament in northern Paraná Basin, Brazil, as inferred from aeromagnetic data. J. Geophys. Res. Solid Earth 119, 1544–1562. https://doi.org/10.1002/2013JB010593.
D'Agrella-Filho, M.S., Cordani, U.G., 2017. The Paleomagnetic Record of the São Francisco-Congo Craton. In: Heilbron, M., Alkmim, F., Cordani, U.G. (Eds.), São Francisco Craton, Eastern Brasil: Tectonic Genealogy of a Miniature Continent,

Regional Geology Review Series. Springer-Verlag, pp. 305–320 Chapter 16.
D'Agrella-Filho, M.S., Bispo-Santos, F., Trindade, R.I.F., Antonio, P.J.Y., 2016. Paleomagnetism of the Amazonian Craton and its role in paleocontinents. Braz. J. Geol. 46 (2), 275–299.
Dall' Agnol, R., Costi, H.T., Leite, A.A.S., Magalhães, M.S., Teixeira, N.P., 1999. Rapakivi granites from Brazil and adjacent areas. Precambrian Res. 95, 9–39.
Dragone, G.N., Ussami, N., Gimenez, M.E., Klinger, F.G.L., Chaves, C.A.M., 2017. Western Paraná suture/shear zone and the limits of Rio Apa, Rio Tebicuary and Rio de la Plata cratons from gravity data. Precambrian Res. 291, 162–177.
Elholou, S., Belousova, E., Griffin, W.L., Peasom, N.J., O'Reilly, S.Y., 2006. Trace elements and isotopic composition of GJ red zircon standard by laser ablation. Geochem. Cosmochem. Acta 70 (i18), A158.
Ernst, R.E., 2014. Large Igneous Provinces, 1–653. Cambridge University Press, Cambridge, UK.
Evans, D.A.D., Mitchell, R.N., 2011. Assembly and breakup of the core of Paleoproterozoic–Mesoproterozoic supercontinent Nuna. Geology 39, 443–446. https://doi.org/10.1130/G31654.1.
Faleiros, F.M., Pavan, M., Remédio, M.J., Rodrigues, J.B., Almeida, V.V., Caltabeloti, F.P., Pinto, L.G.R., Oliveira, A.A., Pinto de Azevedo, E.J., Costa, V.S., 2016. Zircon U-Pb ages of rocks from the Rio Apa Cratonic Terrane (Mato Grosso do Sul, Brazil): new insights for its connection with the Amazonian Craton in pre-Gondwana times. Gondwana Res. 34, 187–204.
Fernandes, C.M.D., Juliani, C., Monteiro, L.V.S., Lagler, B., Echeverri-Misas, C.M., 2011. High-K calc-alkaline to A-type fissure-controlled volcano-plutonism of the São Fidelix do Xingu region, Amazonian craton, Brazil: exclusively crustal sources or only mixed Nd model ages? J. S. Am. Earth Sci. 32, 351–368.
Ganade, C.E., Cordani, U.G., Agbossoumoude, Y., Renaud, C., Basei, M.A.S., Weinbert, R.F., Sato, K., 2016. Tightening-up NE Brazil and NW Africa connections: new U-Pb/Lu-Hf zircon data of a complete plate tectonic cycle in the Dahomey belt of the West Gondwana Orogen in Togo and Benin. Precambrian Res. 276, 24–42.
Gaucher, C., Frei, R., Chemale Jr., F., Frei, D., Bossi, J., Martínez, G., Chiglino, L., Cernuschi, F., 2011. Mesoproterozoic evolution of the Rio de la Plata Craton in Uruguay: at the heart of Rodinia? Int. J. Earth Sci. 100, 273–288. https://doi.org/10.1007/s00531-01100562-x.
Geraldes, M.C., Van Schmus, W.R., Condie, K.C., Bell, S., Teixeira, W., Babinski, M., 2001. Proterozoic geologic evolution of the SW part of the Amazonian Craton in Mato Grosso state, Brazil. Precambrian Res. 111, 91–128.
Godoy, A.M., Manzano, J.C., Araújo, L.M.B., Silva, J.A., 2010. Suíte Vulcânica Serra da Bocaina, Grupo Amoguijá, Maciço Rio Apa – MS. Geociências 28, 485–499.
Godoy, A.M., Manzano, J.C., Araujo, L.M.B., Godoy, L.P., 2014. Magmatismo da Serra da Alegria, Grupo Amonguijá, Maciço Rio Apa, sudeste do estado de Mato Grosso do Sul. Geociências 33, 558–578.
Halls, H.C., Campal, N., Davis, D.W., Bossi, J., 2001. Magnetic studies and U–Pb geochronology of the Uruguayan dike swarm, Río de la Plata Craton, Uruguay: paleomagnetic and economic implications. J. S. Am. Earth Sci. 14, 349–361.
Johansson, Å., 2009. Baltica, Amazonia and the SAMBA connection—1000 million years of neighbourhood during the Proterozoic? Precambrian Res. 175, 221–234.
Johansson, Å., 2014. From Rodinia to Gondwana with the 'SAMBA' model—a distant view from Baltica towards Amazonia and beyond. Precambrian Res. 244, 226–235.
Kroonenberg, S.B., de Roever, E.W.F., Fraga, L.M., Reis, N.J., Faraco, T., Lafon, J.-M., Cordani, U., Wong, T.E., 2016. Paleoproterozoic evolution of the Guiana Shield in Suriname: a revised model. Geol. Mijnb. 1–32. https://doi.org/10.1017/njg.2016.10.
Lacerda Filho, J.V., 2015. Bloco Rio Apa: origem e evolução tectônica. Unpublished Doctoral Thesis. Universidade de Brasília, Brasília, Brazil. (181p).
Lacerda Filho, J.V., Fuck, R.A., Ruiz, A.S., Dantas, E.L., Scandolara, J.E., Rodrigues, J.B., Nascimento, N.D.C., 2016. Palaeoproterozoic tectonic evolution of the Alto Tererê Group, southernmost Amazonian Craton, based on field mapping, zircon dating and rock geochemistry. J. S. Am. Earth Sci. 65, 121–141.
Lacerda-Filho, J.V., de Brito, R.S.C., Silva, M.G., de Oliveira, C.C., Moreton, L.C., Martins, E.G., Lopes, R.C., Lima, T.M., Larizatti, J.H., Valente, C.R., 2006. Geologia e Recursos Minerais do Estado de Mato Grosso do Sul. Programa Integração, Atualização e Difusão de Dados da Geologia do Brasil: Convênio CPRM/SEPROTUR/MS, Campo Grande, 121, escala 1: 1.000.000.
Lamarão, C.N., Dall'Agnol, R., Lafon, J.M., Lima, E.F., 2002. Geology, geochemistry and Pb–Pb zircon geochronology of the Paleoproterozoic magmatism of Vila Riozinho, Tapajós gold province, Amazonian craton, Brazil. Precambrian Res. 119, 189–223.
Lamarão, C.N., Dall'Agnol, R., Pimentel, M.M., 2005. Nd isotopic composition of Paleoproterozoic volcanic and granitoid rocks of Vila Riozinho: implications for the crustal evolution of the Tapajós gold province, Amazon craton. J. S. Am. Earth Sci. 18, 277–292.
Leite, J.A.D., Saes, S., 2003. Geocronologia Pb/Pb de zircões detríticos e análise estratigráfica das coberturas sedimentares proterozóicas do sudoeste do Cráton Amazônico. Sér. Científ. São Paulo Rev. Inst. Geociênc. USP 3, 113–127.
Li, Z.X., Bogdanova, S.V., Collins, A.S., Davidson, A., De Waele, B., Ernst, R.E., Fitzsimons, I.C.W., Fuck, R.A., Gladkochub, D.P., Jacobs, J., Karlstrom, K.E., Lu, S., Natapov, L.M., Pease, V., Pisarewsky, S.A., Thrane, K., Vernikovsky, V., 2008. Assembly, configuration, and break-up history of Rodinia: a synthesis. Precambrian Res. 160, 179–210.
Litherland, M., Annells, R.N., Appleton, J.D., Berrangé, J.P., Bloomfield, K., Burton, C.C.J., Darbyshire, D.P.F., Fletcher, C.J.N., Hawkins, M.P., Klinck, B.A., Llanos, A., Mithcell, W.I., O'Connor, E.A., Pitfield, P.E.J., Power, G.E., Webb, B.C., 1986. The Geology and Mineral Resources of the Bolivian Precambrian Shield.
Litherland, M., Annells, R.N., Darbyshire, D.P.F., Fletcher, C.N.J., Hawkings, M.P., Klinck, B.A., Mitchell, W.I., O'Conner, E.A., Pitfeild, P.E.J., Power, G., Webb, B.C., 1989. The Proterozoic of Eastern Bolivia and its relationship to the Andean mobile belt. Precambrian Res. 43, 157–174.
Ludwig, K.R., 2003. User's Manual for ISOPLOT 3.00. A Geochronological Toolkit for Microsoft Excel. Berkeley Geochronological Center Special Publication 4, 70 pp.
Ludwig, K.R., 2009a. Isoplot 4.1. A Geochronological Toolkit for Mircosoft Excel. Berkeley geochronology Center, Berkeley, CA Special Publications 4. 75p.
Ludwig, K., 2009b. SQUID 2: A User's Manual, rev. 12 Apr, 2009. Berkeley Geochronology Center, Special Publication 5, 110 p.
Manzano, J.C., Godoy, A.M., Araujo, L.M.B., Godoy, L.P., 2012. Suite plutônica Alumiador, Grupo Amoguijá, Maciço Rio Apa – MS. Geociências 31, 351–370.
Matos, R., Teixeira, W., Geraldes, M.C., Bettencourt, J.S., 2009. Geochemistry and isotopic evidence of the Pensamiento Granitoid Complex, Rondonian–San Ignacio province, eastern Precambrian Shield of Bolivia: petrogenetic constraints for a Mesoproterozoic magmatic arc setting. Rev. Geol. USP Sér. Científ. 9 (2), 89–117.
Meert, J.G., 2012. Whats the name? The Columbia (Paleopangaea/Nuna) supercontinent. Gondwana Res. 21, 987–993.
Meert, J.G., Santosh, M., 2017. The Columbia supercontinent revisited. Gondwana Res. 50, 67–83.
Nedel, I.M., Ruiz, A.S., Matos-Salinas, G., Sousa, M.Z.A., Pimentel, M.M., Pavaneto, P., 2017. Front San Diablo na região de Miraflores, Faixa Sunsás, Bolívia: implicações tectônicas e estratigráficas. Geol. USP Sér. Científ. 17 (3), 125–147.
Nogueira, S.F., Sousa, M.Z.A., Ruiz, A.S., Batata, M.E.F., Cabrera, R.F., Costa, J.T., 2013. Granito Aquidabã – Suíte Intrusiva Alumiador – Sul do Cráton Amazônico Geologia, Petrografia e Geoquímica. Anais do 13° Simpósio de Geologia da Amazônia, Belém, pp. 368–371.
Payolla, B.L., Bettencourt, J.S., Kozuch, M., Leite Jr., W.B., Fetter, A.H., Van Schmus, W.R., 2002. Geological evolution of the basement rocks in the east-central part of the Rondônia Tin Province, SW Amazonian Craton, Brazil: U–Pb and Sm–Nd isotopic constraints. Precambrian Res. 119, 141–169.
Peri, V.G., Barcelona, H., Pomposiello, M.C., Favetto, A., 2015. Magnetotelluric characterization through the Ambargasta-Sumampa Range: the connection between the northern and southern trace of the Río de La Plata Craton – Pampean Terrane tectonic boundary. J. S. Am. Earth Sci. 59, 1–12.
Pinho, M.A.S.B., Chemale Júnior, F., Van Schmus, W.R., Pinho, F.E.C., 2003. U–Pb and Sm–Nd evidence for 1.76–1.77 Ga magmatism in the Moreru region, Mato Grosso, Brazil: implications for province boundaries in the SWAmazon Craton. Precambrian Res. 126, 1–25.
Pisarevsky, S.A., Elming, S.-A., Pesonen, L.J., Li, Z.-X., 2014. Mesoproterozoic paleogeography: supercontinent and beyond. Precambrian Res. 244, 207–225.
Plens, D.P., 2018. Petrogênese e Análise Estrutural da Suíte Caracol: Implicações para a Evolução Geodinâmica do Bloco Rio Apa – Sul do Cráton Amazônico. Unpublished Doctoral Thesis Universidade de Brasília. Brasília, Brasil, 117p.
Plens, D.P., Ruiz, A.S., Sousa, M.Z.A., Batata, M.E.F., Lafon, J.-M., Brittes, A.F.N., 2013. Cerro Porã Batholith: post-orogenic A-type granite from the Amoguijá Magmatic Arc – Rio Apa Terrane – South of the Amazonian Craton. Braz. J. Geol. 43, 515–534.
Ramos, V.A., 2018. Tectonic evolution of the Central Andes: from terrane accretion to crustal delamination. In: Zamora, G., McClay, K.M., Ramos, V.A. (Eds.), Petroleum Basins and Hydrocarbon Potential of the Andes of Peru and Bolivia: AAPG Memoir. 117. pp. 1–34.
Ramos, V.A., Vujovicha, G., Martino, R., Otamendic, J., 2010. Pampia: a large cratonic block missing in the Rodinia supercontinent. J. Geodyn. 50, 243–255. https://doi.org/10.1016/j.jog.2010.01-019.
Rapalini, A.E., 2018. The Assembly of Western Gondwana: reconstruction based on paleomagnetic data. In: Siegesmund, S., Basei, M., Oyhantçabal, P., Oriolo, S. (Eds.), Geology of Southwest Gondwana. Regional Geology Reviews. Springer, pp. 3–18. https://doi.org/10.1007/978-3-319-68920-3_1.
Redes, L.A., Sousa, M.Z., Ruiz, A.S., Lafon, J.-M., 2015. Petrogenesis and U-Pb and Sm-Nd geochronology of the Taquaral granite: record of an orosirian continental magmatic arc in the region of Corumbá – MS. Braz. J. Geol. 45 (1), 431–451.
Reis, N.J., Bahia, R.B.C., Almeida, M.E., Costa, U.A.P., Betiollo, L.M., Oliveira, A.C., Oliveira, A.A., Splendor, F., 2013. O Supergrupo Sumaúma no contexto geológico da Folha SB.20-Z-D (Sumaúma), sudeste do Amazonas: modo de ocorrência, discussão de idades em zircões detríticos e correlações no SW do Cráton do Amazonas. Contrib. Geol. Amazôn. 8, 199–222.
Remédio, M.J., Faleiros, F.M., 2014. Programa Geologia do Brasil – PGB. Geologia e Recursos Minerais da Folha Fazenda Margarida – SF.21-X-C-IV, Estado de Mato Grosso do Sul, Escala 1:100.000. CPRM, São Paulo.
Rizzotto, G.J., Santos, J.O.S., Hartmann, L.A., Tohver, E., Pimentel, M.M., McNaughton, N.J., 2013. The Mesoproterozoic Central Brazil suture in the SW Amazonian Craton: geotectonic implications based on field geology, zircon geochronology and Nd-Sr isotope geochemistry. J. S. Am. Earth Sci. 48, 271–295.
Rizzotto, G.J., Hartmann, L.A., Santos, J.O.S., McNaughton, N.J., 2014. Tectonic evolution of the southern margin of the Amazonian craton in the late Mesoproterozoic based on field relationships and zircon U-Pb geochronology. An. Acad. Bras. Cienc. 86, 57–84.
Rizzotto, G.J., Alves, C.L., Rios, F.S., Sant'Ana, M.B., 2019a. The Nova Monte Verde metamorphic core complex: Tectonic implications for the southern Amazonian craton. J. S. Am. Earth Sci. 91, 154–172. https://doi.org/10.1016/j.jsames.2019.01.003.
Rizzotto, G.J., Alves, C.L., Rios, F.S., Sant'Ana, M.B., 2019b. The Western Amazonia igneous belt. J. S. Am. Earth Sci. 96. https://doi.org/10.1016/j.jsames.2019.201326.
Roberts, N.M.W., 2013. The boring billion? Lid tectonics, continental growth and environmental change associated with the Columbia supercontinent. Geosci. Front. 4, 681–691.
Rosa, J.W.C., Rosa, J.W.C., Fuck, R.A., 2016. The structure of the Amazonian craton: available geophysical evidence. J. S. Am. Earth Sci. 70, 162–173. https://doi.org/10.1016/j.jsames.2016.05.006.
Ruiz, A.S., 2005. Evolução geológica do sudoeste do Craton Amazônico, região limítrofe

Brasil-Bolivia-Mato Grosso. Unpublished Doctoral Thesis. Universidade Estadual de São Paulo, Rio Claro, Brazil (260 p).
Ruiz, A.S., Lima, G.A., D'Agrella-Filho, M.S., 2014. Ar-Ar step heating ages for mylonitic low angle shear zones rocks in the Rio Apa Terrane, South Amazonian Craton. In: 9th SSAGI- South American Symposium on Isotope Geology, pp. 96 Program and Abstracts. São Paulo, Brazil.
Santos, J.O.S., Hartmann, L.A., Gaudette, H.E., Groves, D.I., McNaugthon, N.J., Fletcher, I.R.A., 2000. New understanding of the Provinces of Amazon Cráton based on integration of Field Mapping and U–Pb and Sm–Nd Geochronology. Gondwana Res. 4 (3), 453–488.
Santos, J.O.S., Groves, D.I., Hartmann, L.A., McNaughton, N.J., Moura, M.B., 2001. Gold deposits of the Tapajós Province, Amazon Craton. Mineral. Deposita 36, 278–299.
Santos, J.O.S., Van Breemen, O.B., Groves, D.I., Hartmann, L.A., Almeida, M.E., McNaughton, N.J., Fletcher, I.R., 2004. Timing and evolution of multiple Paleoproterozoic magmatic arcs in the Tapajós Domain, Amazon Craton: constraints from SHRIMP and TIMS zircon, baddeleyite and titanite U-Pb geochronology. Precambrian Res. 131 (1/2), 73–109.
Santos, J.O.S., Rizzotto, G.J., Potterd, P.E., McNaughton, N.J., Matos, R., Hartmann, L.A., Chemale Jr., F., Quadros, M.L.E.S., 2008. Age and autochthonous evolution of the Sunsás Orogen in West Amazon Craton based on mapping and U–Pb geochronology. Precambrian Res. 165, 120–152.
Santos, G., Ruiz, A.S., Sousa, M.Z.A., Batata, M.E.F., Cabrera, R.F., Lafon, J.M., 2019. Petrologia, deformação e Geocronologia U-Pb (SHRIMP) do Granito Coimbra: Bloco Rio Apa na região de Corumbá – Brasil. Geol. USP Sér. Científ. 19 (1), 171–192.
Santosh, M., Zhao, G., 2009. Supercontinent dynamics. Gondwana Res. 15, 225–470.
Sato, K., Tassinari, C.C.G., 1997. Principais eventos de acresção continental no Cráton Amazônico, baseados em idade modelo Sm-Nd, calculadas em evoluções de estágio único e estágio duplo. In: Costa, M.L., Angélica, R.S. (Eds.), Contribuições à Geologia da Amazônia. 1. SBG, Belém, Brazil, pp. 91–142.
Sato, K., Basei, M.A.S., Siga Junior, O., Onoi, A.T., 2010. In situ U-Th-Pb Isotopic Analyses by Excimer Laser Ablation/ICP-MS on Brazilian Megacrystal Xenotime: First Results on U-Pb Isotopes at CPGeo-IGC-USP. VII SSAGI-South American Simposium on Isotope Geology, Brasília, Brazil. Abstracts. pp. 349–352.
Sato, K., Tassinari, C.C.G., Basei, M.A.S., Siga Jr., O., Onoe, A.T., Souza, M.D., 2014. Sensitive High Resolution Ion Microprobe (SHRIMP IIe/MC) of the Institute of Geosciences of the University of São Paulo, Brazil: analytical method and first results. Geol. USP Sér. Científ. 14 (3), 3–14.
Scandolara, J.E., Fuck, R.A., Dantas, E.L., Souza, V.S., 2013a. Geochemistry of Jamari complex, Central-Eastern Rondônia: Andean type magmatic arc and Paleoproterozoic crustal growth of the southwestern Amazonian Craton, Brazil. J. S. Am. Earth Sci. 46 (1–28).
Scandolara, J.E., Fuck, R.A., Dall Agnol, R., Dantas, E.L., 2013b. Geochemistry and origin of the Early Mesoproterozoic mangerite-charnockite-rapakivi granite association of the Serra da Providência suite and associated gabbros, Central-Eastern Rondônia, SWAmazonian Craton, Brazil. J. S. Am. Earth Sci. 4, 166–193.
Scandolara, J.E., Ribeiro, P.S.E., Frasca, A.A.S., Fuck, R.A., Rodrigues, J.B., 2014. Geochemistry and geochronology of mafic rocks from the Vespor suite in the Juruena arc, Roosevelt-Juruena terrain, Brazil: implications for Proterozoic crustal growth and geodynamic setting of the SW Amazonian craton. J. S. Am. Earth Sci. 53, 20–49.
Scandolara, J.E., Correa, R.T., Fuck, R.A., Souza, V.S., Rodrigues, J.B., Ribeiro, P.S.E., Frasca, A.A.S., Saboia, A.M., Lacerda Filho, J.V., 2017. Paleo-Mesoproterozoic arc-accretion along the southwestern margin of the Amazonian craton: the Juruena accretionary orogen and possible implications for Columbia supercontinente. J. S. Am. Earth Sci. 73, 223–247.
Siqueira, R., Hollanda, M.H.B., Basei, M.A.S., 2014. A novel approach to (LA-ICP-MS acquired) U–Th–Pb data processing. In: 9th South American Symposium on Isotope Geology – SSAGI, Brazil, pp. 306 Program and Abstracts.
Souza, C.D., Souza, M.Z.A., Ruiz, A.S., Batata, M.E.F., Brittes, A.F.N., Lafon, J.-M., 2016. Formação Serra da Bocaina: Contribuição do Vulcanismo Paleoproterozoico do Arco Magmático Amoguijá no Bloco Rio Apa, Sul do Cráton Amazônico. Geochim. Bras. 30 (2), 136–157. https://doi.org/10.21715/GB2358-2812.2016302136.
Stacey, J.S., Kramers, J.D., 1975. Approximation of terrestrial lead isotope evolution by a two-stage model. Earth Planet. Sci. Lett. 26 (203), 207–221.
Stern, R.J., 2004. Subduction initiation: spontaneous and induced. Earth Planet. Sci. Lett. 226, 275–292.
Tassinari, C.C.G., Macambira, M., 2004. A evolução tectônica do Craton Amazônico. In: Mantesso-Neto, V., Bartorelli, A., Carneiro, C.D.R., Brito Neve, B.B. (Eds.), Geologia do Continente Sul Americano: Evolução da obra de Fernando Flávio Marques Almeida. São Paulo, pp. 471–486.
Tassinari, C.C.G., Cordani, U.G., Nutman, A.P., Van Schmus, W.R., Bettencourt, J.S., Taylor, P.N., 1996. Geochronological systematics on basement rocks from the Rio Negro-Juruena Province (Amazonian Craton) and tectonic implications. Int. Geol. Rev. 38, 161–175. https://doi.org/10.1080/00206819709465329.
Teixeira, W., Tassinari, C.C.G., Cordani, U.G., Kawashita, K., 1989. A review of the geochronology of the Amazonian Craton: tectonic implications. Precambrian Res. 42, 213–227.
Teixeira, W., Geraldes, M.C., Matos, R., Ruiz, A.S., Saes, G., Vargas-Mattos, G., 2010. A review of the tectonic evolution of the Sunsas belt, SW Amazonian Craton. J. S. Am. Earth Sci. 29, 47–60.
Teixeira, W., D'Agrella-Filho, M.D., Hamilton, M.A., Ernst, R.E., Girardi, V.A.V., Mazzucchelli, M., Bettencourt, J.S., 2013. U–Pb (ID-TIMS) baddeleyite ages and paleomagnetism of 1.79 and 1.59 Ga tholeiitic within the Columbia supercontinent dyke swarms, and position of the Rio de la Plata Craton. Lithos 174, 157–174.
Teixeira, W., Hamilton, M., Girardi, V.A.V., Faleiros, F.M., 2019a. U-Pb baddeleyite ages of key dyke swarms in the Amazonian Craton (Carajás/Rio Maria and Rio Apa areas): tectonic implications for events at 1880, 1110 Ma, 535 Ma and 200 Ma. Precambrian Res. 329, 138–155. https://doi.org/10.1016/j.precamres.2018.02.008.
Teixeira, W., Hamilton, M.A., Lima, G.A., Matos, R., Ernst, R.E., 2015. Precise ID-TIMS U-Pb baddeleyite ages (1110-1112 Ma) for the Rincón del Tigre-Huanchaca large igneous province (LIP) of the Amazonian Craton: Implications for the Rodinia supercontinent. Precambrian Res. 265, 273–285.
Teixeira, W., Reis, N.J., Bettencourt, J.S., Klein, E.F., Oliveira, D., 2019b. Intraplate Proterozoic magmatism in the Amazonian Craton reviewed: geochronology, crustal tectonics and global barcode matches. In: Rajesh (Ed.), Dyke Swarms of the World-A Modern Perspective, pp. 111–154. https://doi.org/10.1007/978-981-13-1666-1_4. Springer Geology.
Tohver, E., Van der Pluijm, B.A., Mezger, K., Essene, E., Scandorala, J.E., Rizzotto, G.J., 2004. Significance of the Nova Brasilândia metasedimentary belt in western Brazil: redefining the mesoproterozoic boundary of the Amazon Craton. Tectonics 23https://doi.org/10.1029/2003TC001563. TC6004.
Tohver, E., Teixeira, W., Van Der Pluijm, B.A., Geraldes, M.C., Bettencourt, J.S., Rizzotto, G., 2006. Restored transect across the exhumed Grenville orogen of Laurentia and Amazonia, with implications for crustal architecture. Geology 34 (8), 669–672. https://doi.org/10.1130/G22534.1.
Vargas-Matos, G., Geraldes, M.C., Mattos, R., Teixeira, W., 2011. LA-ICPMS U-Pb Ages of Paleo- and Mesoproterozoic Granites in Bolivia. Goldschmidt Conference Abstracts. pp. 2074.
Vervoot, J.D., Kemp, A.I.S., 2016. Clarifying the Zr Hf isotopic record of crust-mantle evolution. Chem. Geol. 425, 65–75.
Wiens, F., 1986. Zur lithostratigraphischen, petrographischen und strukturellen Entwicklung des Rio-Apa Hochlandes, Nordost Paraguay: Clausthal, Geologisches Institut der Technischen Universität Clausthal, Clausthaler Geowissenschaftliche. Unpublished Master Thesis 19. 280 p.
Xu, H., Yang, Z., Peng, P., Meert, J.G., Zhu, R., 2014. Paleo-position of the North China craton within the Supercontinent Columbia: constraints from new paleomagnetic results. Precambrian Res. 255, 276–293.
Youbi, N., Kouyate, D., Soderlund, U., Ernst, R.E., Soulaimani, A., Hafid, A., Ikenne, M., El Bahat, A., Bertrand, H., Chaham, K.R., Abbou, M.B., Mortaji, A., El Ghorfi, M., Zouhair, M., El Janati, M., 2013. The 1750 Ma Magmatic event of the West African Craton (Anti-Atlas, Morocco). Precambrian Res. 236, 106–123.
Zhao, G.C., Cawood, P.A., Wilde, S.A., Sun, M., 2002. Review of global 2.1–1.8 Ga orogens: implications for a pre-Rodinia supercontinent. Earth Sci. Rev. 59, 125–162.